NASA CONTRACTOR REPORT

NASA CR-2571

NASA CR-

THEORY OF AN AIRFOIL EQUIPPED WITH A JET FLAP UNDER LOW-SPEED FLIGHT CONDITIONS

F. L. Addessio and J. G. Skifstad

Prepared by
PURDUE UNIVERSITY
West Lafayette, Ind. 47907
for Langley Research Center

NATIONAL AERONAUTICS AND SPACE ADMINISTRATION • WASHINGTON, D. C. • JULY 1975

1. Report No. NASA CR-2571	2. Government Accession No.
3.	
4. Title and Subtitle THEORY OF AN AIRFOIL EQUIPPED WITH A JET FLAP UNDER LOW-SPEED FLIGHT CONDITIONS	5. Report Date July 1975
	6. Performing Organization Code
7. Author(s) F. L. Addessio and J. G. Skifstad	8. Performing Organization Report No.
	10. Work Unit No. 505-06-11-04
9. Performing Organization Name and Address Purdue University School of Mechanical Engineering West Lafayette, Indiana 47907	11. Contract or Grant No. NGL 15-005-094
	13. Type of Report and Period Covered CONTRACTOR REPORT
12. Sponsoring Agency Name and Address National Aeronautics and Space Administration Washington, D.C. 20546	14. Sponsoring Agency Code

15. Supplementary Notes

Final report.

16. Abstract

A theory is developed, for the inviscid, incompressible flow past a thin airfoil equipped with a thin, part-span jet flap, by treating the induced flowfields of the jet and the wing separately and by obtaining the fully coupled solution in an iterative manner. Spanwise variation of the jet vortex strength is assumed to be elliptical in the analysis. Since the method considers the vorticity associated with the jet to be positioned on the computed locus of the jet, the downwash aft of the wing can be evaluated as well as forces and moments on the wing. A lifting-surface theory is incorporated for the aerodynamics of the wing.

Computational results are presented for a rectangular wing at momentum coefficients above 2.0 and compared with existing linear theories and experimental data. Good agreement is found for small angles of attack, jet-deflection angles, and jet-momentum coefficients where the linear theories and experimental data are applicable. In addition, results are presented for larger values of the above parameters where the linear theories are not suitable. Downwash data at a point in the vicinity of a control surface, the load distribution on the airfoil, and the jet, and the jet location are also presented for representative flight conditions.

17. Key Words (Suggested by Author(s)) (STAR category underlined) Jet-Flap Theory, Powered Lift, Flowfield analysis	18. Distribution Statement Unclassified - Unlimited. Subject Category 02 Aerodynamics

19. Security Classif. (of this report)	20. Security Classif. (of this page)	21. No. of Pages	22. Price*
Unclassified	Unclassified	140	$5.75

*Available from The National Technical Information Service, Springfield, Virginia 22151; STIF/NASA Scientific and Technical Information Facility, P.O. Box 33, College Park, MD 20740

TABLE OF CONTENTS

$\vec{A}$ vector potential

A constant defined by Equation (A15)

A_n, B_n constants defined in Appendix C

a,b,d arbitrary constants (see Appendices A and B)

a_m constant employed in the series expansion for the jet sheet location

a_{mn}, b_{mn} constants defined in Appendix C

B constant defined by Equation (A16)

b_m constant defined by Equation (D5)

CA constant defined in Appendix B

C_D drag coefficient

C_J jet-momentum coefficient

C_n constant employed in the expansion for the streamwise distribution of the vortex strength

C_L lift coefficient

C_p pressure coefficient

c airfoil chord, arbitrary constant (see Appendices A and B)

c_m, d_m, e_m constants defined in Appendix C

D drag force on the airfoil

E complete elliptic integral of the second kind

E_n remainder in Simpson's compound integration rule

$\vec{e}$ unit vector

e damping factor

F variable defined by Equation (59)

f arbitrary function

G streamwise distribution of the jet vortex strength

G_j variable defined by Equation (58)

g streamwise distribution of the jet vortex strength such that $g(x) = G[\xi(x,f_J)]$, constant (see Appendix A)

g_n function employed in the series expansion of g

H spanwise distribution of the jet vortex strength such that $H = dh/d\eta$

h spanwise distribution of the jet eortex strength, step size employed in the numerical algorithms

I arbitrary integral

J arbitrary integral, jet momentum flux per unit span

K	complete elliptic integral of the first kind
k	modulus of the complete elliptic integrals
k_c	complimentary modulus such that $k_c^2 = 1-k^2$
L	lift force on the airfoil
l.e.	leading edge of the airfoil
MO	constant defined in Appendix B
m,n	constants defined in Appendix B
$\vec{n}$	unit normal vector
P	variable defined by Equation (A25)
PIFO	constant defined in Appendix B
p	pressure
Q	variable defined by Equation (A26)
Q_i	variable defined by Equation (52)
q	arbitrary constant (see Appendix A)
$\vec{R}$	distance from a source point to a field point
R	magnitude of $\vec{R}$, variable defined by Equation (A27)
r	residual of a least square fit for a function, integration variable (see Appendix A)

S surface

s span

s_i variable defined by Equation (54)

T_i variable defined by Equation (53)

t jet thickness

t_{ni} variable defined by Equation (55)

t.e. trailing edge of the airfoil

U,V,W components of the total velocity vector

u x-component of the disturbance velocity vector, integration variable (see Appendix A)

v,w components of the disturbance velocity vector

$\vec{V}$ total velocity vector

$\vec{v}$ disturbance velocity vector

x,y,z rectangular

$\vec{x}$ vector in a rectangular coordinate system

x_b location of the bound vortex line

$\bar{x}$ nondimensional variable such that $x = \nu x/s_J$

$\bar{x}_i$ variable defined in Appendix E

α angle of attack, integration constant defined by Equation (A21)

α_A parameter of the elliptic integral of the third kind (see Eq. (65))

α_2 integration constant defined by Equation (A22)

β scale factor employed in the expansion for the streamwise distribution of the vortex strength

Γ circulation of the horseshoe vortex system

$\vec{\gamma}$ vortex strength vector

γ parameter of the elliptic integral of the third kind (see Appendices A and B)

Δ difference between the values of a variable on each side of a vortex sheet; step size (see Appendix E)

δ small neighborhood of the origin

ε small parameter

$\varepsilon_1, \varepsilon_2$ define a small neighborhood of the control point

Φ scalar potential for the total velocity vector

ϕ scalar potential for the disturbance velocity vector

ϕ_1 variable defined by Equation (C4)

ϕ_m constant defined by Appendix C

Θ downwash angle

θ angle between the normal to the jet sheet and $\vec{e}_z$

κ curvature

κ_o curvature obtained from a previous iterate

Λ_n variable defined by Equation (D3)

ν scale factor employed in the series expansion for the jet sheet location

Ξ variable defined by Equation (E1)

ξ,η,ζ coordinate system located within the jet sheet, arbitrary integration variables (see Appendix A)

$\bar{\xi}_i$ variable defined in Appendix E

Π complete elliptic integral of the third kind

π = 3.1415926...

ρ mass density of the free stream, arbitrary integration variable (see Appendix A)

Σ summation symbol

τ jet-deflection angle

τ_d doublet strength

T a region in space

ψ	slope of the airfoil surface in an x-z plane
$\vec{\omega}$	vorticity vector

Subscripts

A	pertaining to the airfoil
J	pertaining to the jet
m	average of the values for a parameter on each side of a vortex sheet
O	pertaining to the plane of symmetry (y=0)
p	pertaining to the pressure force on the airfoil
x,y,z	components in a rectangular coordinate system
ξ,η,ζ	components in a coordinate system located on the jet sheet
∞	pertaining to the free stream

Superscripts

+	value of a parameter above the vortex sheet
-	value of a parameter below the vortex sheet
'	pertaining to a source point
*	complex conjugate

pertaining to the point which defines the boundary between the inner and outer regions of the jet sheet, pertaining to a region containing the starting vortex of the system

vector

I. INTRODUCTION

Recent interest in STOL aircraft has stimulated investigations of airfoil configurations employing both powered and unpowered devices for obtaining high lift coefficients and improved stability characteristics at low flight speeds. The practical feasibility of the powered schemes, such as jet flaps, blown flaps, and augmentor wings was greatly enhanced with the advent of high by-pass ratio engines. This provided substantial incentive for obtaining theories capable of predicting induced velocity fields and forces for configurations employing such devices.

A jet flap comprises a thin jet of air exhausting from the trailing edge of the airfoil at an angle to the direction of the freestream (refer to Figure 1). The presence of the jet contributes to the lift of the airfoil in two ways: (1) the aerodynamic field is altered by the jet, increasing the net lifting pressure force on the wing's surface, and (2) the reaction to the momentum flux of the jet contributes to the lift. Two related devices, the blown flap and the augmentor wing are also shown in Figure 1. In the blown flap scheme the high velocity jet is ejected over the upper surface of a mechanical flap utilizing the Coanda effect to direct the jet stream. The augmentor wing employs an ejector system combined with the trailing edge flap design in order to augment the thrust of the primary jet. This latter device develops an increased thrust and also produces smaller nose-down pitching moments than the other devices. The jet flap remains the simplest of the configurations.

One of the first analytic investigations of the jet flap scheme was a two-dimensional theory developed by Spence.[1] This was later extended to handle the three-dimensional problem with limitation to elliptic loadings, constant jet momentum coefficients, and constant jet deflection angles.[2] Several theories seeking to provide more generality have been published. Those of Kerney[3] and Tokuda[4] who employed matched asymptotic expansions to provide a method capable of handling more general wing-flap configurations and the lifting surface theory of Lopez and Shen[5] which offered the further advantage of also providing solutions for augmentor wings and blow flaps are representative. Other theories which have considered the ground effects problem[6] or provided more rapid computation techniques[7] are now available. All of these methods, however, employed approximations inherent in linear theories. That is, all flow angles were assumed to be small. Although it might be expected that such theories should be capable of providing good results for the forces and moments on the airfoil, at least for situations where the jet flap is at a small angle to the free stream, or where the momentum flux is small, the accuracy with which the downwash field could be obtained is open to serious question. In the past few years, two-dimensional theories which accounted for nonlinearities have been reported.[8,9]

Each of the existing theories may adequately account for parts of the overall problem, but none may be expected to be capable of treating the entire spectrum of flight regimes and jet loadings. With low jet loadings and sufficient airspeed, for example, the field induced by the jet may be regarded properly as a small perturbation to the basic aerodynamic field. With higher jet loadings and lower airspeeds, this may not be acceptable. If computation of the downwash field near airframe members such as the tail surface is to be required, along with forces and moments on the wing, additional care in the treatment of the jet is required. And there are regimes of flight demanding yet other factors, such as consideration of the ground plane, be included in the theory.

The analysis described herein is intended to handle the situation where the induced aerodynamic field of the jet is not small in comparison with the normal aerodynamic field of the vehicle. It is to apply to wings with jet flaps of either high or low loadings and offers the additional benefit of improved downwash computations.

Formulation of the complete inviscid, incompressible, three-dimensional jet flap problem is formidable. Even if the thin sheet approximations are employed, it is still necessary to apply a nonlinear boundary condition at the jet boundary, the position of which must be determined in the solution. It is essential, therefore, to employ further simplifications in order to obtain a solution for the nonlinear three-dimensional problem. It was considered important to account for the position of the vorticity associated with the jet, departing substantially from the plane of the airfoil in the flight regime of interest. When rollup of the jet sheet may be neglected, as it is here, it is necessary to introduce either an approximation for the spanwise geometry of the jet or the functional form of the spanwise distribution of vorticity in the jet. The latter offers significant simplification of the theory and was chosen in this theoretical model. The streamwise variation of the deflection of the jet sheet remains to be solved as an important element in the solution. The specific assumptions and approximations made in the present theory, are discussed in Chapter II along with a general discussion of the solution procedure. Chapters III, IV, and V are concerned with the detailed development of the theory. The theory is then applied to a number of situations and compared with a few of the linear theories as well as the experimental results of Williams and Alexander[10] in Chapter VI. Chapter VII concludes with a discussion of the strengths and weaknesses of the theory as well as areas of possible further study.

II. FORMULATION OF THE ANALYTICAL MODEL

A theoretical model attempting to represent the forces, moments, and induced aerodynamic field in the vicinity of an airfoil equipped with a jet flap must represent the jet reasonably well within a few chord lengths of the wing. This was an accepted premise of the analysis. By virtue of the dominant streamwise momentum flux of the jet in the near field, the rolling up process of the streamwise vorticity in the jet sheet plausibly could be neglected in the near field region. But the position of the jet sheet was retained as an important element in the theory even though the precise spanwise geometry would not be represented. It is this feature which primarily distinguishes the present theory from the linear theories. Viscous effects are known to contribute to the induced field of the jet, but they are neglected along with compressibility effects which play a role in the flow within the jet. The entrainment properties of the jet, however, could be added to the theory with little difficulty.

Even neglecting viscous and compressibility effects from the outset in contemplating a theoretical model for a jet flap, an intractable, three-dimensional, inviscid problem in aerodynamic theory remains. It would be necessary to obtain solutions for the flow within the jet (the internal flow problem) and the external aerodynamic field, subject to the pressure (dynamic) and kinematic boundary conditions at the interfaces between the two flows. These interfaces could be expected to be highly convoluted sheets of semi-infinite extent. The geometry of the sheet is not known initially and would have to be obtained as part of the solution. It is essential to introduce further assumptions to obtain a tractable problem with an appropriate reduction as to what may be expected of the theory. Moreover, for the information sought in the analysis (forces and moments on the airfoil and downwash data), a precise solution of the complete inviscid problem would seem unnecessarily detailed and unwarranted.

A. Principal Assumptions

The principal assumptions in the formulation of the analytical model may be outlined conveniently as follows.

1. The flow field is assumed to be inviscid and incompressible. The inviscid approximation, as in most aerodynamic theories, sacrifices the capability of accounting for boundary layer phenomena such as skin friction on the airfoil surface and anticipation of separation phenomena. These phenomena may be treated in a separate manner, given the basic aerodynamic flow field, as in more conventional aerodynamic problems. Two aspects of the inviscid approximation relevant to the jet flow which could be of some importance in the jet flap problem are the viscous entrainment by the jet and the growth of the jet thickness by virtue of mass and momentum exchange with the external flow. The former is likely to be most important. The aerodynamic field induced by viscous entrainment could be accommodated by employing a suitable distribution of sources and sinks in the inviscid model. This is left for possible extension of the present theory. Under the conditions of highly loaded flaps, the contribution should be a small one. Compressibility may be of significance in some parts of the jet flow and possibly in the concentrated vortex cores of the wake. Considering the fact that most of the jet is in a low subsonic flow regime and that the near field is of more importance than the distant wake, compressibility should not exert a significant influence on the results. For higher freestream velocities where the aerodynamic field might be locally compressible, compressibility could possibly be accounted for by employing the Göethert rule.

2. The airfoil and the jet flap are assumed to be symmetric about a plane containing the undisturbed freestream velocity vector. This is an essential part of the analysis; more general geometries would require a much more elaborate analysis.

3. Airfoils equipped with both full span and part span jet flaps with constant jet momentum coefficients and which issue from a straight trailing edge are considered. Variable distributions of the jet momentum coefficient would be admissible in the basic theory, but such situations were not considered in the computations.

4. The thickness of the wing is neglected; however, camber and variations in the wing planform are included. This procedure follows the usual thin airfoil approximation in aerodynamic theory. The resulting force system on the airfoil may later be modified to account for the thickness effects of the airfoil in an approximate manner by employing a modified lift slope as initially used by Spence[1] and discussed in greater detail by Lissaman.[7] Furthermore, such effects also might be represented by a suitable distribution of sources along the surfaces used to denote the airfoil.

5. Several approximations are introduced pertaining to the representation of the jet.

(a) The thickness of the jet is neglected, and the jet momentum coefficient is taken to be constant. Interaction between the jet and the external field then arises solely from the normal force due to pressure differences across the jet sheet. The jet is assumed to have no spanwise component of velocity.

(b) Rollup of the jet sheet at its edges is not considered. This may be of importance for lightly loaded jets, at high freestream velocities, or far enough downstream. For the situations of interest here, however, the rollup is likely to be delayed to a point far enough downstream to be of little influence on the results.

(c) The vorticity associated with the jet is assumed to lie in a sheet generated by a system of straight lines normal to the free stream direction (refer to Figure 2a) and tangent to the actual jet sheet at the plane of symmetry. The position of the stream surface associated with the jet may not be composed of straight line generators, as indicated in Figure 2a, but this arrangement does place the vorticity close to the actual surface, an important factor when the jet lies significantly below the plane of the wing. The small difference between the actual jet sheet and the sheet on which the singularities are placed should not compromise the solution in a serious manner. Similar approximations have met with ample success in conventional aerodynamics.

(d) The lateral (spanwise) distribution of the spanwise component of vorticity in the jet sheet is assumed to be elliptical. This distribution falls to zero at the edges of the jet in the proper manner and greatly simplifies the theory. To be sure, the spanwise distribution in an actual jet will not follow this pattern, but will vary in the streamwise direction leading to concentrated vortex cores far downstream. Nonetheless, in the near field of primary importance, at least, the distribution probably will have a form approximating an elliptical loading.

Moreover, in view of the neglect of the fact that rollup occurs, a plausible assumption of this sort remains consistent with the framework of the balance of the model. It should be observed that employing such an assumption for the spanwise distribution of the vortex strength is tantamount to specifying the lateral geometry of the jet and it is far more effective in simplifying the theory. One or the other must be given if rollup is neglected. In order to provide greater care in modeling the jet while retaining convenient working equations, the former was chosen. The merit of this assumption ultimately may be tested, of course, by comparisons with experimental data.

6. Certain assumptions are made as to the mathematical convergence of the solution procedure. This method amounts to (a) starting with a first approximation for the flowfield of the wing alone from an elementary linear theory, (b) solving the jet problem subject to the freestream and the disturbance field of the wing alone, and (c) employing the jet solution so obtained, together with the undisturbed freestream, as the externally imposed field in a more complete solution for the disturbance field of the wing. If these last results prove unsatisfactory, the procedure may be continued, obtaining a new jet flow, etc. It is assumed this procedure does converge to a solution.

7. In computations involving the influence of the disturbance field of the airfoil, the vorticity in the wake of the wing alone is assumed to lie in the plane of the surface used to represent the airfoil in a manner similar to existing lifting surface theories. For a lightly

loaded wing and in the region close to the airfoil, this vorticity will have a primary effect of distorting the jet sheet laterally. Because this effect is not a primary consideration, and since the influence of the disturbance field of the wing is small compared with that of the free-stream for the jet solution, such a contribution might be reasonably neglected altogether. However, the wake vorticity is retained and treated in the above manner because it does result in simpler equations. A more accurate accounting of the vorticity shed by the wing would add significant complication to the analysis unless some assumptions as to its position could be made *a priori*. That part within the spanwise extent of the jet presumably would follow the jet contour. But that near the wing tips would lie somewhere between the plane of the wing and the location of the jet for an airfoil equipped with a part span jet flap.

B. Mathematical Formulation

The coordinate systems employed in the analysis, along with the principal geometric parameters of concern are illustrated in Figure 2. A right-handed cartesian coordinate system is employed, taking the x-axis along the direction of the freestream velocity, the y-axis along the intersection of the airfoil's trailing edge and the jet, and the z-axis in the vertically upward direction. For some computations in the jet analysis it is convenient to employ an orthogonal, curvilinear coordinate system located within the jet sheet: ξ in the streamwise direction, η in the spanwise direction, and ζ normal to the sheet.

Referring to Figure 2b, the two principal angles are defined in the cross sectional view. The angle of attack (α) is the angle measured from the x-axis to the chord line and the jet deflection angle (τ) from the chord line to a line which is tangent to the jet as it leaves the trailing edge of the airfoil. The notation pertinent to the span lengths and the wing chord are also shown in the figure.

The positions of the physical elements employed in the problem, the jet sheet and the (thin) wing, are shown in bold outline in Figure 2a. The locations of the singularities used to represent these elements are shown in lighter outline. The singularities used to represent the airfoil surface are placed in the $z = 0$ plane in an area corresponding to the planform of the wing. Those for the jet are positioned on a surface tangent to the actual jet sheet in the plane of symmetry (the $y = 0$ plane) having straight line generators (parallel to the y-axis) as already mentioned.

Given a specific wing planform and camber distribution, together with the span length of the jet flap, the necessary parameters for this problem are:

(a) the angle of incidence of the wing (α)

(b) the freestream velocity (U_∞)

(c) the angle of deflection of the jet (τ), and

(d) the jet momentum coefficient (C_J).

The objective of the analysis, then, is to obtain results for the forces and moments on the airfoil, and the velocity field at points of interest with respect to the airframe design (e.g., the downwash in the vicinity of tail surfaces).

1. General Relations

Within the framework of the assumptions discussed above, the analytical problem amounts to one of the Neumann type in potential theory. The flow is everywhere irrotational and solenoidal* giving rise to a representation of the field in terms of a scalar potential. The normal derivative of the scalar potential on the airfoil and on the jet sheet must be zero; these are stream surfaces. The great difficulty of the problem arises from the fact that the position of the jet sheet is not known initially and must be determined in the solution. This requires matching the pressure difference across the sheet with the normal acceleration of an element of fluid in the jet (dynamic condition).

The relations required in the theory may be obtained from the Fundamental Theorem of Vector Analysis (Helmholtz's Theorem)[11,12]. Referring to Figure 3a, consider for the moment a closed, singly connected domain surrounding the wing and jet and containing both (the domain envisioned here is large enough to contain even the starting vortex of the system). Define the perturbation velocity $\vec{v}$ in the usual manner

$$\vec{v} = \vec{V} - U_\infty \vec{e}_x$$

where $\vec{V}$ is the complete velocity vector. Then

$$\vec{v} = -\nabla\phi + \nabla \times \vec{A}$$

---

*excluding the singular surfaces representing the wing and the jet.

where

$$\phi(\vec{x}) = \frac{1}{4\pi} \iiint \frac{\nabla' \cdot \vec{v}'}{R} d\hat{T}'$$

$$\vec{A}(\vec{x}) = \frac{1}{4\pi} \iiint \frac{\nabla' \times \vec{v}'}{R} d\hat{T}'$$

and

$$R = |\vec{R}| = \sqrt{(x-x')^2 + (y-y')^2 + (z-z')^2}$$

In these relations, integration is with respect to the source coordinates $(\vec{x}')$ and the potentials ϕ and $\vec{A}$ are functions of the field point $\vec{x}$. Combining the above equations a general relation may be obtained for the vector $\vec{v}$[13]

$$\vec{v}(\vec{x}) = \frac{1}{4\pi} \left[\iiint (\nabla' \cdot \vec{v}') \frac{\vec{R}}{R^3} d\hat{T}' - \iint (\vec{v}' \cdot \vec{n}') \frac{\vec{R}}{R^3} d\hat{S}' + \right.$$

$$\left. \iiint (\nabla' \times \vec{v}') \times \frac{\vec{R}}{R^3} d\hat{T}' + \iint (\vec{v}' \times \vec{n}') \times \frac{\vec{R}}{R^3} d\hat{S}' \right] \tag{1}$$

$\hat{S}$ represents the surface bounding the region $\hat{T}$ and $\vec{n}$ represents the unit outward normal of $\hat{S}$.

The vector field of concern is solenoidal ($\nabla \cdot \vec{v} = 0$ everywhere); therefore, the first term of Equation (1) is zero. For a domain $\hat{T}$ large enough, $\vec{v}$ is zero at every point on the surface $\hat{S}$. Then the vector field is entirely given within the domain as

$$\vec{v}(\vec{x}) = \frac{1}{4\pi} \iiint \frac{(\nabla' \times \vec{v}') \times \vec{R}}{R^3} d\hat{T}' \tag{2}$$

This situation, of course, is not quite what is needed for the problem at hand. Rather, one is interested in a part of the domain in which the flow and jet geometry are stationary in time, a domain contained within the one described above and far enough removed from the time varying starting vortex region so as not to be influenced by it (refer again to Figure 3a). From the foregoing discussion, it should be clear that the velocity at a point of interest within the inner domain will be determined as the sum of two integrals of the form of Equation (2): one over the inner domain and one over its complement. Since these regions may be chosen for our purposes to be as large as desired, the contribution of the second integral to field points of interest within the inner domain (not too near the intersection of the jet sheet with the boundary of the domain) can be made small enough to be inconsequential in the analysis. Equation (2), then, may be written as

$$\vec{v}(\vec{x}) = \frac{1}{4\pi} \iiint \frac{(\nabla' \times \vec{v}') \times \vec{R}}{R^3} \, d\tau'$$

Now, the vorticity in the domain of interest is assumed to be concentrated in the form of vortex sheets.[14] These singular sheets are related to the actual distributed vorticity regions by introducing the vortex strength of the sheet, $\vec{\gamma}$, such that (refer to Figure 3b)

$$\lim_{\substack{t \to 0 \\ \vec{\omega} \to \infty}} \vec{\omega} \, t \, dS = \vec{\gamma} \, dS$$

where $\vec{\omega}$ is the vorticity vector ($\vec{\omega} = \nabla \times \vec{v}$) and the element of area S lies in a vortex region of thickness t. It may be shown[14,15] that the strength of the vortex sheet is related to the vector difference of velocities on either side of the sheet

$$\vec{\gamma} \times \vec{n} = \Delta \vec{v} = (\vec{v}^{+} - \vec{v}^{-}) \tag{3}$$

where $\vec{n}$ is a unit normal to the sheet and $\vec{v}^{+}$ ($\vec{v}^{-}$) is the velocity vector above (below) the sheet. Employing the definition of $\vec{\gamma}$, the velocity field $\vec{v}(\vec{x})$ may now be expressed in the form

$$\vec{v}(\vec{x}) = \frac{1}{4\pi} \iint \frac{\vec{\gamma}' \times \vec{R}}{R^3} dS' \tag{4}$$

where S now represents the totality of vortex sheets within the domain of interest. Equation (4) is the starting point of this analysis as it is for most other problems in aerodynamics.

The problem now is to determine the vortex strength distribution on these sheets so that the flow is everywhere tangent to them. Suppose for the moment the sheet positions may be described in the form

$$f(x, y) - z = 0$$

The kinematic condition of tangency then becomes

$$\vec{V} \cdot \nabla (f - z) = 0$$

or

$$(U_\infty + u)\frac{\partial f}{\partial x} + v\frac{\partial f}{\partial y} - w = 0 \tag{5}$$

Furthermore, since $\vec{\gamma}$ must be solenoidal and since by definition it lies in the vortex sheet, it has only one independent component. Equations (4) and (5) then provide four equations for the variables u, v, w and, say, γ_y. If the positions of the vortex sheets were known, then, by substitution of Equation (4) for u, v, and w, along with a relation between γ_x and γ_y obtained from the solenoidal character of $\vec{\gamma}$, into Equation (5), a single integral equation over a two-dimensional sheet results for the determination of γ_y. In view of the assumption to be made as to the spanwise distribution of vorticity, the condition given by Equation (5) may be met at the plane of symmetry where the sheet of singularities and the stream surface of the jet coincide. Application of Equation (5), starting at the trailing edge of the airfoil, may then yield the form of the actual jet sheet at points not in the plane of symmetry. This will not, in general, coincide with the sheet of singularities representing the vorticity of the jet (refer to Figure 2).

The location of the vortex sheet associated with the jet unfortunately is not known initially. Moreover, the jet sheet must be positioned such that the pressure force acting on it balances the local normal acceleration of the flow within the jet. This <u>dynamical condition</u>, then, provides the necessary additional relation for the determination of the position of the jet sheet.

Consider a jet sheet generated by straight lines such that it has only one finite curvature and with its normal vectors lying in planes parallel to the x-z plane. Applying the momentum theorem of fluid mechanics to an element of the jet sheet, it may be shown[2] simply that

$$\kappa = \frac{p^- - p^+}{J}$$

where κ represents the curvature of the jet sheet, p^+ (p^-) is the pressure above (below) the sheet, and J is the momentum flux of the jet per unit length of span. This relation may be placed in a more suitable form as follows. By employing Bernoulli's equation along with Equation (3) the pressure difference across the jet may be written

$$\Delta p = p^+ - p^- = -\frac{1}{2}\rho\ (V^{+2} - V^{-2}) = -\rho\ (\vec{\gamma} \times \vec{n}) \cdot \vec{V}_m$$

where

$$\vec{V}_m \equiv \frac{1}{2}(\vec{V}^+ + \vec{V}^-)$$

is the mean velocity at a point located on the jet sheet. Utilizing the definition of the jet momentum coefficient[2]

$$C_J \equiv \frac{J}{\frac{1}{2}\rho\ U_\infty^2\ c}$$

the dynamic condition may be written in the form

$$\kappa = \frac{2\ (\vec{\gamma} \times \vec{n}) \cdot \vec{V}_m}{C_J\ U_\infty^2\ c} \tag{6}$$

By definition, the curvature is related to the geometry of the jet sheet under consideration through the relation

$$\kappa = \frac{\left|\frac{d^2f}{dx^2}\right|}{\left[1 + \left(\frac{df}{dx}\right)^2\right]^{3/2}}$$

where the surface in question is given by the relation

$$f(x) - z = 0$$

This form of the dynamical condition is to be satisfied at points on the jet sheet in the plane of symmetry where the jet sheet coincides with the sheet of singularities representing the jet vorticity. This condition is not met strictly at any other point on the jet sheet, of course, within the approximations involved in the analysis. This is again a consequence of the neglect of rollup in the theory.

Equations (4), (5), and (6) provide the basic relations from which the vortex strength distribution and the position of the jet sheet may be determined. An iterative procedure was adopted for that purpose in the analysis.

2. Method of Solution

The solution procedure adopted for the analysis is most conveniently presented by considering the perturbation velocity field on the airfoil and the jet separately. Employing equation (4) the required relations may be expressed as

$$\vec{v}(\vec{x}_J) = \frac{1}{4\pi}\iint_{S_A} \frac{\vec{\gamma}' \times \vec{R}}{R^3}\, dS' + \frac{1}{4\pi}\iint_{S_J} \frac{\vec{\gamma}' \times \vec{R}}{R^3}\, dS' \tag{7}$$

$$\vec{v}(\vec{x}_A) = \frac{1}{4\pi}\iint_{S_A} \frac{\vec{\gamma}' \times \vec{R}}{R^3}\, dS' + \frac{1}{4\pi}\iint_{S_J} \frac{\vec{\gamma}' \times \vec{R}}{R^3}\, dS' \tag{8}$$

where the subscript J (A) refers to the jet (airfoil). Equations (7) and (8) provide a set of coupled equations for the vortex strengths on the airfoil and the jet. They are analogous in some respect to the bi-plane[16] problem. In choosing a method of solution for this problem, it is helpful to keep in mind the physical conditions of primary interest. The influence of the disturbances produced by the wing on the jet (represented by the first surface integral in Equation (7)) may be expected to be small compared with the interaction of the jet and the freestream for the flight conditions of interest, whereas the reverse is not true. The jet induced disturbances (represented by the second surface integral of Equation (8)) should have a significant influence on the wing field for a highly loaded jet.

A solution for this set of equations may be obtained as follows.

(a) A solution for the wing alone is obtained as a first approximation for the use of modeling the influence of the wing on the jet in Equation (7). This may be as simple as a lifting line approximation or a more detailed solution if readily available.

(b) A solution for the jet is obtained subject to the influence of the combined fields of the wing and the freestream. This solution comprises obtaining the distribution of the vortex strength along the jet and the position of the jet sheet.

(c) The jet solution and the freestream are taken as a new imposed field for a detailed solution of the wing problem. The solution procedure employed herein is of the lifting surface type.

Given these results, the forces and moments on the wing may be obtained by direct integration, and the velocity field at points of interest in the vicinity of the wing or jet may be computed as needed. Should the results for the last wing solution prove inaccurate, it is possible to employ that solution as a new initial approximation and repeat the entire procedure.

The analysis of the jet subject to the influence of the freestream and the disturbance field of the airfoil may be referred to here as the jet problem. That of determining the aerodynamic field of the wing subject to the freestream and the field of the jet may be termed the airfoil problem in the following treatment.

3. Working Equations

A solution for the jet problem requires determination of the distribution of vortex strength ($\vec{\gamma}_J$) on the jet sheet as well as the location of the jet in the plane of symmetry ($z = f_J(x,0)$). For a given f_J, obtained either by an initial assumption or from the results of a previous iterate, the vortex strength may be determined by satisfying the kinematic condition,

$$[U_\infty \vec{e}_x + \vec{v}(x,0,f_J)] \cdot \nabla (f_J - z) = 0 \tag{9}$$

where

$$\vec{v}(\vec{x}) = \vec{v}_A + \frac{1}{4\pi} \iint_{S_J} \frac{\vec{\gamma}_J' \times \vec{R}}{R^3} dS_J' \tag{10}$$

and $\vec{v}_A$ accounts for the influence of the downwash field created by the airfoil on the jet. The proper solution is one which also satisfies the dynamic condition

$$\kappa = \frac{2 \, (\vec{\gamma}_J \times \vec{n}_J) \cdot \vec{V}_m}{C_J \, U_\infty^2 \, c} \tag{11}$$

An iterative procedure is adopted for varying $f_J(x)$ so that Equation (11) is met in the solution, along with Equations (9) and (10).

In a similar manner for the airfoil problem, a solution for the vortex strength distribution of the airfoil ($\vec{\gamma}_A$) may be found by applying the kinematic condition

$$(U_\infty \vec{e}_x + \vec{v}) \cdot \nabla \, (f_A - z) = 0 \tag{12}$$

where

$$\vec{v}(\vec{x}) = \frac{1}{4\pi} \iint_{S_A} \frac{\vec{\gamma}_A' \times \vec{R}}{R^3} dS_A' + \vec{v}_J \tag{13}$$

to the location of the projection of the airfoil on the z = 0 plane. In the above equations

$$f_A \, (x,y) - z = 0$$

represents the surface of the airfoil and $\vec{v}_J$ accounts for the downwash field created by the jet on the airfoil.

III. JET ANALYSIS

Consider now the problem of determining the vortex strength distribution and the location of the jet sheet, subject to the influence of both the freestream and the disturbance field created by the airfoil. For present considerations, the field induced by the airfoil will be assumed to be known.

Recalling the curvilinear coordinate system (ξ,η) located in the jet sheet, the vortex strength distribution associated with the jet may be expressed as

$$\vec{\gamma}_J(\xi,\eta) = \gamma_{J\xi}\,\vec{e}_\xi + \gamma_{J\eta}\,\vec{e}_\eta$$

Since the vorticity field is solenoidal, $\gamma_{J\xi}$ and $\gamma_{J\eta}$ are related through the relation

$$\frac{\partial\,\gamma_{J\xi}}{\partial\xi} + \frac{\partial\,\gamma_{J\eta}}{\partial\eta} = 0$$

or

$$\gamma_{J\eta} = -\int_{-s_J}^{\eta} \frac{\partial\,\gamma'_{J\xi}}{\partial\xi}\,d\eta'$$

The assumption that the spanwise distribution of loading on the jet has the same functional form at all streamwise positions along the jet implies that the components of the vortex strength may be represented in terms of products of the form

$$\gamma_{J\xi} = G(\xi)\, H(\eta) \tag{14}$$

then

$$\gamma_{J\eta} = - \frac{\partial G}{\partial \xi} \int_{-s_J}^{\eta} H(\eta')\, d\eta'$$

Defining

$$h(\eta) \equiv \int_{-s_J}^{\eta} H(\eta')\, d\eta'$$

the equation for $\gamma_{J\eta}$ may be written

$$\gamma_{J\eta} = - \frac{\partial\, G(\xi)}{\partial \xi}\, h(\eta) \tag{15}$$

If the loading on the jet is to be elliptic, as discussed earlier,

$$h(\eta) = \sqrt{1 - (\eta/s_J)^2}$$

and then

$$H(\eta) = \frac{-\,\eta/s_J^2}{\sqrt{1 - (\eta/s_J)^2}}$$

The choice of an elliptic loading provides the primary advantage of simplifying some of the integrals in the subsequent elements of the theory, and does have the proper characteristics at the edges of the jet.

A. Integro-Differential Equations for the Jet Problem

1. Analytical Relations

Recall first the relations given by Equations (9) to (11)

$$\vec{V}\,(\vec{x}) = U_\infty\,\vec{e}_x + \vec{v}_A + \frac{1}{4\pi}\iint_{S_J} \frac{\vec{\gamma}_J{}' \times \vec{R}}{R^3}\,dS' \tag{16}$$

$$(U_\infty + u)\,\frac{df_J}{dx} - w = 0 \tag{17}$$

$$\kappa = \frac{\left|\dfrac{d^2 f_J}{dx^2}\right|}{\left[1 + \left(\dfrac{df_J}{dx}\right)^2\right]^{3/2}} = \frac{2\,(\vec{\gamma}_J \times \vec{n}_J)\cdot\vec{V}_m}{C_J\,U_\infty^{\,2}\,c} \tag{18}$$

where these relations all pertain to field points located on the jet sheet in the plane of symmetry $(y = 0)$. Then

$$\vec{V}\Big|_{y=0} = (U_\infty + u)\,\vec{e}_x + w\,\vec{e}_z$$

since $v = 0$ in this plane. And

$$\vec{V}_m = \frac{\vec{V}^+ + \vec{V}^-}{2}$$

It has been determined that integrations carried out with respect to x and y rather than ξ and η are most convenient. The cartesian parameters involved may be expressed as

$$\gamma_{Jx} = \gamma_{J\xi} \cos\theta = \gamma_{J\xi} \Big/ \left[1 + \left(\frac{df_J}{dx}\right)^2\right]^{1/2} \tag{19}$$

$$\gamma_{Jy} = \gamma_{J\eta} \tag{20}$$

$$\gamma_{Jz} = \gamma_{J\xi} \sin\theta = \gamma_{J\xi} \frac{df_J}{dx} \Big/ \left[1 + \left(\frac{df_J}{dx}\right)^2\right]^{1/2} \tag{21}$$

$$dS_J' = d\xi' \, d\eta' = \sec\theta' \, dx' \, dy'$$

$$(\vec{\gamma}_J' \times \vec{R})_x = \gamma_{Jy}' \, (z - f_J') - \gamma_{Jz}' \, (y - y')$$

$$(\vec{\gamma}_J' \times \vec{R})_z = \gamma_{Jx}' \, (y - y') - \gamma_{Jy}' (x - x')$$

where $R = \{[x - x']^2 + [y - y']^2 + [z - f_J \, (x')]^2\}^{1/2}$

and, referring to Figure 3

$$\sec\theta = \sqrt{1 + \left(\frac{df_J}{dx}\right)^2}$$

Then the components of Equation (16) take the form

$$u(x,0,z) = u_A(x,0,z) + \frac{1}{4\pi} \int_{-s_J}^{s_J} \int_0^{\infty} \frac{\gamma_{Jy}' (z - f_J) + \gamma_{Jz}' \, y'}{R^3} \sec\theta' \, dx' \, dy' \tag{22}$$

$$w(x,0,z) = w_A(x,0,z) + \frac{1}{4\pi} \int_{-s_J}^{s_J} \int_0^{\infty} \frac{-\gamma_{Jx}' \, y' - \gamma_{Jy}' \, (x - x')}{R^3} \sec\theta' \, dx' \, dy' \tag{23}$$

Introducing Equations (14) and (15) for $\gamma_{J\xi}$ and $\gamma_{J\eta}$ into Equations (19) through (21),

$$\gamma_{Jx} = G\,H \Big/ \left[1 + \left(\frac{df_J}{dx}\right)^2\right]^{1/2}$$

$$\gamma_{Jy} = -\frac{dG}{d\xi}\,h$$

$$\gamma_{Jz} = G\,H\,\frac{df_J}{dx} \Big/ \left[1 + \left(\frac{df_J}{dx}\right)^2\right]^{1/2}$$

and let

$$g(x) = G\,[\xi(x,f_J)]$$

Then since $\frac{dG}{d\xi} = \frac{dg}{dx}\frac{dx}{d\xi} = \frac{dg}{dx}\cos\theta$, Equations (22) and (23) may be written

$$u(x,0,z) = u_A(x,0,z) - \frac{1}{4\pi}\int_0^\infty \frac{dg'}{dx'}(z - f_J')\,dx' \int_{-s_J}^{s_J} \frac{h'\,dy'}{R^3} +$$

$$\frac{1}{4\pi}\int_0^\infty g'\,\frac{df_J'}{dx'}\,dx' \int_{-s_J}^{s_J} \frac{y'\,H'\,dy'}{R^3} \qquad (24)$$

and

$$w(x,0,z) = w_A(x,0,z) - \frac{1}{4\pi} \int_0^{\infty} g' \, dx' \int_{-s_J}^{s_J} \frac{y' \, H' \, dy'}{R^3} +$$

$$\frac{1}{4\pi} \int_0^{\infty} \frac{dg'}{dx'} (x - x') \, dx' \int_{-s_J}^{s_J} \frac{h' \, dy'}{R^3} \tag{25}$$

The integrals with respect to y' may be evaluated directly (refer to Appendix A) to yield

$$u(x,0,z) = u_A(x,0,z) - \frac{1}{2\pi s_J^{\,2}} \int_0^{\infty} \left[g' \frac{df_J'}{dx'} k_J [K(k_J) - E(k_J)] + \right.$$

$$\left. \frac{dg'}{dx'} (z - f_J') \frac{k_J}{k_{cJ}^2} [E(k_J) - k_{cJ}^2 K(k_J)] \right] dx' \tag{26}$$

$$w(x,0,z) = w_A(x,0,z) + \frac{1}{2\pi s_J^{\,2}} \int_0^{\infty} \left[g' k_J \, [K(k_J) - E(k_J)] + \right.$$

$$\left. \frac{dg'}{dx'} (x - x') \frac{k_J}{k_{cJ}^2} [E(k_J) - k_{cJ}^2 K(k_J)] \right] dx' \tag{27}$$

where

$$k_J^2 = \frac{s_J^{\,2}}{s_J^{\,2} + (x - x')^2 + (z - f_J')^2} \tag{28}$$

$$k_J^{\,2} + k_{cJ}^{\,2} = 1$$

and K, E are the complete elliptic integrals of the first and second kinds, respectively, with modulus k.

The dynamical condition given by Equation (18) may be written in the form

$$\kappa = \frac{-2\,\frac{dg}{dx}\,[U_m(x,0,f_J) - \left|\frac{df_J}{dx}\right| W_m(x,0,f_J)]}{C_J\, U_\infty^2\, c \left[1 + \left(\frac{df_J}{dx}\right)^2\right]} \tag{29}$$

since, in the plane of symmetry

$$(\vec{\gamma} \times \vec{n}) \cdot \vec{V}_m = \frac{-\frac{dg}{dx}\,[U_m(x,0,f_J) - \left|\frac{df_J}{dx}\right| W_m(x,0,f_J)]}{1 + \left(\frac{df_J}{dx}\right)^2}$$

where

$$U_m = \frac{1}{2}\,(U^+ + U^-)$$

and

$$W_m = \frac{1}{2}\,(W^+ + W^-)$$

as discussed previously.

The kinematic condition, Equation (17), may be written simply as

$$[U_\infty + u(x,0,f_J)]\,\frac{df_J}{dx} - w(x,0,f_J) = 0 \tag{30}$$

Equations (29) and (30), with u and w substituted from Equations (26) and (27) represent a pair of nonlinear integro-differential equations for $f_J(x)$ and $g(x)$. The jet location and slope are known at $x = 0$. The function g must display the proper behavior; that is $\frac{dg}{dx}$ must vanish at infinity as well as having a logarithmic singularity at the origin of the jet. This system of equations is to be solved numerically for these functions.

2. Forms of the Equations for Numerical Solution

The method adopted here for the solution of the equations discussed in the previous section is related to the integral methods of fluid mechanics.[17,18,19] The functions f_J and g are represented by truncated series with coefficients to be determined in the solution. These functions are chosen to give the proper behavior for large x and to meet the appropriate boundary conditions. The semi-infinite domain, $0 \leq x \leq \infty$, is divided into two regions, a near field $0 \leq x \leq \hat{x}$ and a far field extending beyond $\hat{x}$. The functional representations in the near field are of primary concern here. Those in the far field were chosen to facilitate integration in that domain; the choice there is not particularly critical in the solution since contributions to the integrals from that region are small if $\hat{x}$ is large enough. Choices for $\hat{x}$ in the computations of 5 to 10 wing chord lengths were found to yield satisfactory results. The optimum choice depends on the parameters of the problem, such as C_J. This subject will be discussed further in connection with the computational results.

It may be anticipated that γ_{Jy} will decrease monotonically with increasing x, as it must ultimately approach zero. Moreover, the function dg/dx should display a logarithmic singularity at the origin as suggested by the two-dimensional theory of Spence.[1] The choice made in this analysis is a series of exponentials such that

$$\frac{dg}{dx} = \sum_{n=1}^{N} C_n \frac{dg_n}{dx} = - \sum_{n=1}^{N-1} C_n\, n \exp\left(-\frac{n\beta x}{s_J}\right) + C_N \frac{\ln(x/s_J)}{\left(\frac{x}{s_J} + 1\right)^{3/2}} \tag{31}$$

so that

$$g = \sum_{n=1}^{N} C_n g_n = \sum_{n=1}^{N-1} C_n \frac{s_J}{\beta}\left[\exp\left(-\frac{n\beta x}{s_J}\right) - 1\right] + 2s_J C_N \left[\ln \frac{\sqrt{x/s_J + 1} - 1}{\sqrt{x/s_J + 1} + 1} - \frac{\ln(x/s_J)}{\sqrt{x/s_J + 1}} + 2 \ln 2\right] \tag{32}$$

The factor β is a parameter chosen along with $\hat{x}$ for a particular problem to best represent the function over the near field domain. A value of β between unity and 10 appeared to be suitable for most of the computations attempted. This functional representation is retained in the computations extending from $x = \hat{x}$ to infinity as well as in the near field region.

The function $f_J(x)$ was chosen to have the form

$$\frac{f_J}{s_J} = \frac{1}{\nu}\left[a_{-1}\,(\bar{x} + 1) + a_0 + \frac{a_1}{(\bar{x} + 1)} + \dots + \frac{a_M}{(\bar{x} + 1)^M}\right] \tag{33}$$

where $\bar{x} = \nu x/s_J$ and ν is a scale factor. Values of ν found to yield acceptable results in the computations attempted were in a range from 1 to 10. Since the jet passes through the origin, it is required that

$$\sum_{m=-1}^{M} a_m = 0 \tag{34}$$

Employing Equation (33), the slope given by

$$\frac{\nu}{s_J} \frac{df_J}{dx} = a_{-1} - \frac{a_1}{(\bar{x} + 1)^2} - \frac{2a_2}{(\bar{x} + 1)^3} - \cdots - \frac{M\, a_M}{(\bar{x} + 1)^{M+1}} \tag{35}$$

must agree with that specified in the problem at $x = 0$. Thus

$$\frac{\nu}{s_J} \left.\frac{df_J}{d\bar{x}}\right|_{x = 0} = a_{-1} - \sum_{m=1}^{M} m\, a_m = - \tan (\tau + a) \tag{36}$$

There remain M free coefficients in the function to be determined in the solution.

Now, while the form of Equation (33) was employed for the jet in the near field region $x \leq \hat{x}$, it was not employed to represent the jet for $x > \hat{x}$. There the jet sheet was taken simply to have a constant slope, matching the value of the near field function at $x = \hat{x}$. This representation is not precise, of course, but simplifies the integrals considerably and should not seriously detract from the merit of the solution. Considering the inviscid problem, where the sheet would be allowed to roll up, the resulting trailing vortex pair would have a constant slope, apart from viscous interactions.

Given the above functional forms for g and f_J, the final forms of the equations discussed in Section 1 may be written as

$$[U_\infty + u(x,0,f_J)] \frac{df_J}{dx} - w(x,0,f_J) = 0 \tag{37}$$

$$\kappa(x) = \frac{2\ [U_\infty + u(x,0,f_J) - \left|\frac{df_J}{dx}\right| w(x,0,f_J)]}{C_J\ U_\infty^2\ c\left[1 + \left(\frac{df_J}{dx}\right)^2\right]} \left[\sum_{n=1}^{N-1} C_n\ n \exp\left(-\frac{n\beta x}{s_J}\right) - C_N \frac{\ln(x/s_J)}{(x/s_J + 1)^{3/2}}\right]. \tag{38}$$

$$u(x,0,z) = u_A(x,0,z) - \frac{1}{2\pi\ s_J^2} \sum_{n=1}^{N} C_n \int_0^\infty \left[g_n' \frac{df_J'}{dx'} k_J(K - E) + \frac{dg_n'}{dx'} (z - f_J') \frac{k_J}{k_{cJ}^2} (E - k_{cJ}^2\ K)\right] dx' \tag{39}$$

$$w(x,0,z) = w_A(x,0,z) + \frac{1}{2\pi\ s_J^2} \sum_{n=1}^{N} C_n \int_0^\infty \left[g_n'\ k_J\ (K - E) + \frac{dg_n'}{dx'} (x - x') \frac{k_J}{k_{cJ}^2} (E - k_{cJ}^2\ K)\right] dx' \tag{40}$$

and

$$\kappa = \frac{\left|\frac{d^2 f_J}{dx^2}\right|}{\left[1 + \left(\frac{df_J}{dx}\right)^2\right]^{3/2}} \tag{41}$$

where U_m, W_m in Equation (29) are now given simply by U,W with the understanding that these are the values computed excluding a suitably small region in the vicinity of x in the integrals of Equations (39) and (40).*

B. Method of Solution

Equations (37) and (38), upon substitution of u, w and κ from Equations (39), (40) and (41) comprise a pair of integro-differential equations for the functions f_J and g. Employing the approximate forms for f_J and g, these equations become a pair of algebraic equations for the M + N coefficients in the solution. With a finite number of terms, M + N here, it is not possible, of course, to satisfy these equations at all points in the semi-infinite region $0 \leq x < \infty$. The equations could be satisfied exactly only at $\frac{1}{2}$ (M + N) points at most. Rather than requiring the equations to be met precisely at the $\frac{1}{2}$ (M + N) points, it is advisable to meet the relations in a broader sense over the domain. This is accomplished in the analysis by requiring the equations to be satisfied in a least squares sense over the near field domain $0 \leq x \leq \hat{x}$, subject to values at a larger number of points.

The numerical analysis employs a set of control points spanning the near field domain $0 \leq x \leq \hat{x}$. The number of such points is chosen to

*A region small enough such that its contribution to $U_m = \frac{U^+ + U^-}{2}$ is negligible.

be several times the value $\frac{1}{2}$ (M + N) such that the least squares method will yield smooth functions f_J and g, and so that information of the necessary resolution within the domain is represented.

The procedure employed for the solution is an iterative one. It may be outlined as follows.

(a) A trial function $\kappa(x)$ is first chosen. κ is employed as the primary representation of the jet rather than f_J, because it is of primary importance in the dynamical condition and it is more sensitive than f_J or df_J/dx. Employing κ at the control points, a first integral obtained numerically yields df_J/dx at the control points. These values are employed to find coefficients in the expression for f_J which yield a least squares fit for df_J/dx. f_J and df_J/dx are then evaluated from this function at the points employed in obtaining the necessary integrals.

(b) These values for f_J and df_J/dx are employed to calculate the coefficients of the C_n in Equations (39) and (40) at each control point. Substituting the results into Equation (38), the dynamical condition, the C_n values are obtained so as to meet that condition in a least squares sense over the domain.

(c) Finally, new values for df_J/dx are obtained at the control points through Equation (37). The curvature corresponding to this new distribution of df_J/dx is then estimated. These are compared with the starting values and a new iterate $\kappa(x)$

is generated. When $\kappa(x)$ values obtained in two successive iterates agree within a given error bound a solution is formally obtained for the problem.

The scheme described above is not the only one possible, but it is stable and converges rapidly. It would be possible, for example, to employ the linear tangency condition in step (b) rather than the dynamical condition, for evaluating the C_n. Then the dynamical condition would yield the new κ iterate directly. It was found that this method is not always stable. Halsey[9] found similar results in a two-dimensional theory.

IV. NUMERICAL ASPECTS OF THE JET PROBLEM

The integrals to be evaluated numerically in the analysis require careful attention in several respects. They are discussed together with the numerical integration scheme in this chapter. The relations employed for evaluating the coefficients C_n in step (b) of the iteration scheme are then summarized. A description of a method of evaluation for the starting values and the new jet function is then given followed by a discussion of the procedure adopted for generating a new iterate $\kappa(x)$.

A. Evaluation of the Integrals

The complexity of the integrals involved in the equations for the velocity field requires that they be computed numerically. Three difficulties arise in this connection:

1. singularity of terms in the integrand at $x' = x$, the control point

2. infinite upper bound

3. singularity at the origin caused by the logarithmic term in the vortex strength expansion

1. Singularity at the Control Point

At the point $x' = x$, the modulus of the complete elliptic integrals (k_J) becomes unity and the elliptic integral of the first kind becomes infinite. This presents the problem of numerically integrating through a point in which some of the terms of the integrand are singular. Of course, the integral is finite. It is possible to circumvent this difficulty by applying the identities

$$\frac{z - f_J'}{k_{cJ}^2} = \frac{1}{k_J^2} \frac{\frac{z - f_J'}{x - x'}}{1 + \left(\frac{z - f_J'}{x - x'}\right)^2} \frac{s_J^2}{x - x'} \tag{42}$$

$$\frac{x - x'}{k_{cJ}^2} = \frac{1}{k_J^2} \frac{1}{1 + \left(\frac{z - f_J'}{x - x'}\right)^2} \frac{s_J^2}{x - x'} \tag{43}$$

$$k_J = \frac{k_{cJ}}{\left[1 + \left(\frac{z - f_J'}{x - x'}\right)^2\right]^{1/2}} \frac{s_J}{x - x'} \tag{44}$$

Inserting Equations (42) through (44) into the integrals under consideration results in the expressions

$$u(x,0,f_J) = u_A(x,0,f_J) - \frac{1}{2\pi}\sum_{n=1}^{N} C_n \int \left[\frac{g_n'}{s_J} \frac{df_J'}{dx'} \frac{k_{cJ}\,(K - E)}{\left[1 + \left(\frac{z - f_J'}{x - x'}\right)^2\right]^{1/2}} + \right.$$

$$\left. \frac{dg_n'}{dx'} \frac{z - f_J'}{x - x'} \frac{1}{k_J} \frac{E - k_{cJ}^2 K}{1 + \left(\frac{z - f_J'}{x - x'}\right)^2} \right] \frac{dx'}{x - x'} \qquad (45)$$

and

$$w(x,0,f_J) = w_A(x,0,f_J) + \frac{1}{2\pi}\sum_{n=1}^{N} C_n \int \left[\frac{g_n'}{s_J} \frac{k_{cJ}\,(K - E)}{\left[1 + \left(\frac{z - f_J'}{x - x'}\right)^2\right]^{1/2}} + \right.$$

$$\left. \frac{dg_n'}{dx'} \frac{1}{k_J} \frac{E - k_{cJ}^2 K}{1 + \left(\frac{z - f_J'}{x - x'}\right)^2} \right] \frac{dx'}{x - x'} \qquad (46)$$

Since

$$\lim_{k \to 1} k_c\,(K - E) \to 0$$

$$\lim_{k \to 1} \frac{E - k_c^2 K}{k} \to 1$$

and

$$\lim_{x \to x'} \frac{z - f_J'}{x - x'} \to \left[\frac{df_J'}{dx'}\right]_{x'=x}$$

the expressions within the braces of Equations (45) and (46) are continuous and non-singular in a small neighborhood of the control point ($x' = x$). These terms are plotted in Figure 4 as f_1 and f_2, respectively.

The associated integrals may be written as Cauchy principal values,

$$\oint_{x-\varepsilon_1}^{x+\varepsilon_2} \frac{f_i(x')}{x - x'}\, dx' \qquad ; i = 1,2$$

in a neighborhood of $x' = x$. It is then possible to expand $f_i(x')$ in powers of $(x - x')$ within this neighborhood and to perform the integration analytically. By choosing ε_1 and ε_2 to be small enough, this expansion may be truncated to fourth order in $(x - x')$ without loss of accuracy (refer to Appendix F). In any event the contribution of this element to the total integral is extremely small.

2. Infinite Upper Limit

The problem of numerically integrating to infinity may be removed by employing a change in variables. A natural candidate for this task is the modulus of the ellpitic integrals k_J. From Equation (28) it can be seen that

$$dx' = \frac{s_J^{\,2}}{(x - x') + \frac{df_J'}{dx'}(z - f_J')} \frac{dk_J}{k_J^{\,3}} \tag{47}$$

By employing Equation (47) an integral over the range $\hat{x} \leq x' \leq \infty$ may be transformed into an integral with respect to k_J over the internal $\hat{k}_J \leq k_J \leq 0$ where $\hat{k}_J = k_J(\hat{x})$. For example

$$\int_{\hat{x}}^{\infty} \left[\frac{g_n'}{s_J} \frac{df_J'}{dx'} k_J \,(K-E) + \frac{dg_n'}{dx'} (z-f_J') \frac{k_J}{k_{cJ}^2} (E-k_{cJ}^2 K)\right] dx' =$$

$$s_J \int_{\hat{k}_J}^{0} \left[\frac{g_n'}{x-x'} \frac{df_J'}{dx'} \frac{K-E}{k_J^2} + \frac{dg_n'}{dx'} \frac{z-f_J'}{x-x'} \frac{E-k_{cJ}^2 K}{k_J^2 k_{cJ}^2}\right] \frac{dk_J}{1 + \frac{df_J'}{dx'}\left(\frac{z-f_J'}{x-x'}\right)} \tag{48}$$

By noticing that

$$\lim_{k\to 0} \frac{K - E}{k^2} = \lim_{k\to 0} \frac{E - k_c^2 K}{k^2 k_c^2} \to \frac{\pi}{4}$$

and

$$\lim_{x\to\infty} \frac{g_n'}{x - x'} = \lim_{x\to\infty} \frac{dg_n'}{dx'} \to 0$$

it can be seen that the resulting integrand is zero at $k_J = 0$. The slope df_J/dx is taken to be a constant here, in accord with the approximate representation of the jet in this region as discussed in section A2 of the previous chapter. The resulting integrand for the x (z) velocity component is plotted as f_1 (f_2) in Figure 5.

3. Singularity at the Origin

The final difficulty encountered within the integrands of interest involves the logarithmic singularity at the origin due to the term dg_n/dx. Consider only the integral involving this term in a small δ neighborhood about the origin.

$$\int_0^{\delta} \frac{dg_n'}{dx'} \frac{z - f_J}{x - x'} \frac{1}{k_J} \frac{E - k_{cJ}^2 K}{1 + \left(\frac{z - f_J}{x - x'}\right)^2} \frac{dx'}{x-x'} \tag{49}$$

The group of terms

$$\frac{z-f_J'}{x-x'} \frac{1}{k_J} \frac{E - k_{cJ}^2 K}{1 + \left(\frac{z - f_J'}{x - x'}\right)^2} \frac{1}{x-x'}$$

(plotted as f_1 in Figure 6) may be given their value at a mean point and removed from the integral to provide the resulting approximation for Equation (49)

$$2 s_J \left[\frac{z-f_J'}{x-x'} \frac{1}{k_J} \frac{E - k_{cJ}^2 K}{1 + \left(\frac{z - f_J'}{x - x'}\right)^2} \frac{1}{x-x'} \right]_{\delta/2} \left[\ln \frac{\sqrt{\delta/s_J + 1} - 1}{\sqrt{\delta/s_J + 1} + 1} - \right.$$

$$\left. \frac{\ln (\delta/s_J)}{\sqrt{\delta/s_J + 1}} + 2 \log 2 \right]$$

A similar relation was developed for the z velocity component (the term to be evaluated at the intermediate value is plotted as f_2 in Figure 6).

The integrands of Equations (39) and (40) have been plotted as f_1 and f_2 respectively in Figure 7 for the remaining intervals.

4. Numerical Integration Method

In accord with the factors mentioned above, the integrals were subdivided into at most the sum of five integrals over parts of the domain of interest.

$$0 \leq x' \leq \delta$$

$$\delta \leq x' \leq x - \varepsilon_1$$

$$x - \varepsilon_1 \leq x' \leq x + \varepsilon_2$$

$$x + \varepsilon_2 \leq x' \leq \hat{x}$$

$$\hat{x} \leq x' < \infty$$

where δ, ε_1, and ε_2 are small values chosen on the basis of integration accuracy. Those integrands not involving the logarithmic singularity at $x = 0$ were integrated directly from 0 to $x - \varepsilon_1$.

Now, in order to represent the integrals well for a range of jet geometries, it was decided to choose the main control points at nineteen equally spaced locations along the jet ($\Delta\xi$ = constant). An additional control point was placed at $\Delta\xi/2$, within the initial region of rapid variation of the jet geometry, resulting in a total of twenty control points in the domain $0 \leq x' \leq \hat{x}$. Step sizes for the integrations were taken to be ten times smaller, resulting in a total of 201 points in the numerical grid. These values were found to give satisfactory accuracy. Numerical integration of the functions with nonsingular integrands was performed by means of a compound Simpson's rule.[20]

$$\int_{x_0}^{x_{2n}} f(x)\,dx = \frac{h}{3}\,[f_0 + 4\,(f_1 + f_3 + \ldots + f_{2n-1}) + 2\,(f_2 + f_4 + \ldots +$$

$$f_{2n-2}) + f_{2n}] + E_n$$

where

$$f_i = f(x_i)$$

$$h = (x_{i+1} - x_i) = \text{constant}$$

and the remainder E_n is given by

$$E_n = -\frac{nh^5}{90}\,\frac{d^4 f(\xi)}{dx^4}\;;\; x_0 < \xi < x_{2n}\,.$$

The indices refer to the grid points within the integration interval of concern. Numerical algorithms for the complete elliptic integrals are described in Appendix B.

B. Evaluation of C_n

Upon evaluating the integrals numerically at each of the control points, one has

$$u\,(\vec{x}_i) = u_A\,(x_i) + \sum_{n=1}^{N} C_n\, I_n\,(x_i)$$

and

$$w\,(\vec{x}_i) = w_A\,(x_i) + \sum_{n=1}^{N} C_n\, J_n\,(x_i)$$

where x_i denotes the i^{th} control point and $I_n\ (x_i)$, $J_n\ (x_i)$ are now known coefficients. These expressions may be substituted into the dynamical condition, Equation (38) to yield

$$\left(-\sum_{n=1}^{N} C_n \frac{dg_n}{dx}\right)\left[\left(U_\infty + u_A + \sum_{n=1}^{N} C_n I_n\right) - \left|\frac{df_J}{dx}\right| \left(w_A + \sum_{n=1}^{N} C_n J_n\right)\right] =$$

$$\frac{1}{2} C_J U_\infty^2 c \kappa \left[1 + \left(\frac{df_J}{dx}\right)^2\right] \tag{50}$$

This system of twenty equations in N unknowns (the N C_n values) is an overdetermined system (N was chosen to be 6 in the computations). The C_n values are evaluated such that Equations (50) are satisfied in a least squares sense over the domain.

The least squares solution may be obtained by minimizing the sum of the squares of the residuals

$$r = \sum_{i=1}^{M} [Q_i - T_i]^2 \tag{51}$$

where

$$Q_i = -\sum_{n=1}^{N} C_n \frac{dg_n\ (x_i)}{dx} [s_i + \sum_{n=1}^{N} C_n t_{ni}] \tag{52}$$

$$T_i = \frac{1}{2} C_J U_\infty^2 c\ \kappa(x_i) \left[1 + \left(\frac{df_J\ (x_i)}{dx}\right)^2\right] \tag{53}$$

and

$$s_i = U_\infty + u_A - \left|\frac{df_J(x_i)}{dx}\right| w_A \tag{54}$$

$$t_{ni} = I_n(x_i) - \frac{df_J(x_i)}{dx} J_n(x_i) \tag{55}$$

Thus

$$\frac{1}{2}\frac{\partial r}{\partial C_n} = \sum_{i=1}^{M} (Q_i - T_i)\frac{\partial Q_i}{\partial C_n} = 0 \quad ; \quad n = 1,\ldots,N$$

Substituting the expression for Q into this relation yields

$$\sum_{i=1}^{M}\left[T_i + \left(\sum_{n=1}^{N} C_n \frac{dg_n(x_i)}{dx}\right)\left(s_i + \sum_{n=1}^{N} t_{ni}\right)\right] \cdot \left[s_i \frac{dg_n(x_j)}{dx} + \right.$$

$$\left.\sum_{n=1}^{N} C_n\left(t_{ni}\frac{dg_n(x_j)}{dx} + t_{nj}\frac{dg_n(x_i)}{dx}\right)\right] = 0 \quad ; \quad j = 1,\ldots,N \tag{56}$$

which may be solved for the C_n values.

Equations (56) comprise a nonlinear system of algebraic equations for the N values of the coefficients C_n. A solution may be obtained by employing a variation of the secant method[21,22]. This is an iterative procedure starting from a trial set of values $\{C_n\}$. As for most such nonlinear problems, the trial values for starting the solution must be reasonably close to the solution for rapid convergence of the method. Once the computations are underway, preceding iterates serve this purpose well enough. In a new computation, however, it may be necessary to provide initial values without the guidance of prior solutions. One means for accomplishing this is simply to employ the linear tangency condition, Equation (37), solving for the C_n values employing the current f_J function. These values of C_n may then be used to calculate the velocity components, u and w. Since the velocity components change less rapidly than the vortex strength[9], a linearized dynamic condition may now be employed (with only $\vec{\gamma}$ as an unknown) to obtain an improved set of values $\{C_n\}$. This last set of C_n values can then be employed as a trial set in the solution of the nonlinear dynamical condition. Experience with this procedure has been satisfactory.

C. Evaluation of the Function f_J

The function f_J is determined iteratively in the solution procedure. An initial trial value must be chosen for a new problem. Subsequent values are generated by the program in the iteration scheme. The procedure, outlined in the previous discussion, amounts to (a) starting with a trial function f_J, (b) evaluating $g(x_i)$ given f_J so that the dynamical condition is met, and (c) employing the tangency condition to guide the choice of a new iterate for the function f_J. Both f_J and g must be such as to satisfy both the tangency and dynamical conditions in the solution.

Upon initiating a new computation, it has been found convenient to start with a function f_J derived from the two-dimensional solution of Spence.[1] The appropriate equations for this purpose are listed in Appendix C. While this method is best for small C_J, α, and τ values, it is generally preferable to employ solutions obtained in the present analysis for similar parametric ranges, when they are available, if C_J, α, τ are large. More rapid convergence can then be achieved, as would be expected.

The function f_J giving the position of the jet in the analysis is not itself sensitive enough to be employed either for the estimation of errors involved or for iterative purposes. Since both the first derivative and the curvature involving the second derivative arise in the theory they must be represented with sufficient accuracy and regularity in the numerical scheme. Therefore, the curvature, being most sensitive, was employed both as a basis for the choice of new iterates, and as the factor on which accuracy was judged.

The computations start with a set of values for $\kappa(x_i)$ at the twenty control points. This function is numerically integrated to yield values for df_J/dx at the control points. The method employed for integration of the curvature may be found in Appendix D. The coefficients in the expansion of Equation (34) for f_J are determined so as to provide a least squares fit to the slope, df_J/dx, at the control points. Thus one has[23,24]

$$\sum_{j=1}^{J} a_j \left[\sum_{i=1}^{M} G_j(x_i)\, G_k(x_i) \right] = \sum_{i=1}^{M} F(x_i)\, G_k(x_i) \quad ; \; k = 1,\ldots,J \qquad (57)$$

where a_j ($j = 1, \ldots, J$) are the coefficients in the expansion for f_J (cf. Equation 33) and

$$G_j(x_i) = j\left[1 - \frac{1}{(x_i + 1)^{j+1}}\right] \tag{58}$$

$$F(x_i) = \frac{df_J}{dx} - \frac{df_J\ (x = 0)}{dx} \tag{59}$$

Upon determining the coefficients a_j in the representation of f_J, it is necessary to determine positions of the new grid points x_k such that they are equally spaced along the jet. Equal spacing of the grid points is desirable for better representation of the functions involved in the numerical work as mentioned in Section A4. This amounts to numerical integration at the expression for $d\xi/dx$

$$\hat{\xi} = \int_0^{\hat{x}} \frac{d\xi}{dx}\, dx = \int_0^{\hat{x}} \sqrt{1 + \left(\frac{df_J}{dx}\right)^2}\, dx \tag{60}$$

dividing the interval $\hat{\xi}$ into suitable equal intervals (200 here), and establishing a correspondence between ξ_k and x_k for each grid point. The relations involved and the integration scheme employed are described in Appendix E.

The computations employing f_J proceed as discussed in the previous section to an evaluation of $\{C_n\}$ satisfying the dynamical condition. The tangency condition remains to be met. This relation

$$[U_\infty + u(x,0,f_J)]\,\frac{df_J}{dx} - w(x,0,f_J) = 0$$

may now be employed directly to evaluate df_J/dx at each control point.

D. Generation of a New Iterate

As mentioned in Section C above, it is advantageous to employ $\kappa(x)$ as the basis of the iteration scheme so that the key aspects of the jet with respect to the mechanics of the problem may be represented properly. Values of κ employed at first in the computations are smoothly varying in the domain. New iterates are also to be required to vary smoothly.

The problem here, of course, is that of generating smooth changes for κ based on information at the discrete control points regarding df_J/dx. From the definition of κ, a small change may be related to changes in df_J/dx and d^2f_J/dx^2 as follows

$$\delta\kappa = \frac{\delta\left(\frac{d^2f_J}{dx^2}\right)}{\left[1 + \left(\frac{df_J}{dx}\right)^2\right]^{3/2}} - \frac{3\,\frac{d^2f_J}{dx^2}\,\frac{df_J}{dx}\,\delta\left(\frac{df_J}{dx}\right)}{\left[1 + \left(\frac{df_J}{dx}\right)^2\right]^{5/2}}$$

A procedure for obtaining a set of $\delta\kappa$ values at the control points which proved effective in the iteration procedure was simply to ignore the first term (it could be anticipated to be small), and to employ the relation

$$\delta\kappa_i = -3\,\kappa_{oi}\frac{\left(\frac{df_J}{dx}\right)_{oi}\delta\left(\frac{df_J}{dx}\right)_i}{1 + \left(\frac{df_J}{dx}\right)_{oi}^2}$$

where κ_{oi} represents the value of κ employed in starting the preceding iteration and $\delta(df_J/dx)_i$ represents the difference between the computed values of df_J/dx and those values employed in starting the preceding interation. The iteration procedure converged when the new iterates were chosen according to the relation

$$\kappa_i = \kappa_{oi} + e\,\delta\kappa_i$$

where e is a damping factor chosen to be small initially and to increase to unity as the solution was approached. Initial values for e in a new problem might be on the order of 0.2.

A measure of the error in the result may be obtained by comparing these new values of κ_i at each control point with those employed upon starting the previous iteration. A sum of the absolute value of the relative errors between these two values was employed in the computations for this purpose. The existing method employed of value of 0.6 for this sum (or the average relative error at each point was required to be below 0.03). If this criterion was not met, the new values for the curvature were employed to initiate another iteration.

V. ANALYSIS OF THE FLOWFIELD OF THE AIRFOIL

There are two aspects of the aerodynamic field of the airfoil entering the theory. The first is the need for some initial estimate of the influence of the flowfield induced by the wing on the jet. This may be obtained by means of one of the simpler linear wing theories for example. The second is the solution of the flowfield about the airfoil subject to the full influence of the disturbances introduced by the jet. The first is treated here assuming the airfoil to be represented as a lifting line with the appropriate trailing vortex distribution. An elliptic loading is assumed for this purpose with a total lift estimated to represent the final solution (at least somewhat larger than that for the wing alone). The second is accomplished by numerical methods in an adaptation of lifting surface theory.

A. Initial Estimate of the Flowfield of the Airfoil for Use in the Jet Solution

For an elliptically loaded wing operating with a lift coefficient C_L, the distribution of the vortex strength along the lifting line may be expressed as[14]

$$\Gamma = \Gamma_A \sqrt{1 - \left(\frac{y}{s_A}\right)^2} \tag{61}$$

where

$$\Gamma_A = \frac{1}{2} C_L U_\infty c_0$$

The vorticity associated with the bound vortex may be placed at the quarter chord point ($x = x_b$) of the airfoil[15] and the trailing vorticity may be regarded as lying in the $z = 0$ plane (refer to Figure 8).

The velocity components u_A and w_A induced by this vorticity distribution may be determined from the relations[25]

$$u_A = \frac{1}{4\pi} \frac{z}{(x - x_b)^2 + z^2} \int_{-s_A}^{s_A} \frac{d\Gamma'}{dy'} \frac{y - y'}{R} dy' \tag{62}$$

$$w_A = -\frac{1}{4\pi} \int_{-s_A}^{s_A} \frac{d\Gamma'}{dy'} \left[\frac{(x - x_b)(y - y')}{[(x - x_b)^2 + z^2] R} + \frac{y - y'}{(y - y')^2 + z^2} \left(1 + \frac{x - x_b}{R}\right) \right] dy' \tag{63}$$

Values of u_A and w_A at $y = 0$ are required in the jet solution. These may be obtained by carrying out the integrations of Equations (62) and (63) subject to the vortex strength distribution of Equation (61) to yield (cf. Appendix A)

$$u_A(x,0,z) = \frac{\Gamma_A}{2\pi}\,\frac{z\,k_A}{s_A^{\,2}}\left[\frac{E(k_A)}{k_{cA}^{\,2}} - K\,(k_A)\right] \tag{64}$$

$$w_A(x,0,z) = -\frac{\Gamma_A}{2\pi\,s_A}\left[\frac{(x - x_b)\,k_A}{s_A}\left(\frac{E(k_A)}{k_{cA}^{\,2}} - \frac{z^2}{s_A^{\,2} + z^2}\,\Pi\,(\alpha_A^{\,2},\,k_A)\right) + \frac{\pi}{2}\left(1 - \frac{z}{\sqrt{s_A^{\,2} + z^2}}\right)\right] \tag{65}$$

where K and E are the first and second complete elliptic integrals of modulus k_A and Π is the third complete elliptic integral, which is also a function of the parameter α_A. And

$$\alpha_A^{\,2} = \frac{s_A^{\,2}}{s_A^{\,2} + z^2}$$

$$k_A^{\,2} = \frac{s_A^{\,2}}{(x - x_b)^2 + s_A^{\,2} + z^2}$$

B. Solution of the Flowfield about the Airfoil Subject to the Interference Field of the Jet

Given the solution of the jet problem as described in Chapters III and IV, subject to the estimated interaction of the airfoil of Section A above, it is next required to obtain a more precise solution for the flowfield about the wing. This is formally given by the relations (recall the discussion of Section II B-3)

$$\vec{V}(\vec{x}) = U_\infty \vec{e}_x + \frac{1}{4\pi} \iint_{S_A} \frac{\vec{\gamma}_A{}' \times \vec{R}}{R^3} \, dS_A{}' + \vec{v}_J \, (\vec{x}) \tag{66}$$

subject to the kinematic (tangency) condition

$$U \frac{\partial f_A}{\partial x} + V \frac{\partial f_A}{\partial y} - W = 0 \tag{67}$$

at points on the airfoil whose surface is given by the equation

$$f_A \, (x,y) - z = 0$$

It should be pointed out that unlike linear lifting surface theories the streamwise disturbance velocity is no longer negligible compared to the freestream velocity.

The velocity components u_J and w_J at points on the surface of the airfoil may be evaluated by integration over the vortex strength distribution of the jet

$$\vec{v}_J = \frac{1}{4\pi} \iint\limits_{S_J} \frac{\vec{\gamma}_J{}' \times \vec{R}}{R^3} \, dS_J{}' \tag{68}$$

Only airfoils with little or no dihedral (i.e. $\partial f_A/\partial y$ is negligible) are considered here. In addition it is assumed that the spanwise velocity component is small compared to the downwash and the streamwise velocity components. Therefore, the equation necessary for the evaluation of this component is dropped from the ensuing treatment. In Equation (68), the integrations with respect to y' may be obtained analytically (refer to Appendix A). The remaining integrations must be carried out numerically in a manner already described in Chapter III.

It remains to arrange the surface integral of Equation (66), which gives the contribution of the vorticity associated with the airfoil to the velocity field, in a form suitable for solution of the airfoil problem. The surface over which this integral is evaluated includes the surface used to represent the airfoil (the projection of the wing onto the z = 0 plane) as well as the surface containing the vorticity which is washed downstream, the wake vorticity. The location of the wake vorticity is not known, a priori. For a relatively lightly loaded airfoil the contribution of the vorticity created by the airfoil may be considered negligible compared to the vorticity of the jet in this wake region. However, in order to simplify the resulting equations the vorticity shed by the airfoil will be retained. It is assumed that the location of this vorticity may be taken to lie in the z = 0 plane. This assumption is made in most airfoil theories. It is therefore possible to utilize some of the mathematical aspects of those theories.

Employing the definition of a vortex sheet,[14] the vortex strength of the airfoil may be presented by the equation

$$\vec{\gamma}_A = -\Delta v\, \vec{e}_x + \Delta u\, \vec{e}_y \tag{69}$$

where

$$\Delta u = u^+ - u^-$$

Defining a doublet strength as

$$\tau_d \equiv \Phi^+ - \Phi^-$$

Φ being the velocity potential, Equation (69) may be written as

$$\vec{\gamma}_A = -\frac{\partial \tau_d}{\partial y}\,\vec{e}_x + \frac{\partial \tau_d}{\partial x}\,\vec{e}_y \tag{70}$$

Equation (70) along with the assumptions discussed in the preceeding paragraph may now be employed to provide the resulting equations for the induced velocity field created by the airfoil

$$u_A = \frac{1}{4\pi} \int_{\ell.e.}^{\infty} \int_{-s_A}^{s_A} \frac{\partial \tau_d'}{\partial x'} \frac{z}{R^3}\, dy'\, dx' \tag{71}$$

$$w_A = -\frac{1}{4\pi} \int_{\ell.e.}^{\infty} \int_{-s_A}^{s_A} \left[\frac{\partial \tau_d'}{\partial x'} \frac{(x - x')}{R^3} + \frac{\partial \tau_d'}{\partial y'} \frac{(y - y')}{R^3} \right] dy'\, dx' \tag{72}$$

Solution of the airfoil problem requires these equations be applied to the $z = 0$ plane. It may be seen from Equation (71) that $u_A = 0$ for this plane; therefore, only Equation (72) remains to be evaluated.

Equation (72) as it stands contains a singularity with respect to both integrals at the control point (x,y); therefore, a more suitable kernel will be sought. Following the procedure of Robinson and Laurmann[25] this equation may be written as

$$w_A = -\frac{1}{4\pi} \int_{\ell.e.}^{\infty} \int_{-s_A}^{s_A} \tau_d' \frac{\partial^2}{\partial z^2} \left(\frac{1}{R}\right) dx'\, dy' \tag{73}$$

Further manipulations of Equation (73) provide the final working equation for the downwash induced by the airfoil in the form[26]

$$w_A = -\frac{1}{4\pi} \int_{-s_A}^{s_A} \frac{y - y'}{(y - y')^2 + z^2} \frac{\partial}{\partial y'} \left[\int_{\ell.e.}^{t.e.} \frac{\partial \tau_d'}{\partial x'} \left(1 + \frac{x - x'}{R}\right) dx' \right] dy'$$

$$- \frac{z^2}{4\pi} \int_{-s_A}^{s_A} \int_{\ell.e.}^{t.e.} \frac{\partial \tau_d'}{\partial x'} \frac{x - x'}{[(y - y')^2 + z^2]\, R^3}\, dx'\, dy' \tag{74}$$

for an arbitrary field point (x, y, z). In the limit $z \to 0$ the second term of Equation (74) vanishes and the first is given by the Cauchy principal value

$$w_A(x,y,0) = -\frac{1}{4\pi}\lim_{\varepsilon\to 0}\left[\int_{-s_A}^{y-\varepsilon}\frac{\partial}{\partial y'}\left[\int_{\ell.e.}^{t.e.}\frac{\partial\tau_d'}{\partial x'}\left(1+\frac{x-x'}{R}\right)dx'\right]\frac{dy'}{y-y'} + \right.$$

$$\left.\int_{y+\varepsilon}^{s_A}\frac{\partial}{\partial y'}\left[\int_{\ell.e.}^{t.e.}\frac{\partial\tau_d'}{\partial x'}\left(1+\frac{x-x'}{R}\right)dx'\right]\frac{dy'}{y-y'}\right] \tag{75}$$

By defining

$$f(y') \equiv \int_{\ell.e.}^{t.e.}\frac{\partial\tau_d'}{\partial x'}\left(1+\frac{x-x'}{R}\right)dx'$$

employing integration by parts, and expanding $f(y \pm \varepsilon)$ in a Taylor Series, Equation (75) may be obtained in the final form[26]

$$w_A(x,y,0) = \frac{1}{4\pi}⨎_{-s_A}^{s_A}\frac{dy'}{(y-y')^2}\int_{\ell.e.}^{t.e.}\frac{\partial\tau_d'}{\partial x'}\left(1+\frac{x-x'}{R}\right)dx' \tag{76}$$

where the symbol $⨎$ represents the Mangler principal value.[26] The Mangler principle value is defined by the equation

$$⨎_{-s_A}^{s_A}\frac{f(y')}{(y-y')^2}dy' \equiv \lim_{\varepsilon\to 0}\left[\int_{-s_A}^{y-\varepsilon}\frac{f(y')}{(y-y')^2}dy' + \int_{y+\varepsilon}^{s_A}\frac{f(y')}{(y-y')^2}dy' - \frac{2f(y)}{\varepsilon}\right]$$

Equation (76), found in many of the existing lifting surface theories, is singular with respect to only the outer integral. The integral with respect to x' possess only a discontinuity, since for $y = y'$,

$$\lim_{x\to x'}\left[1+\frac{x-x'}{R}\right] \to \begin{cases}2 : x > x'\\ 0 : x < x'\end{cases}$$

The integral equation, Equation (66), with w_A given by Equation (76), together with the kinematic condition, Equation (67), now are in a form suitable for mathematical solution. Given a solution $\tau_d(x,y)$ on the surface of the airfoil, the flowfield may be computed at a point of interest. There are several methods which may be employed to obtain this desired doublet distribution. The method adopted here is related to the finite element theories.[27]

The pressure difference across the airfoil may be obtained from Bernoulli's Equation

$$\Delta p = \frac{1}{2}\rho\ [-2(U_\infty + u_J)\ \Delta u_A + (u_A^{-2} - u_A^{+2}) - 2\, v_J\ \Delta v_A + (v_A^{-2} - v_A^{+2}) - 2w_J\ \Delta w_A + (w_A^{-2} - w_A^{+2})]$$

As a consequence of the fact that the singularities used to represent the airfoil have been placed in a plane, the resulting velocity potential for a cambered wing at incidence to the freestream is antisymmetric with respect to that plane (z = 0 plane). Thus,

$$u_A^+ = -u_A^-$$

$$v_A^+ = -v_A^-$$

$$w_A^+ = w_A^-$$

Therefore, the pressure difference across the airfoil may be expressed in the form

$$\Delta p = -\rho\ (U_\infty + u_J)\ \Delta u_A \tag{77}$$

where the assumption that the spanwise velocity component is negligible compared to the streamwise component has been employed in this last equation.

Utilizing the definition of the doublet strength along with Equation (77), a relation for the change in the pressure coefficient across the airfoil may be determined

$$\Delta C_p = -\frac{2\,(U_\infty + u_J)}{U_\infty^2}\,\frac{\partial \tau_d}{\partial x} \tag{78}$$

Substituting Equation (78) into Equation (76) provides the result

$$w_A(x,y,0) = \frac{U_\infty^2}{8\pi} \int_{-s_A}^{s_A} \frac{dy'}{(y - y')^2} \int_{\ell.e.}^{t.e.} \frac{\Delta C_p}{(U_\infty + u_J)} \left(1 + \frac{x - x'}{R}\right) dx'$$

Consider the airfoil to be composed of a number of finite, rectangular elements. In a manner similar to finite element theories, it is assumed that the pressure difference across each element is constant. In addition, it will be assumed further that the velocity field induced by the jet is also a constant on each element. The downwash due to the k^{th} element at the i^{th} control point can then be written (refer to Figure 9)

$$w_{A_{ki}} = -\frac{U_\infty^2\,\Delta C_{pk}}{8\pi\,(U_\infty^2 + u_{Jk})} \int_{y_{ak}}^{y_{bk}} \frac{dy'}{(y_i - y')^2} \int_{x_{ak}}^{x_{bk}} \left(1 + \frac{x_i - x'}{R}\right) dx' \tag{79}$$

The resulting surface integral in Equation (79) is only a function of the geometry of the element. The evaluation of this integral is treated in

Appendix A where proper care has been taken for the situation in which $k = i$. Defining

$$I(x_i, y_i; x_{ak}, x_{bk}, y_{ak}, y_{bk}) \equiv I_{ki} \equiv \int_{y_{ak}}^{y_{bk}} \frac{dy'}{(y_i - y')^2} \int_{x_{ak}}^{x_{bk}} \left(1 + \frac{x_i - x'}{R}\right) dx' \tag{80}$$

the total downwash at the i^{th} element, for the case in which the wing planform is divided into 2N elements, may be written

$$w_{Ai} = - \frac{U_\infty^2}{8\pi} \sum_{k=1}^{2N} \frac{\Delta C_{pk}}{(U_\infty^2 + u_{Jk})} I_{ki}$$

Because of geometric symmetry the pressure difference and velocity field induced by the jet must be symmetric about the x-axis, therefore

$$w_{Ai} = - \frac{U_\infty^2}{8\pi} \sum_{k=1}^{N} \frac{\Delta C_{pk}}{U_\infty + u_{Jk}} [I_{k,i} + I_{k+N,i}] \tag{81}$$

where the k^{th} element lies on the right semi-span wing section $(y > 0)$ and has as its reflection about the x-axis the $k + N^{th}$ element (refer to Figure 9). It may be shown further that

$$I_{k+N,i} = - I(x_i, y_i; x_{ak}, x_{bk}, - y_{ak}, - y_{bk})$$

The unknown pressure difference for each element (ΔC_{pk}) may now be obtained by applying the kinematic condition at the N control points, which have been taken to be located at

$$x_i = x_{bi} + 0.1\ (x_{ai} - x_{bi})$$

$$y_i = 0.5\ (y_{ai} + y_{bi})$$

Inserting Equation (81) into the kinematic condition results in a set of N simultaneous, linear equations for the N unknown pressure differences

$$-\frac{U_\infty^2}{8\pi} \sum_{k=1}^{N} \frac{\Delta C_{pk}}{U_\infty + u_{Jk}} [I_{k,i} + I_{k+N,i}] = (U_\infty + u_{Ji}) \left(\frac{df_A}{dx}\right)_i - w_{Ji} \quad ; \quad i = 1,\ldots,N \tag{82}$$

C. Calculation of the Forces on the Airfoil

Once the pressure distribution on the airfoil has been obtained the pressure forces may be computed directly.

$$L_p = -\iint_{S_A} \Delta p' \cos \psi' \, dS_A' \tag{83}$$

$$D_p = -\iint_{S_A} \Delta p' \sin \psi' \, dS_A' \tag{84}$$

where
$$\psi = \tan^{-1} \left(\frac{df_A}{dx}\right)$$

(For the situation under consideration $\psi \equiv \alpha$). In the above equation L_p (D_p) refers to the lift (drag) force experienced by the airfoil due to the pressure difference across it (as opposed to the force created by the reaction to the jet). It should be mentioned that Equations (83) and (84) do not include the leading edge suction force which provides only a negligible contribution to the lift. Since the flow is considered inviscid, the above equations also exclude skin friction effects. Written in terms of non-dimensional variables, Equation (83) has the form

$$C_{Lp} = - \iint_{S_A} \frac{\cos \psi' \, \Delta C_p'}{S_A} \, dS_A'$$

where S_A is the surface area of the airfoil. In terms of finite elements covering the surface,

$$C_{Lp} = - \frac{1}{S_A} \sum_{k=1}^{2N} \cos \psi_k \, \Delta C_{pk} \, S_k \tag{85}$$

where

$$S_k = (x_{bk} - x_{ak}) \cdot (y_{bk} - y_{ak})$$

is the area of the k^{th} element. It should be noticed that the assumption that the angle ψ is constant for an element has been employed in Equation (85). Such practice is inherent to the definition of a finite element in theories such as Woodward's.[27] Utilizing the symmetry conditions, Equation (85) may finally be written in the form

$$C_{LP} = - \frac{2}{S_A} \sum_{k=1}^{N} \cos \psi_k \, \Delta C_{pk} \, S_k \tag{86}$$

Similarly, the drag coefficient resulting from the pressure difference across the wing may be obtained from the equation

$$C_{DP} = - \frac{2}{S_A} \sum_{k=1}^{N} \sin \psi_k \, \Delta C_{pk} \, S_k \tag{87}$$

The total lift and drag coefficients for the airfoil may now be obtained by including the reaction to the jet in Equations (86) and (87)

$$C_L = C_{Lp} + \frac{1}{S_A} \int_{-s_J}^{s_J} C_J \, c \sin (\tau + \alpha) \, dy \tag{88}$$

$$C_D = C_{DP} - \frac{1}{S_A} \int_{-s_J}^{s_J} C_J \, c \cos (\tau + \alpha) \, dy \tag{89}$$

D. Calculation of the Velocity Field in the Vicinity of a Tail Surface

The downwash at a point in the vicinity of a tail or control surface downstream of the wing may be immediately obtained from the equations of the previous sections. For simplicity, a point located on the x-axis is employed for this purpose. The velocity at such a point is written

$$\vec{V} = U_\infty \vec{e}_x + \frac{1}{4\pi} \iint_{S_A} \frac{\vec{\gamma}_A' \times \vec{R}}{R^3} \, dS_A' + \frac{1}{4\pi} \iint_{S_J} \frac{\vec{\gamma}_J' \times \vec{R}}{R^3} \, dS_J'$$

Again the first surface integral will be referred to as $u_A(w_A)$ and the second as $u_J(w_J)$.

1. The Velocity Field Induced by the Jet

The necessary equations for the determination of the velocity field induced by the jet sheet at the point under consideration may be obtained from the formulation of Chapter III. Because of symmetry the spanwise velocity component is zero. Furthermore,

$$u_J(x,0,0) = -\frac{1}{2\pi}\sum_{n=1}^{N} C_n \int_0^{\infty} \left[\frac{g_n'}{s_J} \frac{df_J'}{dx'} \frac{k_{cJ}\,(K - E)}{\sqrt{1 + \left(\frac{f_J'}{x - x'}\right)^2}} - \frac{dg_n'}{dx'} \frac{f_J'}{x - x'} \frac{1}{k_J} \frac{E - k_{cJ}^{\,2} K}{1 + \left(\frac{f_J'}{x - x'}\right)^2} \right] \frac{dx'}{x - x'}$$

$$w_J(x,0,0) = \frac{1}{2\pi}\sum_{n=1}^{N} C_n \int_0^{\infty} \left[\frac{g_n'}{s_J} \frac{k_{cJ}\,(K - E)}{\sqrt{1 + \left(\frac{f_J'}{x - x'}\right)^2}} + \frac{dg_n'}{dx'} \frac{1}{k_J} \frac{E - k_{cJ}^{\,2} K}{1 + \left(\frac{f_J'}{x - x'}\right)^2} \right] \frac{dx'}{x - x'}$$

Proper account is taken for the infinite upper limit and the singularity at the origin in exactly the same manner discussed in Chapter IV.

2. The Velocity Field Induced by the Airfoil

The velocity induced by the airfoil at the point (x,0,0) may be obtained by employing the results of Section B.

$$u_A(x,0,0) = 0$$

$$v_A(x,0,0) = 0$$

$$w_A(x,0,0) = -\frac{U_\infty^2}{8\pi} \int_{-s_A}^{s_A} \frac{dy'}{y'^2} \int_{\ell.e.}^{t.e.} \frac{\Delta C_p}{U_\infty + u_J} \left(1 + \frac{x - x'}{R}\right) dx' \qquad (90)$$

Employing finite elements Equation (90) may be written in the form

$$w_A(x,0,0) = -\frac{U_\infty^2}{8\pi} \sum_{k=1}^{N} \frac{\Delta C_{pk}}{(U_\infty + u_{Jk})} I_k$$

where I_k may be found in Appendix A.

VI. COMPUTATIONAL RESULTS AND COMPARISON WITH EXPERIMENTAL DATA AND OTHER THEORIES

A. Choice of Parameters for the Computations

The airfoil and jet geometries as well as values for the angle of attack of the wing, the jet deflection angle, and the jet momentum coefficient were chosen largely in accord with data available in the literature for the purpose of comparison. Computed results were obtained for a rectangular airfoil with an aspect ratio (AR) of 6.8 equipped with a full span jet flap. Choices for the remaining parameters along with the computed results for the lift coefficient, the induced drag coefficient, and the downwash angle (Θ) and pressure coefficient (C_p) three chord lengths downstream of the airfoil are listed in Table 1.

A first solution was obtained for small values of α, τ, and C_J by employing initial values for the jet geometry obtained from the two-dimensional theory of Spence[1] (refer to Appendix C). Subsequent solutions were obtained using initial values obtained from the results of an existing solution which had input parameters (α, τ, and C_J) close to those under consideration.

Choice of the number of grid points employed to determine the necessary integrals and the number of control points on the airfoil and the jet was made on the basis of providing the highest accuracy for reasonable computational times. By using 201 grid points, 20 control points on the jet, and 32 elements on the wing, execution times of approximately 26 seconds per iteration of the jet problem and 23 seconds to obtain the resulting forces on the wing and induced downwash at a downstream location were obtained. All computations were made on a CDC 6500. The factors β and ν (refer to Equations (32) and (33)) were each given a value of 10 for the computations. The resulting values for C_n and a_n fell in the ranges

$$0.05 < |C_n| < 6$$

$$10 < |a_n| < 160$$

The nearfield calculations were obtained in the region extending from the trailing edge of the airfoil to a point $(\hat{x})$ approximately 5 chord lengths downstream. It will later be observed that this region contained the primary contribution to the vortex strength, as it should.

A solution to the jet problem was assumed to be determined once the sum of the magnitudes of the relative errors between the curvature values obtained from two consecutive iterations was below 0.6 (resulting in an average relative error of 3 percent). However, for larger values of C_J and α it was found that the relative errors of the curvature at each control point were approximately constant prior to satisfying the above convergence criterion. Consequently, when these values were scaled to provide proper integrals (refer to Appendix D) the resulting changes from the previous iteration was small. In such cases convergence became slow when the average relative error became less than about 7 percent. An investigation into this dilemma showed that the application of a decreasing functional form for the damping factor (e) was fruitless. However, by assuming that the value of the jet slope at infinity (refer to Appendix D) was half its value at $\hat{x}$ (a value of zero was employed in the original computations for convenience), it was possible to reduce the average value of the relative errors to 2 percent. Since the resulting value for the relative error of the lift coefficient was only 3.5 percent, however, the above error criterion was reduced to a value of 1.3 for these cases. Iterations of the entire problem were terminated once the relative error between two consecutive values of the lift coefficient was below 0.025. The above convergence criteria required approximately 3 iterations of the entire scheme and an average of 6 iterations of the jet scheme. For the initial values, however, as many as 10 iterations were required to converge on a jet solution.

B. Results

The variations of the lift coefficient with changes in the jet momentum coefficient are provided in Figure 10. Comparison with the linear theories of Maskell[2] and Tokuda[4] are favorable. For small values of C_J (linear region) the disagreement between the theories was less than 10 percent. However, the values of C_L computed by the present theory for large values of C_J (nonlinear region) are evidently higher than what would be predicted by extending the curves obtained from the linear theories. Experimental data[10] are also available for the linear region. It can be seen in Figure 10 that agreement between the present theory and the experimental data is also quite acceptable in that regime. It should be mentioned that the results of Maskell[2] have been increased by an appropriate factor to account for the thickness of the airfoil employed in Alexander's[10] experiments. The factor involved is discussed in greater detail by Lissaman.[7]

It can be seen in Figure 11 that the resulting variations of C_L with changes in α provided by the present (nonlinear) theory lies slightly below the experimental data and the curves obtained from the linear theories. However, it has been observed that linear theories in general tend to overestimate the lift, the difference increasing with larger values of α and τ.[28] The linear theories employed a lifting-line approximation for the airfoil. It might be expected that the utilization of a lifting-surface technique would lower these values in a manner similar to that for conventional wings.[15] It has been suggested that the linear theories provide favorable agreement with the experimental data because of the "fortuitous cancellations" of higher order effects.[1] The results of Lissaman's theory are also depicted in Figure 11. They tend to lie even lower than those of the present theory.

The results for the induced drag coefficient are presented in Figures 12 and 13. As already discussed in the previous chapter, the induced drag (or thrust for the conditions encountered) resulting from the present theory only accounts for the reaction to the jet and the pressure distribution on the airfoil. Contributions to the drag attributed to form drag and to viscous effects, such as skin-friction or jet entrainment, are not represented in this analysis. Drag coefficient values for $\alpha = 0°$ as well as values obtained from Figure 12 for $\alpha \neq 0°$ are presented and compared to Williams'[10] data in Figure 13. The agreement is again quite acceptable.

The distribution of the pressure difference across the wing is shown in Figures 14 through 19 for three different cases. Since only four elements were employed in each of the spanwise and chordwise directions only basic trends can be obtained from these figures. For more refined results it would be necessary to employ more elements at the cost of computing time. As expected, a larger than normal pressure difference is encountered in the vicinity of the trailing edge of the airfoil. For this reason a wing equipped with a jet flap experiences large nose-down pitching moments. The spanwise distribution, however, is not very different from conventional wings. This has also been observed in experiments.[10,28]

The locations of the jet sheets in the plane of symmetry are shown in Figures 20 and 21 for different values of C_J and α. Obviously, the jet lies well below the $z = 0$ plane. For this reason downwash results obtained from linear theories are open to serious question.

The vortex distributions provided in Figures 22 and 23 display the proper logarithmic singularity at the origin. It is also apparent from these figures, that the control points were located in a region which contains most of the vorticity. The distributions indicate that the vortex strength becomes slightly negative beyond $x = s_J$. It is felt that this is a result of errors in the truncated series approximation employed for the vortex strength; it is not likely to be real.

As a result of the large nose-down pitching moment experienced by an aircraft equipped with a jet flap, an exceptionally large amount of trim is required. Consequently, a control surface plays an important role in such configurations. It is important, therefore, to know the flowfield with some degree of accuracy in regions where the tail surfaces would be located. Downwash results obtained from the present theory are shown in Figures 24 through 27 in the form of the downwash angle ($\Theta = \tan^{-1}(-U/W)$) and momentum or pressure information (C_p). The results were obtained at a representative point along the x-axis 3 chord lengths downstream of the trailing edge of the airfoil ($x = 0.88\ s_J$).

VII. CONCLUSIONS

The results of the present theory show ample agreement with the available experimental data and compare well with existing linear theories in the operating regime where they apply. For the lift coefficient, both the variation with C_J and α found in the theory were satisfactory. The values of C_L computed were slightly below the experimental data by an increment which could easily be accounted for by considering the airfoil thickness effect both in magnitude and trend. The induced drag (thrust) coefficient also agreed for the conditions considered. Regrettably, there are no experimental data available for the position of the jet sheet for a wing equipped with a jet flap for larger values of C_J, α, or τ. This situation should be remedied in experimental research. In addition, this theory extends values for the force system of the airfoil over a wide range of values for C_J and α, beyond that for which the linear theories apply. Moreover, the downwash computations are likely to be a substantial improvement over results obtained from the linear theories.

The existing theory easily may be extended to include the increase in the lift due to the thickness of the airfoil and the jet. This may be accomplished by employing a proper source distribution over the vortex sheets used to represent the actual wing and jet. Furthermore, it has been observed that entrainment effects are capable of providing substantial gains in the lift coefficient under some circumstances. This is especially true for the situation in which the jet is exhausted over a small flap.[29] Inclusion of entrainment phenomena into the present theory is also possible. This may be accomplished by locating a proper sink distribution[29] over the surface used to represent the jet.

It should be mentioned that this theory is not limited to rectangular airfoils equipped with full span jet flaps for which data was obtained in the previous chapter. However, as it exists no account can be made for spanwise variations in C_J and τ or a wing with dihedral. More general jet properties may be included by employing a suitable functional form for the spanwise variations of the vortex strength (g).* Furthermore, the present theory was developed in a manner that any wing theory might be employed. Therefore, more general airfoil geometries may be handled by utilizing more sophisticated wing theories such as Woodward's.[27] Finally, it should be noted that the ground effects problem may be treated by employing an imaging technique.

The present theory contains many parameters such as the number of control points, the grid point spacing, the factors β and ν, etc. whose values must be specified ab initio. An investigation of the effects changes in each of these parameters has on the solution procedure and results should be undertaken. Ultimately, it would be desirable to develop an algorithm which would automatically adjust the values of these constants depending on the values of τ, α, and C_J. Furthermore, a study of different functional forms for the damping factor (e) which would achieve convergence at a faster rate should also be considered.

*but not without some additional mathematical complexity in the integrals.

APPENDIX A

Evaluation of the Integrals

The theory developed within the main text contains several integrals of standard form. A brief outline of the integration procedures and a summary of the results are provided herein.

A. Integrals Inherent to the Horseshoe Vortex System

1)
$$I_1 \equiv \int_0^1 \frac{\eta^2\, d\eta}{\sqrt{(1-\eta^2)(\eta^2+c^2)}} \tag{A1}$$

Referring to Equation (213.06) of Byrd and Friedman[30] for the case m = 1

$$I_1 = k \int_0^K cn^2\, u\, du = \frac{1}{k}\left[E(k) - k_c^2\, K(k)\right] \tag{A2}$$

where

$$k = \frac{1}{\sqrt{1+c^2}} \tag{A3}$$

2)
$$I_2 \equiv \int_0^1 \frac{\eta^2\, d\eta}{\sqrt{1-\eta^2}\,(\eta^2+c^2)} \tag{A4}$$

$$= \int_0^1 \frac{d\eta}{\sqrt{1-\eta^2}} - c^2 \int_0^1 \frac{d\eta}{\sqrt{1-\eta^2}\,(\eta^2+c^2)}$$

Employing the equations found on pages 45 and 49 of Petit Bois[31]

$$I_2 = \left[\sin^{-1}(\eta) - \frac{c}{\sqrt{c^2+1}} \tan^{-1} \frac{\sqrt{c^2+1}\ \frac{\eta}{c}}{\sqrt{1-\eta^2}}\right]_0^1 = \frac{\pi}{2}\left[1 - \frac{c}{\sqrt{c^2+1}}\right] \qquad \text{(A5)}$$

3)
$$I_3 \equiv \int_0^1 \frac{\eta^2\, d\eta}{(\eta^2+q)\sqrt{(1-\eta^2)(\eta^2+c^2)}} \qquad \text{(A6)}$$

Consider Equation (213.12) of Byrd and Friedman[30]

$$I_3 = \frac{k}{q+1}\int_0^K \frac{1-\mathrm{sn}^2 u}{1-\left(\frac{1}{1+q}\right)\mathrm{sn}^2 u}\, du = k\left[K(k) - \frac{q}{1+q}\,\Pi\left(\frac{1}{1+q}, k\right)\right] \qquad \text{(A7)}$$

where k satisfies Equation (A3).

B. Integrals Inherent to the Jet Problem

1)
$$I_4 \equiv \int_{-1}^1 \frac{\eta^2\, d\eta}{\sqrt{1-\eta^2}\,(\eta^2+c^2)^{3/2}} \qquad \text{(A8)}$$

Taking advantage of the symmetry of the integrand and employing the transformation

$$\rho = \eta^2 + c^2$$

such that

$$d\eta = \frac{d\rho}{2\sqrt{\rho - c^2}}$$

then

$$I_4 = \int_{c^2}^{c^2+1} \frac{\rho - c^2}{\sqrt{1 - \rho + c^2}\sqrt{\rho - c^2}} \frac{d\rho}{\rho^{3/2}}$$

$$= \int_{c^2}^{c^2+1} \frac{d\rho}{\sqrt{\rho\,[(1 + c^2) - \rho][\rho - c^2]}} - c^2 \int_{c^2}^{c^2+1} \frac{d\rho}{\rho\sqrt{\rho[(1 + c^2) - \rho][\rho - c^2]}}$$

Both of these integrals are elliptic and may be found in Byrd and Friedman[30] (Equations (235.00) and (235.01)).

$$I_4 = 2k\ [K(k) - E(k)] \tag{A9}$$

where k satisfies Equation (A3)

2) $$I_5 \equiv \int_{-1}^{1} \frac{\sqrt{1 - \eta^2}\, d\eta}{(\eta^2 + c^2)^{3/2}} \tag{A10}$$

Consider the transformation

$$\xi^2 = \eta^2 + c^2$$

such that

$$d\eta = \frac{\xi\, d\xi}{\sqrt{\xi^2 - c^2}}$$

The original integral may then be written

$$I_5 = 2 \int_{c}^{\sqrt{1+c^2}} \frac{d\xi}{\xi^2} \sqrt{\frac{(1+c^2) - \xi^2}{\xi^2 - c^2}}$$

From Equations (218.10) and (318.02) of Byrd and Friedman[30]

$$I_5 = 2k^3 \int_0^K sd^2\,u\,du = \frac{2k}{k_c^{\,2}}\,[E(k) - k_c^{\,2}\,K(k)] \qquad \text{(A11)}$$

where k satisfies Equation (A3)

3) $$I_6 \equiv \int_{-1}^{1} \frac{\sqrt{1-\eta^2}}{r^3}\,d\eta \qquad \text{(A12)}$$

where $$r^2 \equiv (x-\xi)^2 + (y-\eta)^2 + \rho^2$$

$$= (\eta - c)\,(\eta - c^*) \qquad \text{(A13)}$$

and $$c = y + i\,\sqrt{(x-\xi)^2 + \rho^2}$$

I_6 may therefore be written

$$I_6 = \int_{-1}^{1} \frac{d\eta}{(\eta - c)\,(\eta - c^*)} \sqrt{\frac{(1-\eta)\,(1+\eta)}{(\eta - c)\,(\eta - c^*)}}$$

Employing Equation (259.05) of Byrd and Friedman[30]

$$I_6 \doteq g^3 \int_0^{2K} sd^2 u \, du$$

$$= \frac{2 g^3}{k^2 k_c^2} [E(k) - k_c^2 K(k)] \tag{A14}$$

where
$$A^2 = (1 - y)^2 + (x - \xi)^2 + \rho^2 \tag{A15}$$

$$B^2 = (-1 - y)^2 + (x - \xi)^2 + \rho^2 \tag{A16}$$

$$g^2 = \frac{1}{AB} \tag{A17}$$

$$k^2 = \frac{4 - (A - B)^2}{4AB} \tag{A18}$$

Furthermore, it can be shown that

$$\lim_{y \to 0} I_6 \to \frac{2k}{k_c^2} (E - k_c^2 K) = I_5$$

as should be expected.

4)
$$I_7 \equiv \int_{-1}^{1} \frac{\eta \, (y - \eta)}{\sqrt{1 - \eta^2} \; r^3} \, d\eta \tag{A19}$$

where r^2 satisfies Equation (A13) above. Employing the identity

$$\frac{y - \eta}{r^3} = - \frac{\partial}{\partial y} \left(\frac{1}{r} \right)$$

Equation (A19) may be written

$$I_7 = - \frac{\partial}{\partial y} \int_{-1}^{1} \frac{\eta \, d\eta}{\sqrt{(1 - \eta)(1 + \eta)(\eta - c)(\eta - c^*)}}$$

Referring to Equation (259.03) of Byrd and Friedman[30]

$$I_7 = \frac{\partial}{\partial y} \left[g \sum_{j=0}^{1} \frac{\alpha_2^{1-j} (\alpha - \alpha_2)^j}{(1 - j)! \, j!} \int_0^{2K} \frac{du}{(1 + \alpha \operatorname{cn} u)^j} \right]$$

$$= \frac{\partial}{\partial y} \left[2 \, g \, \alpha_2 \, K(k) + \frac{g \, (\alpha - \alpha_2)}{1 - \alpha^2} \, \Pi \left(\pi, \frac{\alpha^2}{\alpha^2 - 1}, k \right) \right] \qquad \text{(A20)}$$

when A, B, g, and k satisfy Equations (A15) through (A18) and

$$\alpha = \frac{A - B}{A + B} \qquad \text{(A21)}$$

$$\alpha_2 = \frac{A + B}{A - B} \qquad \text{(A22)}$$

By utilizing the "Addition Equations" (Equation (10) of Byrd and Friedman)[30] it can be shown that

$$\Pi \, (\pi, \gamma^2, k) = 2 \, \Pi \, (\gamma^2, k)$$

Employing the additional relations

$$\frac{\partial}{\partial y}\left(\frac{g}{\alpha}\right) = -\frac{g^3}{\alpha^2\,(1-\alpha^2)}\{(\alpha^2-1)[2\alpha\, y + 1 + \alpha^2] + \alpha[y(1+\alpha^2) + 2\alpha]\}$$

$$\frac{\partial K}{\partial k} = \frac{E - k_c{}^2\, K}{k\, k_c{}^2}$$

$$\frac{\partial\, \Pi\,(\gamma^2, k)}{\partial k} = \frac{k}{k_c{}^2\,(k^2-\gamma^2)}\,[E - k_c{}^2\,\Pi]$$

$$\frac{\partial\, \Pi\,(\gamma^2, k)}{\partial \gamma^2} = \frac{\gamma^2 E + (k^2-\gamma^2)K + (\gamma^4 - k^2)\,\Pi}{2\,\gamma^2\,(1-\gamma^2)\,(\gamma^2-k^2)}$$

$$\frac{\partial\, \gamma^2}{\partial y} = -\frac{2\,g^2\,\gamma^2}{\alpha\,(1-\alpha^2)}\,[2\,y\,\alpha + 1 + \alpha^2]$$

$$\frac{\partial k}{\partial y} = -\frac{g^2}{2k}\left\{y + \frac{2k^2-1}{1-\alpha^2}\,[y(1+\alpha^2) + 2\,\alpha]\right\}$$

where

$$\gamma^2 = \frac{\alpha^2}{\alpha^2 - 1} \tag{A23}$$

the resulting form for Equation (A20) may be obtained

$$I_7 = g^3\left[\frac{\gamma^2\, P}{k^2\, k_c{}^2\,(k^2-\gamma^2)}\,E + \left(Q - R + \frac{P}{k^2}\right)K + \left((\gamma^2-1)\,Q + R - \frac{P}{k^2-\gamma^2}\right)\Pi\right.$$

$$\left. + \,Q(E - K)\right] \tag{A24}$$

where

$$P = \frac{1}{\alpha}\left(y + \frac{2k^2 - 1}{1 - \alpha^2}\,[y(1 + \alpha^2) + 2\alpha]\right) \tag{A25}$$

$$Q = \frac{-2\gamma^2}{\alpha^2\,(k^2 - \gamma^2)}\,[2\,y\,\alpha + 1 + \alpha^2] \tag{A26}$$

$$R = \frac{2}{\alpha}\left(\frac{y(1 + \alpha^2) + 2\alpha}{1 - \alpha^2}\right) \tag{A27}$$

It can be shown, with some difficulty that

$$\lim_{y \to 0} I_7 \to 2k\,(E - K) = -I_4$$

as it should.

C. Integrals Inherent to the Finite Element Technique

$$I_8 \equiv \oint \frac{d\eta}{(y - \eta)^2} \int \left(1 + \frac{x - \xi}{r}\right) d\xi \tag{A28}$$

where

$$r^2 = (x - \xi)^2 + (y - \eta)^2$$

Defining the inner integral as J

$$J = \xi + \int \frac{x - \xi}{\sqrt{(x - \xi)^2 + (y - \eta)^2}}\, d\xi$$

Using the transformation $\rho = (x - \xi)$, the resulting integral may be found in Dwight[32]

$$J = \xi - \sqrt{(x - \xi)^2 + (y - \eta)^2} \tag{A29}$$

in which ξ is given the value of the limits.

The remaining integral must be considered over two intervals, one containing the point $y = \eta$ and one not containing this point. The latter situation provides no difficulty

$$I_8 = \int \frac{\xi - \sqrt{(x - \xi)^2 + (y - \eta)^2}}{(y - \eta)^2}\, d\eta$$

$$= \xi \int \frac{d\eta}{(y - \eta)^2} - \int \frac{\sqrt{(x - \xi)^2 + (y - \eta)^2}}{(y - \eta)^2}\, d\eta$$

The first integral can be found immediately

$$\int \frac{d\eta}{(y - \eta)^2} = \frac{1}{y - \eta}$$

The second integral may be determined by employing the transformation

$$\rho = y - \eta$$

Then

$$- \int \frac{\sqrt{(x - \xi)^2 + (y - \eta)^2}}{(y - \eta)^2}\, d\eta = \int \frac{\sqrt{(x - \xi)^2 + \rho^2}}{\rho^2}\, d\rho$$

$$= \frac{\sqrt{(x - \xi)^2 + \rho^2}}{\rho} + \int \frac{d\rho}{\sqrt{(x - \xi)^2 + \rho^2}}$$

$$= - \frac{\sqrt{(x - \xi)^2 + \rho^2}}{\rho} + \ln\, [\rho + \sqrt{(x - \xi)^2 + \rho^2}]$$

The final result may be written

$$I_8 = \frac{\xi - \sqrt{(x - \xi)^2 + (y - \eta)^2}}{(y - \eta)} + \ln\left[(y - \eta) + \sqrt{(x - \xi)^2 + (y - \eta)^2}\right] \quad \text{(A30)}$$

If the interval of integration includes the point $y = \eta$ one must handle the resulting singular integrand. This may be accomplished by employing the Mangler Principal Value[26] which is defined as

$$\oint_a^b \frac{f(\eta)\, d\eta}{(y - \eta)^2} = \lim_{\varepsilon \to 0} \left[\int_a^{y - \varepsilon} \frac{f(\eta)\, d\eta}{(y - \eta)^2} + \int_{y + \varepsilon}^{b} \frac{f(\eta)\, d\eta}{(y - \eta)^2} - \frac{2\, f(y)}{\varepsilon} \right]$$

It may be shown that the resulting limit is identical to the result given in Equation (A30).

By substituting arbitrary constant limits into Equation (A28), the functional form employed in Chapter V may be obtained

$$I_8(x, y; a, b, c, d) \equiv \int_c^d \frac{d\eta}{(y - \eta)^2} \int_a^b \left(1 + \frac{x - \xi}{r}\right) d\xi$$

$$= \frac{(b - a) + \sqrt{(y - d)^2 + (x - a)^2} - \sqrt{(y - d)^2 + (x - b)^2}}{y - d}$$

$$- \frac{(b - a) + \sqrt{(y - c)^2 + (x - a)^2} - \sqrt{(y - c)^2 + (x - b)^2}}{y - c}$$

$$+ \ln \frac{y - c + \sqrt{(y-c)^2 + (x-a)^2}}{y - c + \sqrt{(y-c)^2 + (x-b)^2}}$$

$$- \ln \frac{y - d + \sqrt{(y-d)^2 + (x-a)^2}}{y - d + \sqrt{(y-d)^2 + (x-b)^2}} \qquad \text{(A31)}$$

Although the integral employed for the downwash calculations is a special case of Equation (A28) use was made of the fact that the integrand was symmetric. The integrations were therefore performed over an element and its reflection about the x-axis.

$$I_9 \equiv \int_c^d \frac{d\eta}{\eta^2} \int_a^b \left(1 + \frac{x - \xi}{r}\right) d\xi + \int_{-d}^{-c} \frac{d\eta}{\eta^2} \int_a^b \left(1 + \frac{x - \xi}{r}\right) d\xi \qquad \text{(A32)}$$

$$I_9 = 2 \left[- \frac{(b-a) + \sqrt{d^2 + (x-a)^2} - \sqrt{d^2 + (x-b)^2}}{d} \right.$$

$$+ \frac{(b-a) + \sqrt{c^2 + (x-a)^2} - \sqrt{c^2 + (x-b)^2}}{c}$$

$$\left. + \ln \frac{d + \sqrt{d^2 + (x-a)^2}}{d + \sqrt{d^2 + (x-b)^2}} - \ln \frac{c + \sqrt{c^2 + (x-a)^2}}{c + \sqrt{c^2 + (x-b)^2}} \right] \qquad \text{(A33)}$$

where use has been made of the identity[32]

$$\ln\left(x+\sqrt{x^2+b}\right) = -\ln\left(-x+\sqrt{x^2+b}\right)$$

For elements lying along the x-axis (c = 0) the Mangler Principal Value[26] must be obtained. The resulting form is

$$I_9\,(x,\,y;\,a,\,b,\,0,\,d) \equiv \int_{-d}^{d} \frac{d\eta}{\eta^2} \int_a^b \left(1+\frac{x-\xi}{r}\right) d\xi$$

$$= 2\left[-\frac{(b-a)+\sqrt{d^2+(x-a)^2}-\sqrt{d^2+(x-b)^2}}{d} + \ln\frac{d+\sqrt{d^2+(x-a)^2}}{d+\sqrt{d^2+(x-b)^2}} - \ln\frac{x-a}{x-b}\right]$$

(A34)

APPENDIX B

Algorithms for the Complete Elliptic Integrals

There are a number of existing algorithms which are capable of providing extremely accurate results for the three types of elliptic integrals. Because of the frequent number of times it is necessary to compute these integrals it was also important to obtain methods which were relatively quick. It was for this reason that the below algorithms were chosen for the first and second elliptic integrals over methods which employed Landen or Gaub transformations.

A. Algorithm for the Computation of the First Complete Elliptic Integral[33]

$$K(k) = (((0.032024666\, k_c^{2} + 0.054544409)\, k_c^{2} + 0.097932891)\, k_c^{2} + 1.3862944) - (((0.010944912\, k_c^{2} + 0.060118519)\, k_c^{2} + 0.12475074)\, k_c^{2} + 0.5)\ \ln (k_c^{2}) \qquad \text{(B1)}$$

where $k_c^{2} = 1 - k^{2}$

B. Algorithm for the Computation of the Second Complete Elliptic Integral[34]

$$E(k) = (((0.040905094\, k_c^{2} + 0.085099193)\, k_c^{2} + 0.44479204)\, k_c^{2} + 1.0)$$

$$(((0.01382999\, k_c^{2} + 0.08150224)\, k_c^{2} + 0.24969795)\, k_c^{2})\ \ln (k_c^{2})$$

where $k_c^{2} = 1 - k^{2}$ (B2)

C. Algorithm for the Computation of the Third Complete Elliptic Integral[35]

Existing algorithms for the computation of the third complete elliptic integral are more complex than the above algorithms. The method of computation employed herein uses the Landen transformation and was found to provide excellent results.

Given: k_c, k^2, γ^2

$d = 1 - \gamma^2$

$PIFO = \pi/4$

$CA = 10^{-D/2}$ (yields about D significant figures)

IF $k_c \times d = 0$: FAILS

IF $k_c \times d \neq 0$: BEGINS

$k_c = |k_c|$

$MO = 1$

IF $d > 0$:

$c = 1/d + 1$

$d = \sqrt{d}$

$b = 1/d$

$f = 1$

IF $d < 0$:

$a = 1 - d$

$f = k_c \times k_c - d$

$d = \sqrt{f/a}$

$b = m/(a \times d)$

$c = -m/f$

$f = 0$

L1: $a = MO \times k_c$

$n = a/d$

$b = 2 \times (f \times n + b)$

$f = c$

$d = n + d$

$n = MO$

$c = b/d + c$

$MO = k_c + MO$

IF $|n - k_c| > CA \times n$:

$k_c = 2\sqrt{a}$

Go to L1

IF $|n - k_c| \leq CA \times n$:

$\Pi(\gamma^2, k) = PIFO \times c/MO$

APPENDIX C

Calculation of the Initial Values for the Geometry of the Jet

For small values of the parameters C_J, α, and τ, results of Spence's[1] two-dimensional theory was utilized for the determination of initial values for the jet geometry in the plane of symmetry. The necessary equations are summarized below.

$$f_J(\phi_1) = 2\tau\,(1 - \cos\tfrac{1}{2}\phi_1) + \alpha[\tan^2\tfrac{1}{2}\phi_1(\sin\tfrac{1}{2}\phi_1 - 1) + \sin\tfrac{1}{2}\phi_1 - \ln(\tan(\tfrac{\phi_1}{4} + \tfrac{\pi}{4}))] + 2\,(A_0\tau + B_0\alpha)[\sin\tfrac{1}{2}\phi_1 - \ln(\tan(\tfrac{\phi_1}{4} + \tfrac{\pi}{4}))] + \sum_{n=1}^{N-1}\frac{2(A_n\tau + B_n\alpha)}{4n^2 - 1}[2n\cos n\phi_1 \sin\tfrac{1}{2}\phi_1 - \sin n\phi_1\cos\tfrac{1}{2}\phi_1] \tag{C1}$$

$$\frac{df_J(\phi_1)}{dx} = -\tau\cos^3\tfrac{1}{2}\phi_1 + \alpha(\sin\tfrac{1}{2}\phi_1 - 1) - (A_0\tau + B_0\alpha)\sin\tfrac{1}{2}\phi_1\cos^2\tfrac{1}{2}\phi_1 + \cos^3\tfrac{1}{2}\phi_1\sum_{n=1}^{N-1}(A_n\tau + B_n\alpha)\sin n\phi_1 \tag{C2}$$

$$\kappa(\phi_1) = \frac{2}{C_J}\cos^3\tfrac{1}{2}\phi_1\left[-\frac{2\tau}{\pi}\ln(\tan\tfrac{1}{2}\phi_1) + \sum_{n=0}^{N-1}(A_n\tau + B_n\alpha)\cos n\phi_1\right] \tag{C3}$$

where

$$x = \frac{1}{\cos^2\tfrac{1}{2}\phi_1} - 1 \quad ; \quad 0 \leq x \leq \infty \tag{C4}$$

and A_n, B_n are solutions to the sets of simultaneous linear equations

$$(a_{m0} + \frac{4}{C_J} b_{m0})A_0 + \sum_{n=1}^{N-1} (a_{mn} + \frac{4}{C_J} b_{mn}) A_n = c_m + \frac{4}{C_J} d_m \quad ; m=0,\ldots,N-1$$

$$(a_{m0} + \frac{4}{C_J} b_{m0})B_0 + \sum_{n=1}^{N-1} (a_{mn} + \frac{4}{C_J} b_{mn}) B_n = e_m \quad ; m=0,\ldots,N-1$$

where

$$a_{m0} = \sin \phi_m$$

$$a_{mn} = (1 + \cos \phi_m) \sin n\phi_m \quad ; n > 0$$

$$b_{mn} = \frac{4}{4n^2-1} (\cos n\phi_m + 2n \tan \frac{1}{2} \phi_m \sin n\phi_m)$$

$$c_m = -(1 + \cos \phi_m)$$

$$d_m = \frac{8}{\pi} [\sec \frac{1}{2} \phi_m \ln (\tan \frac{1}{4} \phi_m) - \ln (\tan \frac{1}{4} \phi_m)]$$

$$e_m = - 2 \sec \frac{1}{2} \phi_m (1 - \sin \frac{1}{2} \phi_m)$$

and

$$\phi_m = \frac{m\pi}{n} \quad ; m=0,\ldots,N-1$$

Because Spence employed assumptions inherent to linear aerodynamic theory, the relation for the curvature, Equation C3, was obtained from the approximation

$$\kappa \sim \frac{d^2 f_J}{dx^2}$$

APPENDIX D

Curvature Integration Algorithm

The computations of the iteration scheme employed for the solution of the jet problem are initiated with a set of values for the jet curvature at the control points. These values are utilized to determine the resulting jet slope values at the same locations. This task is not as straightforward as might be presumed since the integrals of the curvature must be properly bounded in order to ensure the evaluation of the jet slopes. The definition of curvature

$$\kappa = \frac{\left| \frac{d}{dx} \left(\frac{df_J}{dx} \right) \right|}{\left[1 + \left(\frac{df_J}{dx} \right)^2 \right]^{3/2}} \tag{D1}$$

along with the condition

$$\left(\frac{df_J}{dx} \right)_{x=0} = - \tan\,(\tau + \alpha)$$

provides a first order differential equation for the jet slope which has the solution

$$\left(\frac{df_J}{dx} \right)_{x_n} = \frac{\Lambda_n}{\sqrt{1 - \Lambda_n^2}} \tag{D2}$$

where

$$\Lambda_n \equiv \frac{-\tan(\tau + \alpha)}{\sqrt{1 + \tan^2(\tau + \alpha)}} \int_0^{x_n} \kappa(x')\, dx' \tag{D3}$$

Obviously Λ_n and therefore the integral of the curvature must be properly bounded in order to ensure that the term under the radical of Equation (D2) does not become negative ($|\Lambda| \leq 1$). In addition, it is expected that the slope of the jet remains negative. Unfortunately, the set of curvature values predicted from a previous iterate may not satisfy this criterion. This dilemma is circumvented by bounding the integral

$$\int_0^{\infty} \kappa'\, dx' = \int_0^{x_N} \kappa'\, dx' + \int_{x_N}^{\infty} \kappa'\, dx' \tag{D4}$$

where x_N is the largest control point.

Because the curvature exhibits a logarithmic behavior, it has been established that the best method for obtaining the integral of the curvature at each of the N control points is by analytically integrating the approximation

$$s_J\ \kappa\left(\frac{x}{s_J}\right) = b_{-1}\ \frac{\ln\left(\frac{x}{s_J}\right)}{\left(\frac{x}{s_J} + 1\right)^{3/2}} + \sum_{m=0}^{M} b_m \left(\frac{x}{s_J}\right)^m \tag{D5}$$

The coefficients (b_m) in the above series are determined for each interval ($x_{n+1} - x_n$) by satisfying Equation (D5) at the M+1 control points closest to this interval. In this manner a set of values for the integrals

$$\int_0^{x_n} \kappa' \, dx' \tag{D6}$$

necessary for the evaluation of Λ_n (cf. Equation D3) and ultimately the first integral on the right hand side of Equation (D4) may be determined.

The remaining integral of Equation (D4) is obtained by employing the series approximation for the slope (refer to Section A2 of Chapter III).

$$\frac{df_J}{dx} = - \tan (\tau + \alpha) + \sum_{i=1}^{M} i \, a_i \left[1 - \frac{1}{(\bar{x} + 1)^{i+1}}\right]$$

where $\bar{x} = \nu x/s_J$. The second derivative of f_J may therefore be written

$$\frac{d^2 f_J}{dx^2} = \frac{\nu}{s_J} \sum_{i=1}^{M} i \, (i + 1) \, \frac{a_i}{(\bar{x} + 1)^{i+2}}$$

For large values of x, the above series may be truncated to provide the approximations

$$\frac{df_J}{dx} \sim - \tan (\tau + \alpha) + a_1 \left[1 - \frac{1}{(\bar{x} + 1)^2}\right] \tag{D7}$$

$$\frac{d^2 f_J}{dx^2} \sim \frac{2a_1 \nu}{s_J \, (\bar{x} + 1)^3} \tag{D8}$$

Substitution of Equations (D7) and (D8) into (D1) provides the resulting approximation for the curvature

$$\kappa \sim \frac{\dfrac{2a_1 \nu}{s_J (\bar{x} + 1)^3}}{\left(1 + \left[-\tan (\tau + \alpha) + a_1 \left(1 - \dfrac{1}{(\bar{x} + 1)^2}\right)\right]^2\right)^{3/2}}$$

where, from Equation (D7)

$$a_1 = \left(\frac{df_J}{dx}\right)_\infty + \tan (\tau + \alpha)$$

Therefore

$$\kappa \sim \frac{2\nu}{s_J} \frac{\left(\dfrac{df_J}{dx}\right)_\infty + \tan (\tau + \alpha)}{\left[1 + \left(\dfrac{df_J}{dx}\right)_\infty^2\right]^{3/2} (\bar{x} + 1)^3} \tag{D9}$$

Employing Equation (D9), it is now possible to obtain an approximate value for the remaining integral of Equation (D4)

$$\int_{x_N}^{\infty} \kappa' \, dx' \sim 2 \frac{\left(\dfrac{df_J}{dx}\right) + \tan (\tau + \alpha)}{\left[1 + \left(\dfrac{df_J}{dx}\right)^2\right]^{3/2}} \int_{\bar{x}_N}^{\infty} \frac{d\bar{x}'}{(\bar{x}' + 1)^3} \sim \frac{\bar{x}_N + 1}{2\nu} s_J \kappa_N \tag{D10}$$

Combining Equations (D2), (D3), (D4), and (D10)

$$\frac{\left(\dfrac{df_J}{dx}\right)_\infty}{\sqrt{1 + \left(\dfrac{df_J}{dx}\right)_\infty^2}} + \frac{\tan (\tau + \alpha)}{\sqrt{1 + \tan^2 (\tau + \alpha)}} = \int_0^{x_N} \kappa' \, dx' + \frac{\bar{x}_N + 1}{2\nu} s_J \kappa_N \tag{D11}$$

A value for the right hand side of Equation (D11) has already been obtained. Therefore, by assuming a value for $(df_J/dx)_\infty$ (one would expect the slope of the jet at infinity to lie within the range $\left(\frac{df_J}{dx}\right)_{x_N} < \left(\frac{df_J}{dx}\right)_\infty \leq 0$) a ratio of the values of the left and right hand sides of Equation (D11) may be obtained. This ratio provides a multiplying factor for the set of integral values of Equation (D6) resulting in a properly bounded set.

APPENDIX E

Calculation of the Grid Point Locations

The region of the jet located closest to the airfoil obviously supplies the dominant effects on the wing not only because of its proximity but also because it contains the largest values of the vortex strength. It is therefore advantageous to employ more control points in this region, the number increasing with increasing values of C_J, τ, and α. For this reason, the grid points (which ultimately provide the control point locations) are chosen to lie at equidistant intervals along the jet sheet.

With the jet slope known as a continuous function of x (refer to Section A2 of Chapter III) the arclength (ξ) along the jet is determined from the first order, linear ordinary differential equation

$$\frac{d\xi}{dx} = \sqrt{1 + \left(\frac{df_J}{dx}\right)^2} \equiv \Xi\ (x) \qquad \text{(E1)}$$

where

$$\xi(x = 0) = 0$$

The solution to this system is obtained by utilizing a fourth order Runge-Kutta[23] technique to obtain the necessary starting values and a fourth order Adams-Moulton[24] scheme for the determination of the remaining values. For the problem of concern these two techniques may be written as

$$\xi_{n+1} = \xi_n + \frac{\Delta_n}{6} [\Xi(x_n) + 2\,\Xi(x_n + \tfrac{1}{2}\Delta_n) + \Xi(x_n + \Delta_n)] \tag{E2}$$

where $\Delta_n = x_{n+1} - x_n$

and

$$\xi_{n+1} = \xi_n + \frac{\Delta}{24} [9\,\Xi(x_{n+1}) + 19\,\Xi(x_n) - 5\,\Xi(x_{n-1}) + \Xi(x_{n-2})] \tag{E3}$$

where $\Delta = (x_{n+1} - x_n) = \text{constant}$

respectively.

Given a suitable interval ($\Delta\xi = h$), values of x_i ($i = 1, \ldots, 201$ herein) which provide equally spaced values for the arc length (ξ_i) may now be determined. Since x_2 ($\xi_1 = x_1 = 0$) is less than $\Delta\xi$ the procedure is initiated by choosing $\bar{x}_2 = h$ (the barred variables are used in or calculated from Equations (E2) and (E3), whereas the unbarred variables are those being sought) and calculating the resulting $\bar{\xi}_2$ from Equation (E2). If $\bar{\xi}_2$ (refer to Figure 28a) is greater than $\xi_2 = \xi_1 + \Delta\xi$ (which must be the case for the initial attempt) $\bar{x}_3$ and $\bar{\xi}_3$ are set equal to $\bar{x}_2$ and $\bar{\xi}_2$ respectively, the values of $\bar{x}_2$ and h are halved, and a new value for $\bar{\xi}_2$ is determined. This procedure is continued until $\bar{\xi}_2 < \xi_2$, is obtained (refer to Figure 28b). At this point the values of $\bar{\xi}_1$, $\bar{\xi}_2$, and $\bar{\xi}_3$ as well as their absissa ($\bar{x}_1$, $\bar{x}_2$, and $\bar{x}_3$), and ξ_2, are known therefore an interpolation scheme may be utilized to obtain x_2.

Having determined the three necessary starting values ($\bar{x}_1$, $\bar{x}_2$, $\bar{x}_3$) the implicit Adams-Moulton technique is now employed. $\bar{\xi}_3$ is first checked to insure its value is less than ξ_3 ($\xi_n = \xi_{n-1} + \Delta\xi$). If it is not $\bar{\xi}_4$, which is the value of $\bar{\xi}$ at $\bar{x}_3 + h$ (where h is now the final result of the halving procedure described in the previous paragraph), is obtained from Equation (E3). This marching technique is continued until $\bar{\xi}_i$ is determined such that $\bar{\xi}_i > \xi_3$. The value of x_3 is then obtained from the interpolation scheme (refer to Figure 28c). This method is continued until an array containing the desired number of abscissa (x_i) has been determined.

A second order, divided difference interpolation technique[24] was chosen for the determination of the abscissa (x_k). This scheme has the form

$$x_k = x[\bar{\xi}_{i-2}] + (\xi_k - \bar{\xi}_{i-2})\, x[\bar{\xi}_{i-2}, \bar{\xi}_{i-1}] + (\xi_k - \bar{\xi}_{i-2})(\xi_k - \bar{\xi}_{i-1})\, x[\bar{\xi}_{i-2}, \bar{\xi}_{i-1}, \bar{\xi}_i]$$

where $x[\bar{\xi}_{i-j},\ldots,\bar{\xi}_i]$ is a divided difference. Therefore,

$$x[\bar{\xi}_{i-2}] = \bar{x}_{i-2}$$

$$x[\bar{\xi}_{i-2}, \bar{\xi}_{i-1}] = \frac{\bar{x}_{i-1} - \bar{x}_{i-2}}{\bar{\xi}_{i-1} - \bar{\xi}_{i-2}}$$

$$x[\bar{\xi}_{i-2}, \bar{\xi}_{i-1}, \bar{\xi}_i] = \frac{1}{\bar{\xi}_i - \bar{\xi}_{i-2}}\left(\frac{\bar{x}_i - \bar{x}_{i-1}}{\bar{\xi}_i - \bar{\xi}_{i-1}} - \frac{\bar{x}_{i-1} - \bar{x}_{i-2}}{\bar{\xi}_{i-1} - \bar{\xi}_{i-2}}\right)$$

The values $\bar{\xi}_i$, $\bar{\xi}_{i-1}$, and $\bar{\xi}_{i-2}$ are chosen such that only $\bar{\xi}_i$ is greater than ξ_k (refer to Figure 28c).

APPENDIX F

Evaluation of the Integrals Associated With the Jet Problem in a Neighborhood of the Control Point

Consider the problem of evaluating the Cauchy principal value

$$\oint_{x-\varepsilon_1}^{x+\varepsilon_2} \frac{f(x')}{x-x'}\,dx' \tag{F1}$$

which involves a singularity at the point $x' = x$. The function $f(x')$ is continuous and non-singular in the region of concern (refer to Section A1 of Chapter IV). Consequently, for small values of ε_1 and ε_2, a sufficient approximation for this integral may be obtained by employing a fourth degree polynomial approximation for $f(x')$. The resulting integration may then be performed analytically.

The method used herein employs Lagrange's interpolation formula[24] for approximating $f(x')$ in the region $x_o \leq x' \leq x_4$ (where $x_o < x-\varepsilon_1$ and $x_4 > x+\varepsilon_2$)

$$f(x') = \sum_{i=0}^{4} Q_i(x')\ f(x_i) \tag{F2}$$

where

$$Q_i = \frac{(x'-x_j)(x'-x_k)(x'-x_m)(x'-x_n)}{(x_i-x_j)(x_i-x_k)(x_i-x_m)(x_i-x_n)} \quad ;\ j,k,m,n \neq i \tag{F3}$$

and

$$x_1 = x-\varepsilon_1$$

$$x_2 = x$$

$$x_3 = x+\varepsilon_2$$

Defining

$$A_i = \frac{1}{(x_i-x_j)(x_i-x_k)(x_i-x_m)(x_i-x_n)} \qquad ; \; j,k,m,n \neq i \qquad \text{(F4)}$$

Equation (F3) may be written

$$Q_i = A_i \; (x'^4 - a_{3i}\, x'^3 + a_{2i}\, x'^2 - a_{1i}\, x' + a_{0i}) \qquad \text{(F5)}$$

where

$$a_{0i} = x_j\, x_k\, x_m\, x_n$$

$$a_{1i} = x_j (x_k(x_m+x_n) + x_m\, x_n) + x_k\, x_m\, x_n$$

$$a_{2i} = x_j (x_k + x_m + x_n) + x_k(x_m + x_n) + x_m\, x_n$$

$$a_{3i} = x_j + x_k + x_m + x_n$$

for $j,k,m,n \neq i$. Employing the identity $x' = x - (x-x')$, Equation (F5) may be expressed in the form

$$Q_i = A_i \; \{(x-x')^4 + [a_{3i} - 4x]\; (x-x')^3 + [a_{2i} - 3x\, a_{3i} + 6x^2]$$
$$(x-x')^2 + [a_{1i} - 2x\, a_{2i} + 3x^2\, a_{3i} - 4x^3]\; (x-x') +$$
$$[a_{0i} - x\, a_{1i} + x^2\, a_{2i} - x^3\, a_{3i} + x^4]\} \qquad \text{(F6)}$$

Substitution of Equation (F6) into Equation (F2) provides the result

$$f(x') = \sum_{i=0}^{4} B_i (x-x')^i$$

where

$$B_0 = \sum_{j=0}^{4} f(x_j)\, A_j [a_{0j} - x\, a_{1j} + x^2\, a_{2j} - x^3\, a_{3j} + x^4]$$

$$B_1 = \sum_{j=0}^{4} f(x_j)\, A_j [a_{1j} - 2x\, a_{2j} + 3x^2\, a_{3j} - 4x^3]$$

$$B_2 = \sum_{j=0}^{4} f(x_j)\, A_j [a_{2j} - 3x\, a_{3j} + 6x^2]$$

$$B_3 = \sum_{j=0}^{4} f(x_j)\, A_j\, [a_{3j} - 4x]$$

$$B_4 = \sum_{j=0}^{4} f(x_j)\, A_j$$

This last expression for f(x') may now be used in Equation (F1) to obtain desired approximation

$$\oint_{x-\varepsilon_1}^{x+\varepsilon_2} \frac{f(x')}{(x-x')} dx' = \sum_{j=1}^{4} \frac{B_j}{j} \cdot [\varepsilon_1{}^j + (-1)^{j+1}\, \varepsilon_2{}^j] + B_0 \ln \left|\frac{\varepsilon_1}{\varepsilon_2}\right| \tag{F8}$$

TABLE

COMPUTED RESULTS

τ = 31.3 degrees

C_J	α (degrees)	C_L	C_D	θ (degrees)	C_p
2.08	0	2.548	-1.777	8.62	0.02874
2.08	5	3.259	-1.499	11.01	0.04397
2.08	10	3.925	-1.113	13.28	0.06248
2.0	0	2.434	-1.709	8.22	0.02662
3.0	0	3.326	-2.563	10.37	0.04341
4.0	0	4.197	-3.418	12.35	0.06199
6.0	0	5.817	-5.127	15.43	0.09904
8.0	0	7.388	-6.836	18.00	0.13562

REFERENCES

1. Spence, D. A., "The Lift Coefficient of a Thin, Jet-Flapped Wing," Proc. Roy. Soc., Vol. A 238, 1956, pp. 46-68.

2. Maskell, E. C. and Spence, D. A., "A Theory of the Jet Flap in Three Dimensions," Proc. Roy. Soc., Vol. A 251, 1959, pp. 407-425.

3. Kerney, K. P., An Asymptotic Theory of the High-Aspect-Ratio Jet Flap, Ph.D. Thesis, School of Aeronautical Engineering, Cornell University, 1967.

4. Tokuda, N., "An Asymptotic Theory of the Jet Flap in Three Dimensions," J. Fluid Mech., Vol. 46, Pt. 4, 1971, pp. 705-726.

5. Lopez, M. L. and Shen, C. C., "Recent Developments in Jet Flap Theory and its Application to STOL Aerodynamic Analysis," Paper No. 71-578, AIAA Fourth Fluid and Plasma Dynamics Conference, June 21-23, 1971.

6. Lissaman, P. B. S., "A Linear Theory of the Jet Flap in Ground Effect," AIAA Journal, Vol. 6, No. 7, July 1968, pp. 1356-1362.

7. Lissaman, P. B. S., "Analysis of High-Aspect-Ratio Jet-Flapped Wings of Arbitrary Geometry," NASA CR-2179, 1973, pp. 1-56.

8. Leamon, R. G. and Plotkin, A., "An Improved Solution of the Two-Dimensional Jet-Flapped Airfoil Problem," J. Aircraft, Vol. 9, No. 9, Sept. 1972, pp. 631-635.

9. Halsey, N. D., "Methods for the Design and Analysis of Jet-Flapped Airfoils," J. Aircraft, Vol. 11, No. 9, Sept. 1974, pp. 540-546.

10. Williams, J. and Alexander, A. J., "Three-Dimensional Wind-Tunnel Tests of a 30° Jet Flap Model," A.R.C. C.P. No. 304, Nov. 1955, p. 1-49.

11. Panofsky, W. K. H. and Phillips, M., Classical Electricity and Magnetism, Addison-Wesley, 1962, pp. 1-7.

12. Morse, P. M. and Feshbach, H., Methods of Theoretical Physics, McGraw-Hill, 1953, Pt. I, pp. 52-54.

13. Russell, H. L., Application of the Scalcr and Vector Potentials to the Aerodynamics of Jets, Ph.D. Thesis, School of Mechanical Engineering, Purdue University, Jan. 1971.

14. Karamcheti, K., Principles of Ideal-Fluid Aerodynamics, Wiley, 1966.

15. Thwaites, B., Incompressible Aerodynamics, Oxford University Press, 1960.

16. Ashley, H. and Landahl, M. T., Aerodynamics of Wings and Bodies, Addison-Wesley, 1965.

17. Ames, W. F., Nonlinear Partial Differential Equations in Engineering, Academic, Vol. 18, 1965.

18. Ames, W. F., Nonlinear Partial Differential Equations in Engineering, Academic, Vol. 18-II, 1972.

19. Finlayson, B. A., The Method of Weighted Residuals and Variational Principles, Academic, 1972.

20. Davis, P. J. and Rabinowitz, P., Numerical Integration, Blaisdell, 1967.

21. Householder, A. S., Principles of Numerical Analysis, McGraw Hill, 1953.

22. Wolfe, P., "The Secant Method for Simultaneous Nonlinear Equations," CACM, Vol. 2, 1959, pp. 12-13.

23. Ralston, A., A First Courst in Numerical Analysis, McGraw Hill, 1965.

24. Hildebrand, F. B., Introduction to Numerical Analysis, McGraw Hill, 1956.

25. Robinson, A. and Laurmann, J. A., Wing Theory, Cambridge, 1956.

26. Multhopp, H., "Methods for Calculating the Lift Distribution of Wings," R. A. E. Rept. No.: AERO 2353, Appendix I, 1950.

27. Woodward, F. A., "Analysis and Design of Wing-Body Combinations at Subsonic and Supersonic Speeds," J. Aircraft, Vol. 5, No. 6, Nov.-Dec. 1968, pp. 528-534.

28. Williams, J., Butler, S. F. J., and Wood, M. N., "The Aerodynamics of Jet Flaps," Advances in Aeron. Sci., MacMillian, Vol. 4, 1960, pp. 619-656.

29. Wygnanski, I. and Newman, B. G., "The Effect of Jet Entrainment on Lift and Moment for a Thin Airfoil with Blowing," Aeron. Quart., Vol. XV, Pt. 2, May 1964, pp. 122-150.

30. Byrd, P. F. and Friedman, M. D., Handbook of Elliptic Integrals for Engineers and Physicists, Springer-Verlag, 1954.

31. Bois, G. P., Tables of Indefinite Integrals, Dover, 1961.

32. Dwight, H. B., Tables of Integrals and Other Mathematical Data, MacMillian, 1961.

33. Herndon, J. R., "Algorithm 55, Complete Elliptic Integral of the First Kind," CACM, 4, 1961, p. 180.

34. Herndon, J. R., "Algorithm 56, Complete Elliptic Integral of the Second Kind," CACM, 4, 1961, p. 180.

35. Bulirsch, R., "Numerical Calculation of Elliptic Integrals and Elliptic Functions," Numerische Mathematik, Vol. 7, 1965, pp. 78-90.

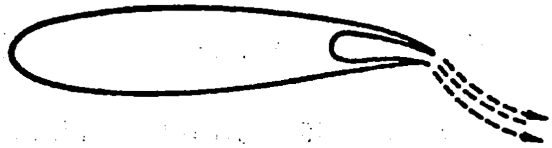

a) Jet Flap.

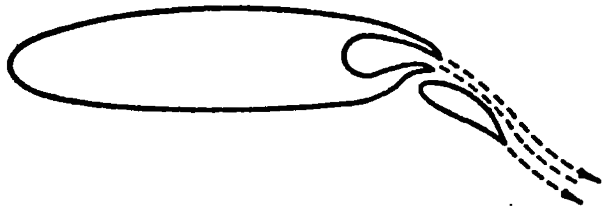

b) Blown Flap.

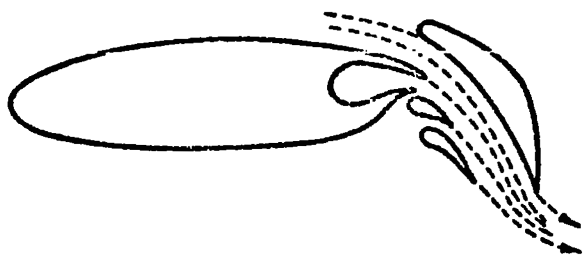

c) Augmentor Wing.

Figure 1. Powered Flap Configurations.

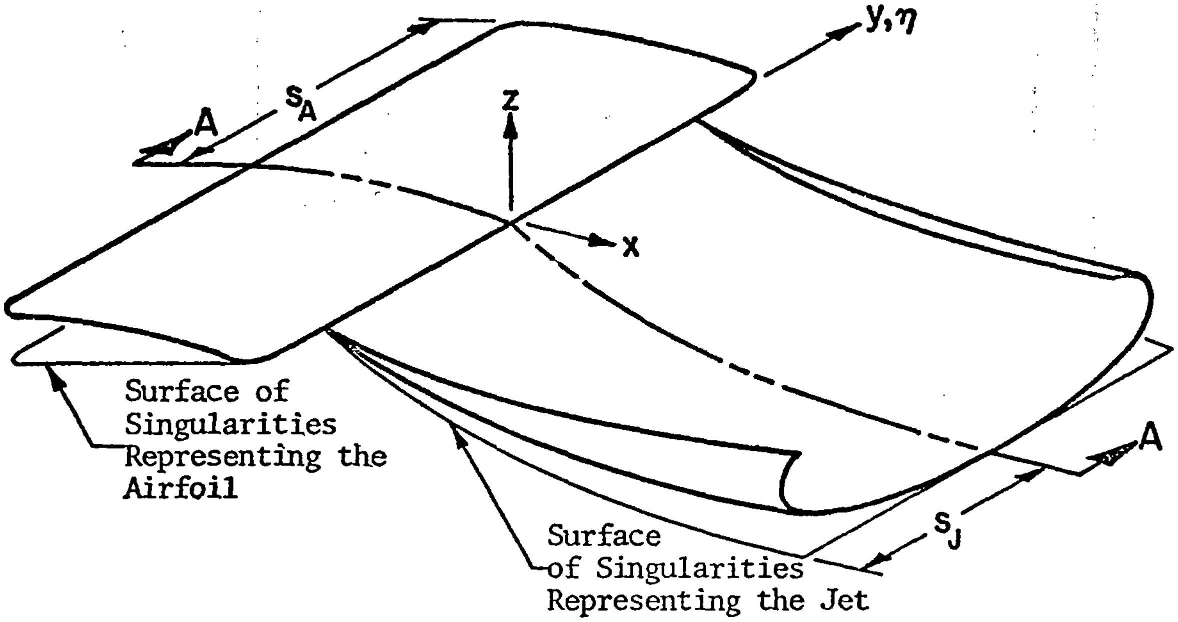

a) Locations of the Singularities and the Stream Surfaces.

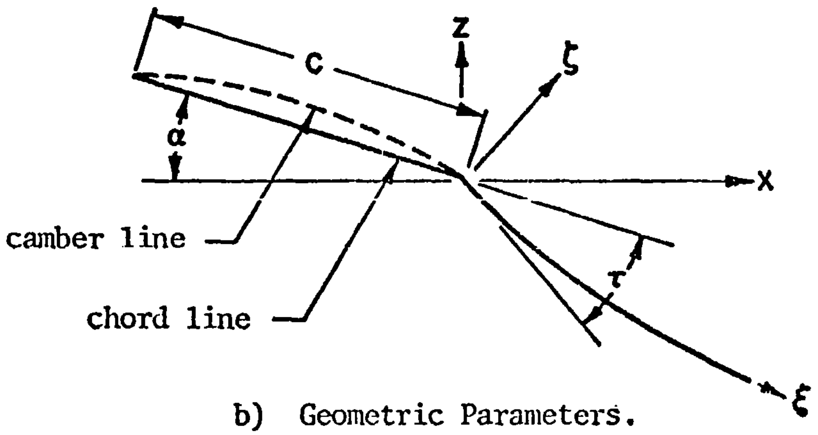

b) Geometric Parameters.

Figure 2. Jet-Flap and Airfoil Geometry.

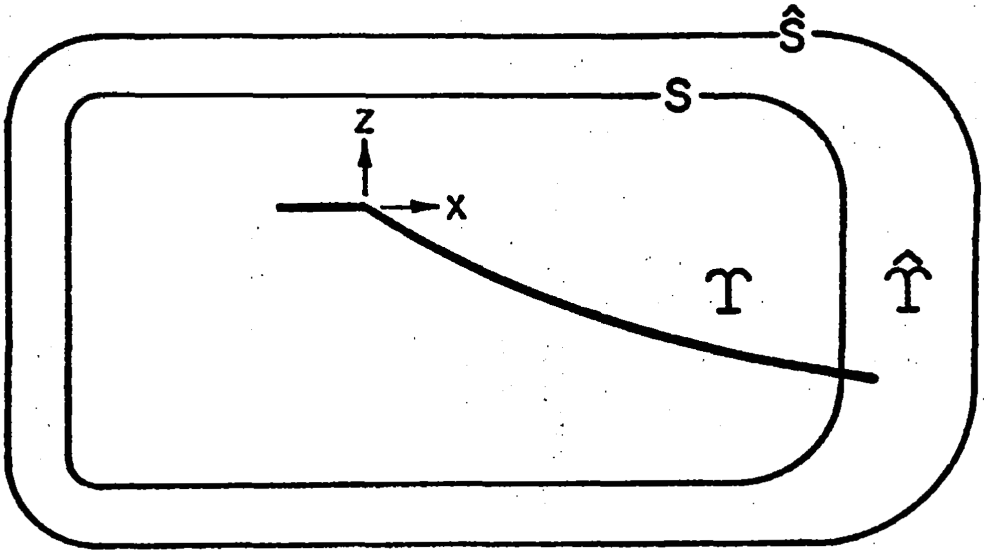

a) Control Volumes.

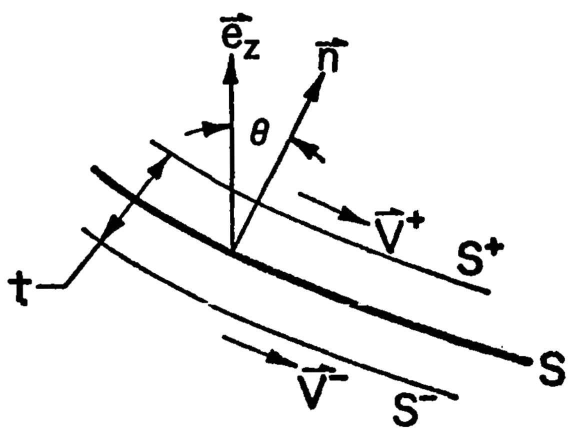

b) Nomenclature Associated with the Vortex Sheet.

Figure 3. Basic Flow Considerations.

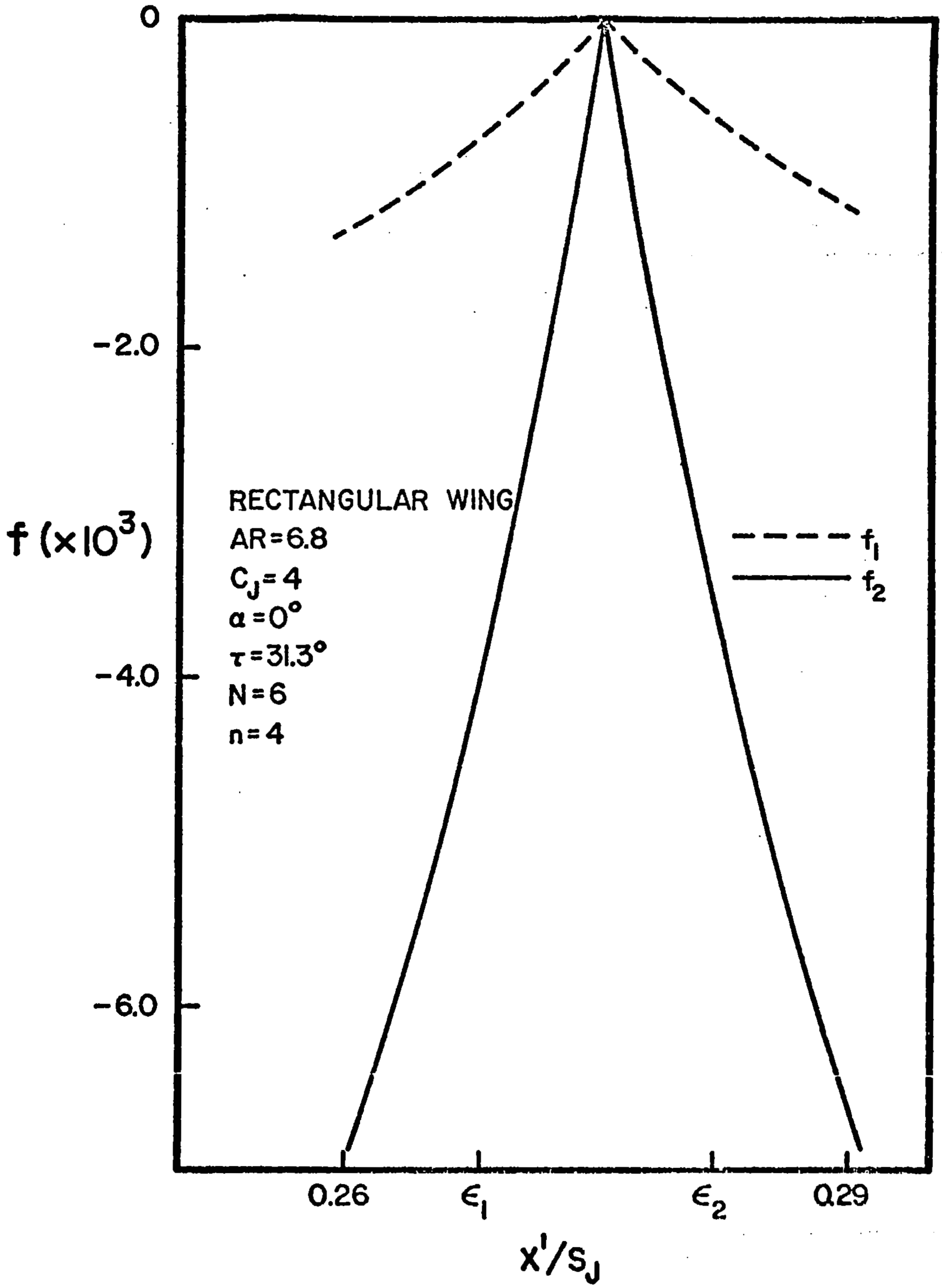

Figure 4. Variation of the Functions Employed in Obtaining the Cauchy Principal Value.

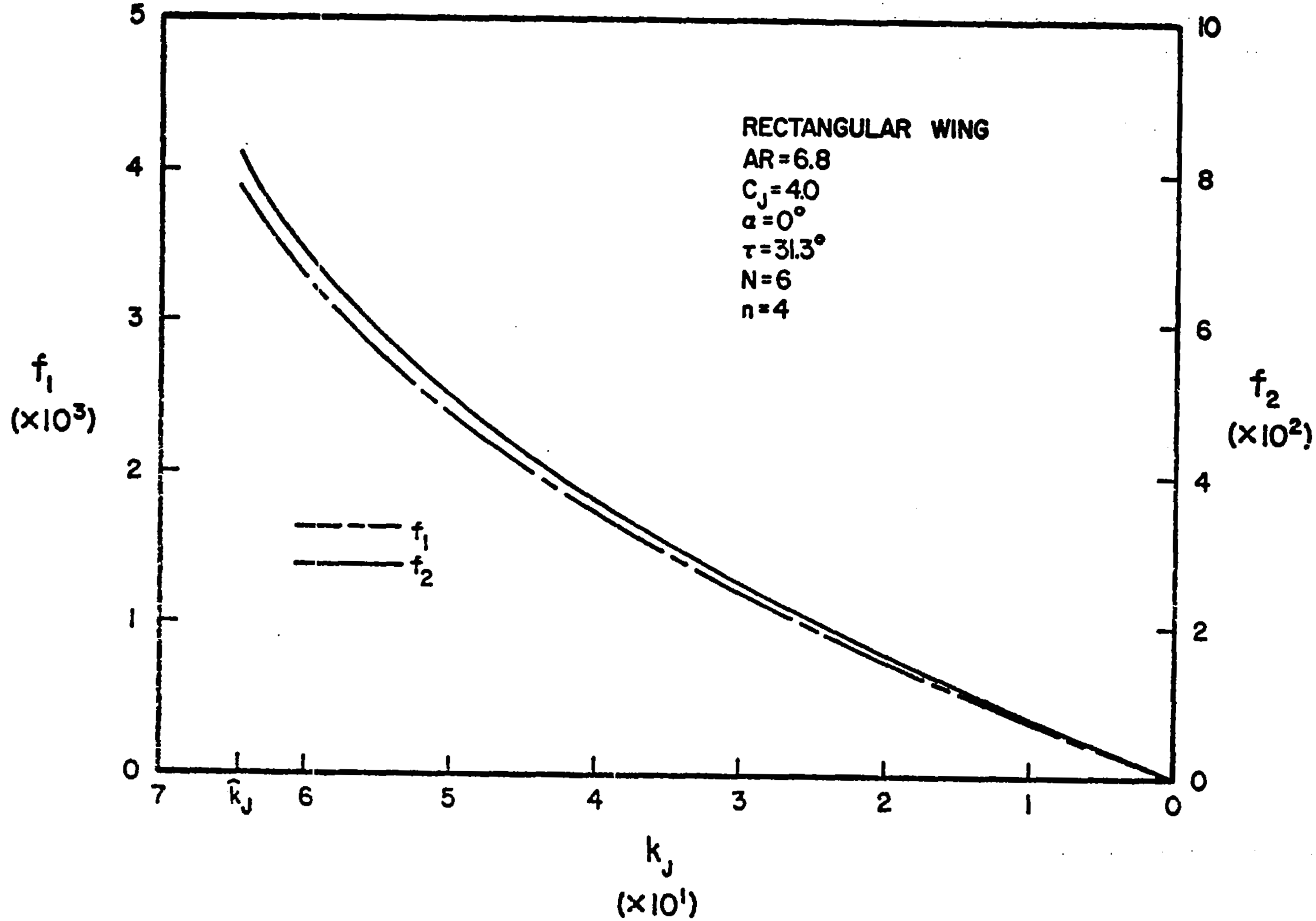

Figure 5. Variation of the Integrands Employed for Obtaining the Integrals with the Infinite Upper Limit.

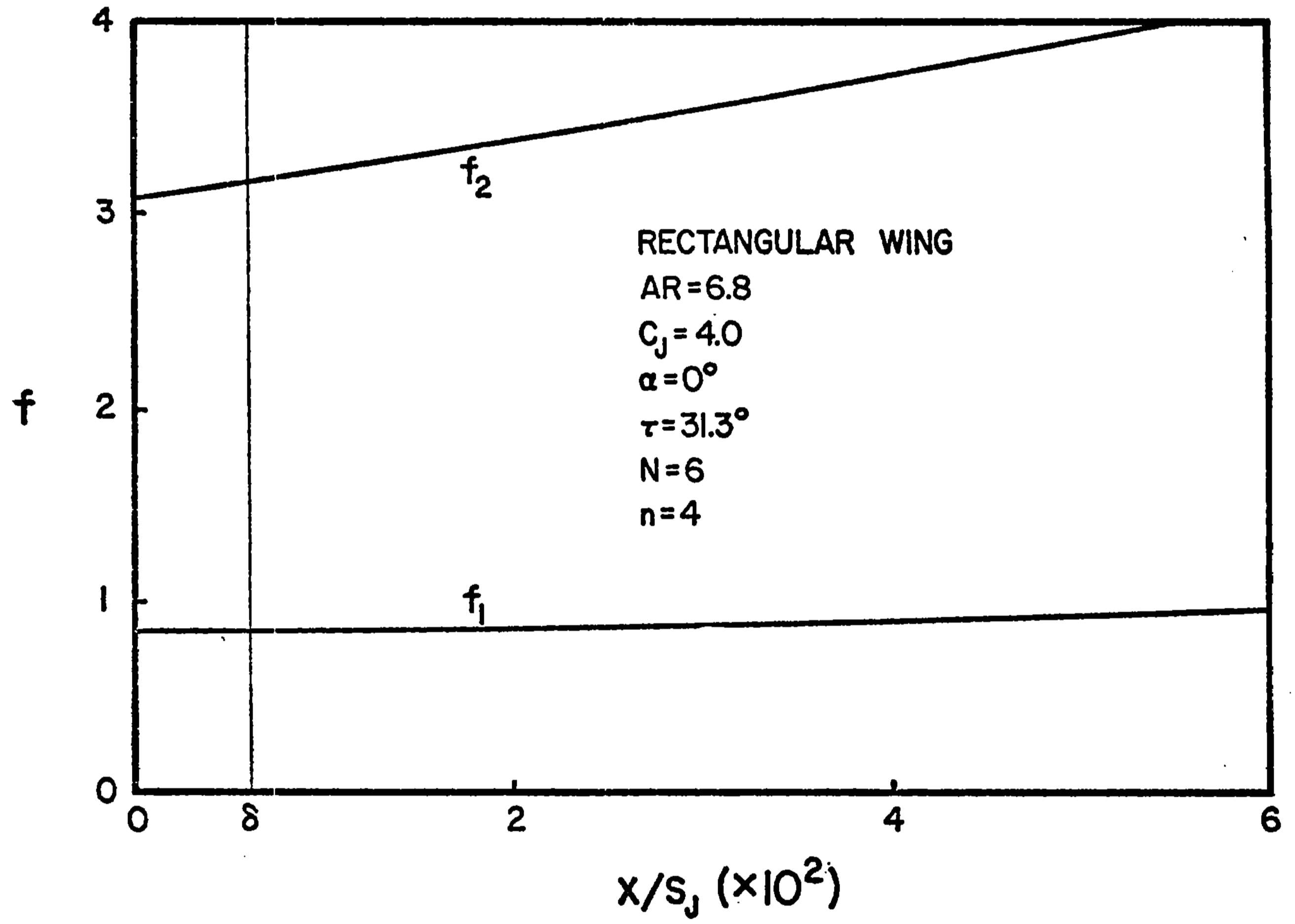

Figure 6. Variation of Terms Which are Factored from the Integrals in a δ Neighborhood of the Origin.

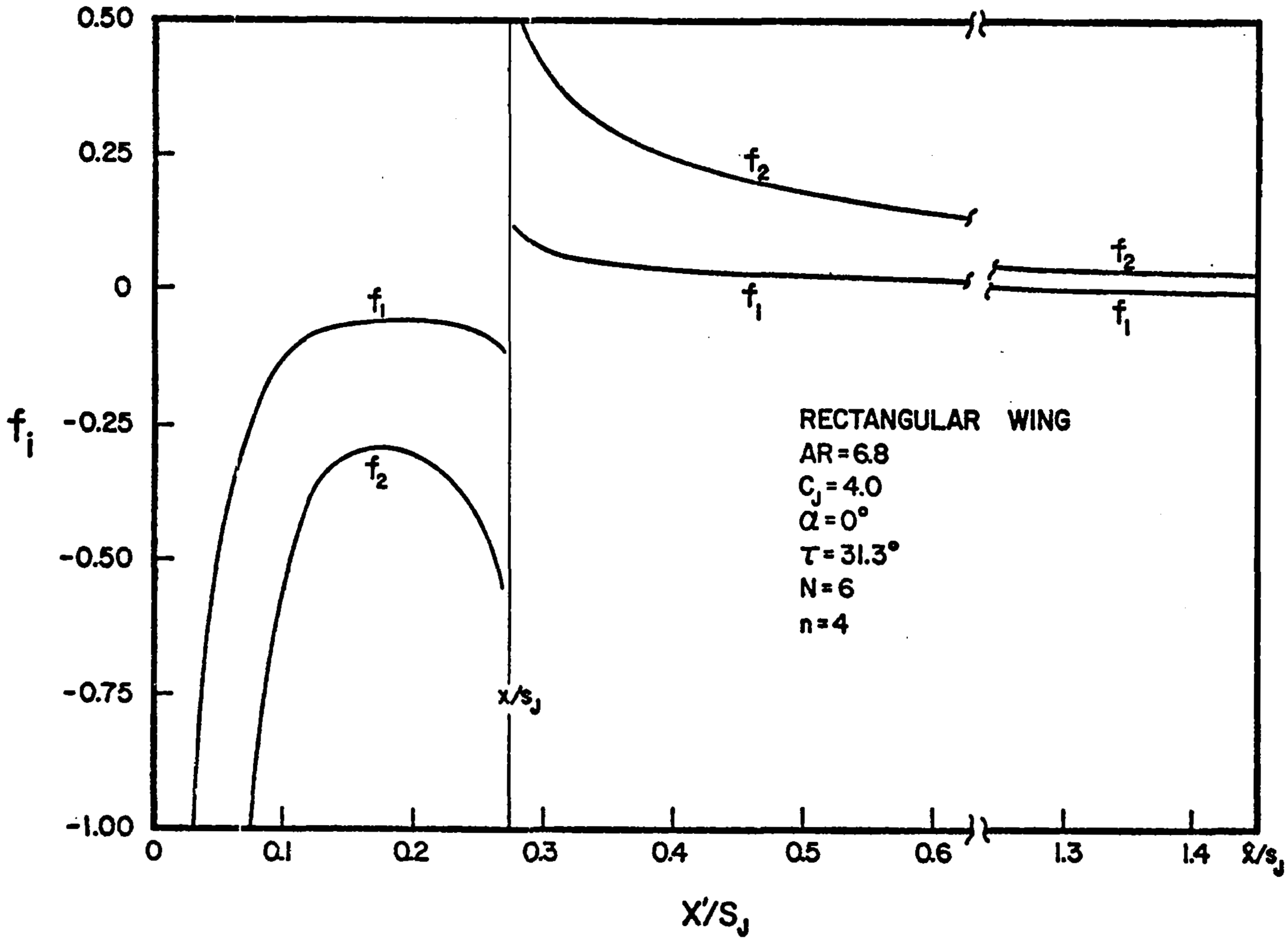

Figure 7. Variation of the Integrands About the Control Point.

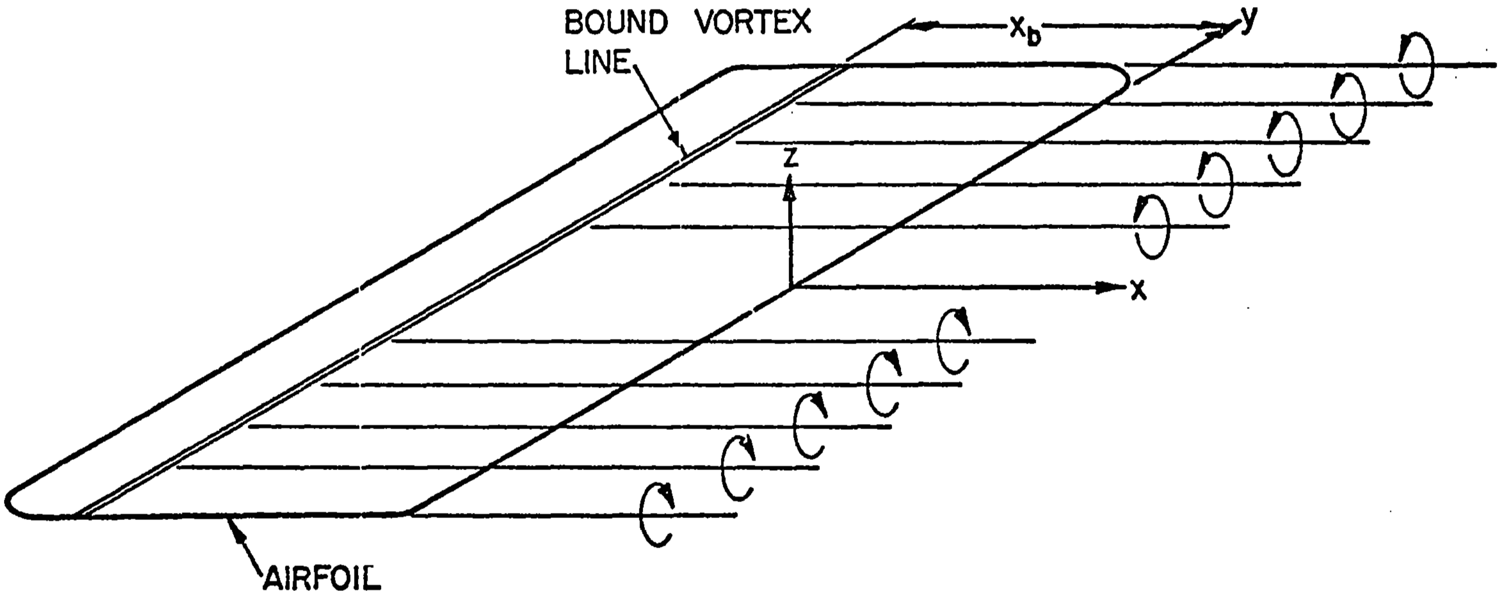

Figure 8. Horseshoe Vortex System.

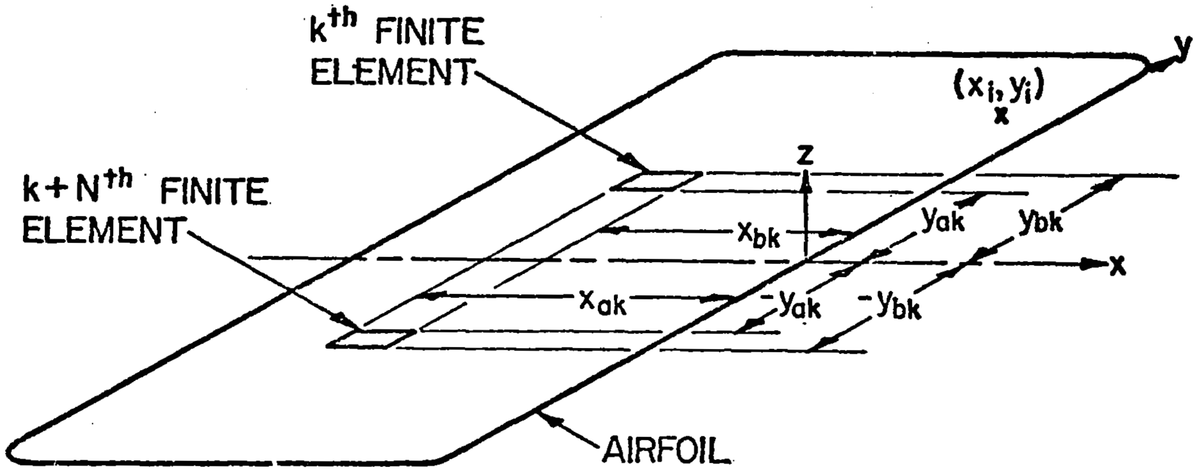

a) Location of the k^{th} Finite Element and its Reflection.

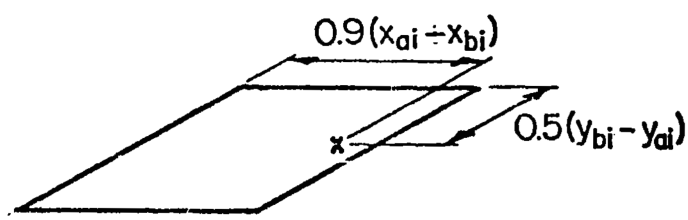

b) Location of the Control Point on the i^{th} Element.

Figure 9. Finite Element Geometry.

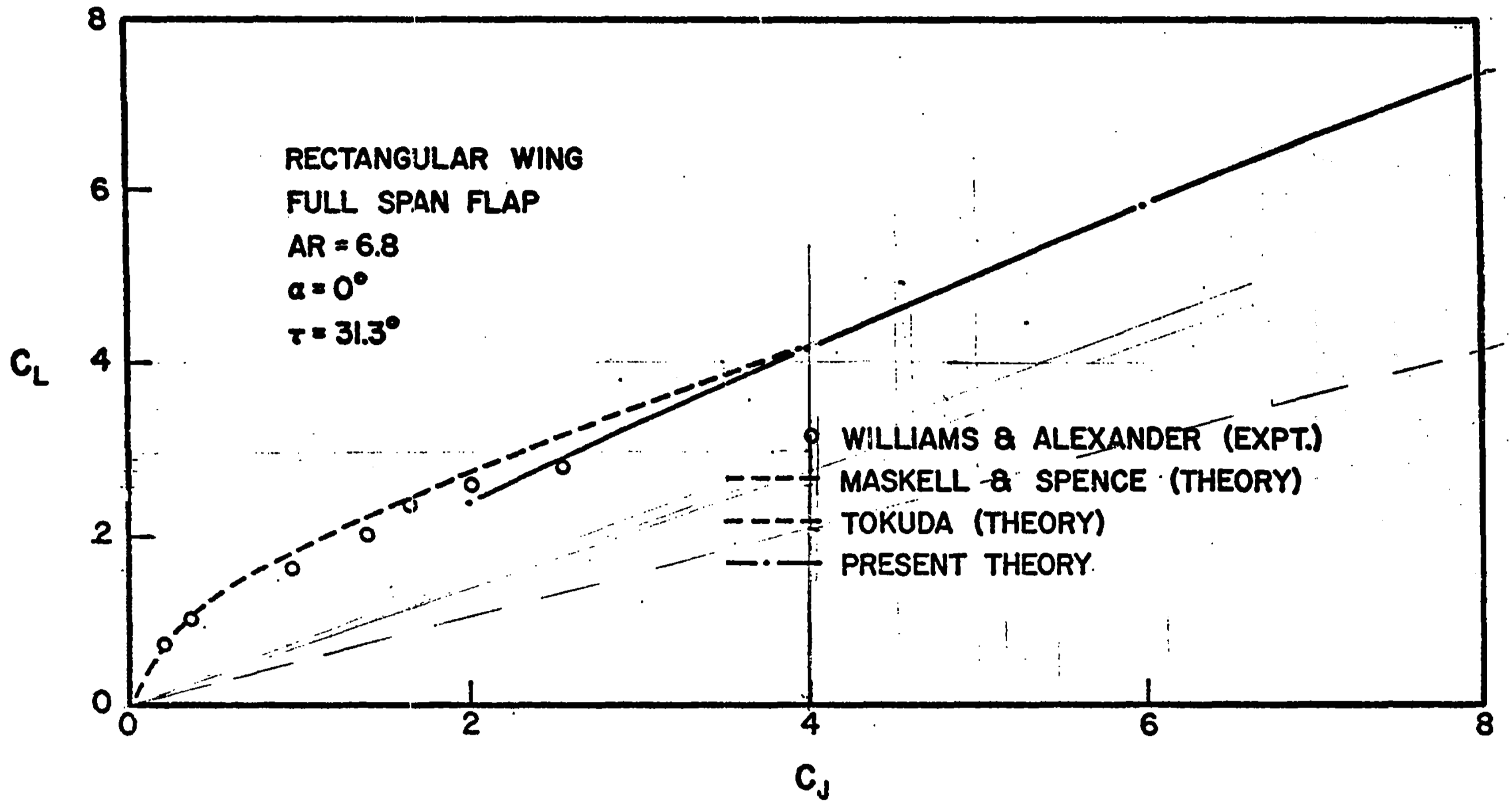

Figure 10. Variation of the Lift Coefficient with Jet Momentum Flux for $\alpha = 0°$.

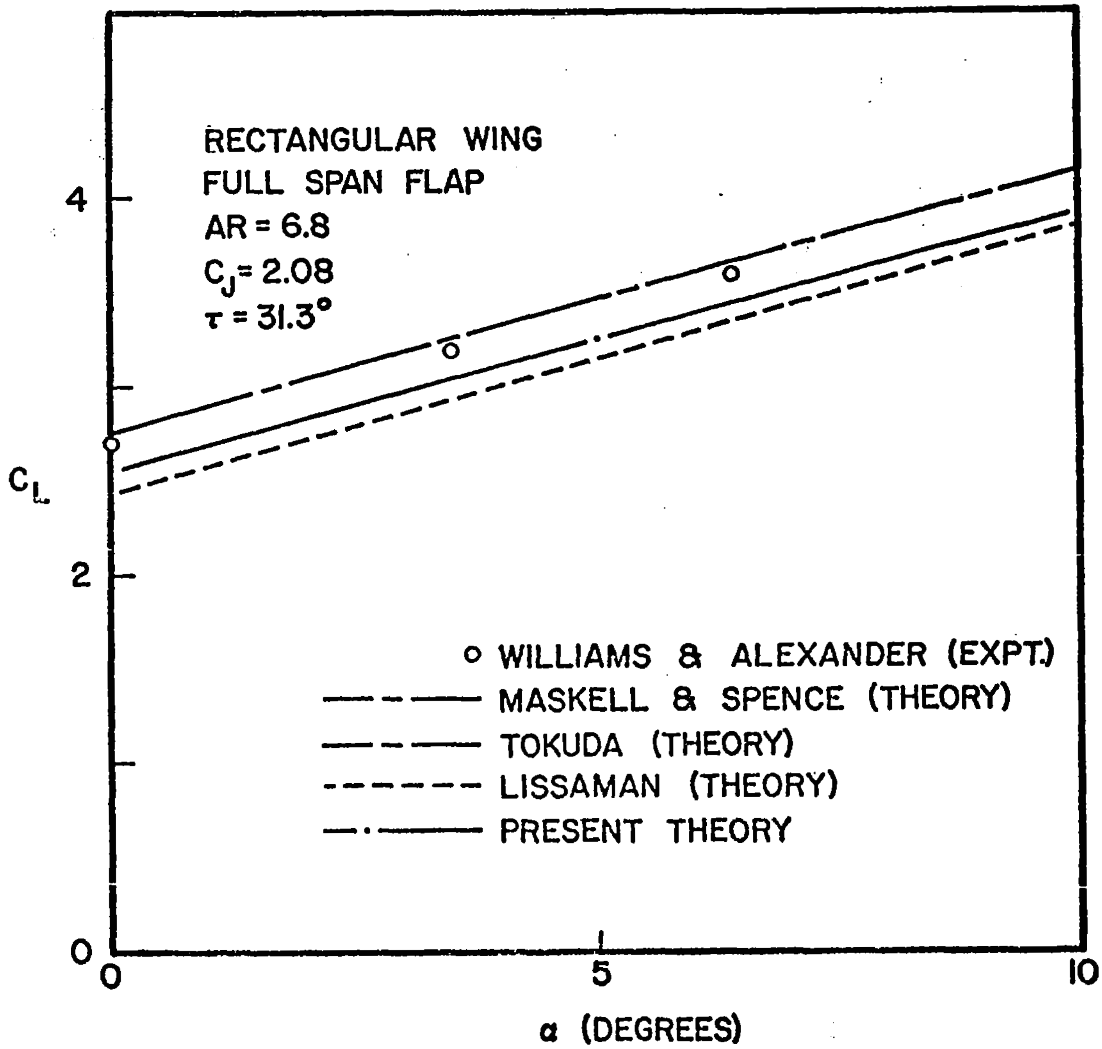

Figure 11. Variation of the Lift Coefficient with Angle of Attack for C_J = 2.08.

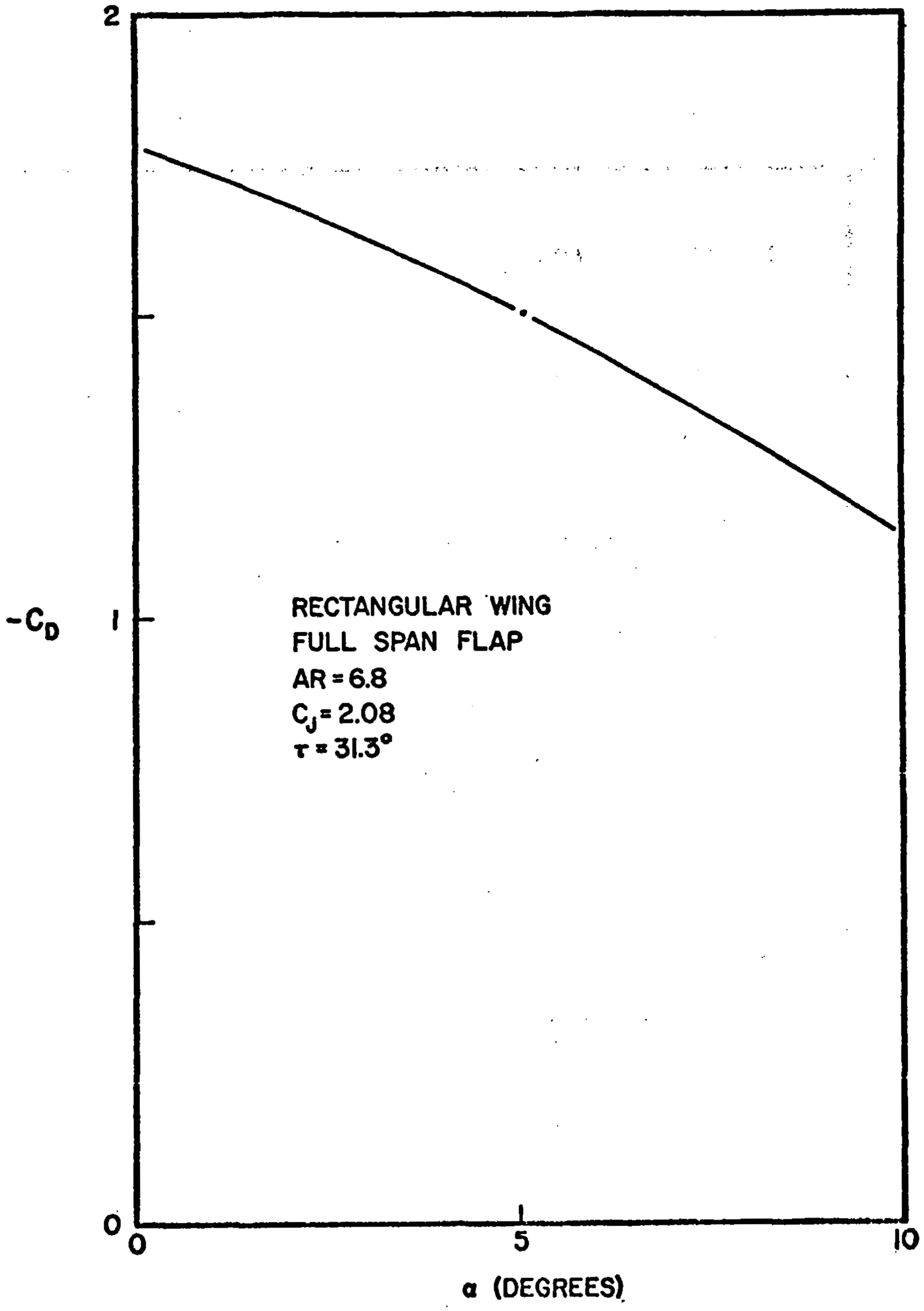

Figure 12. Variation of the Drag Coefficient with Angle of Attack for C_J = 2.08.

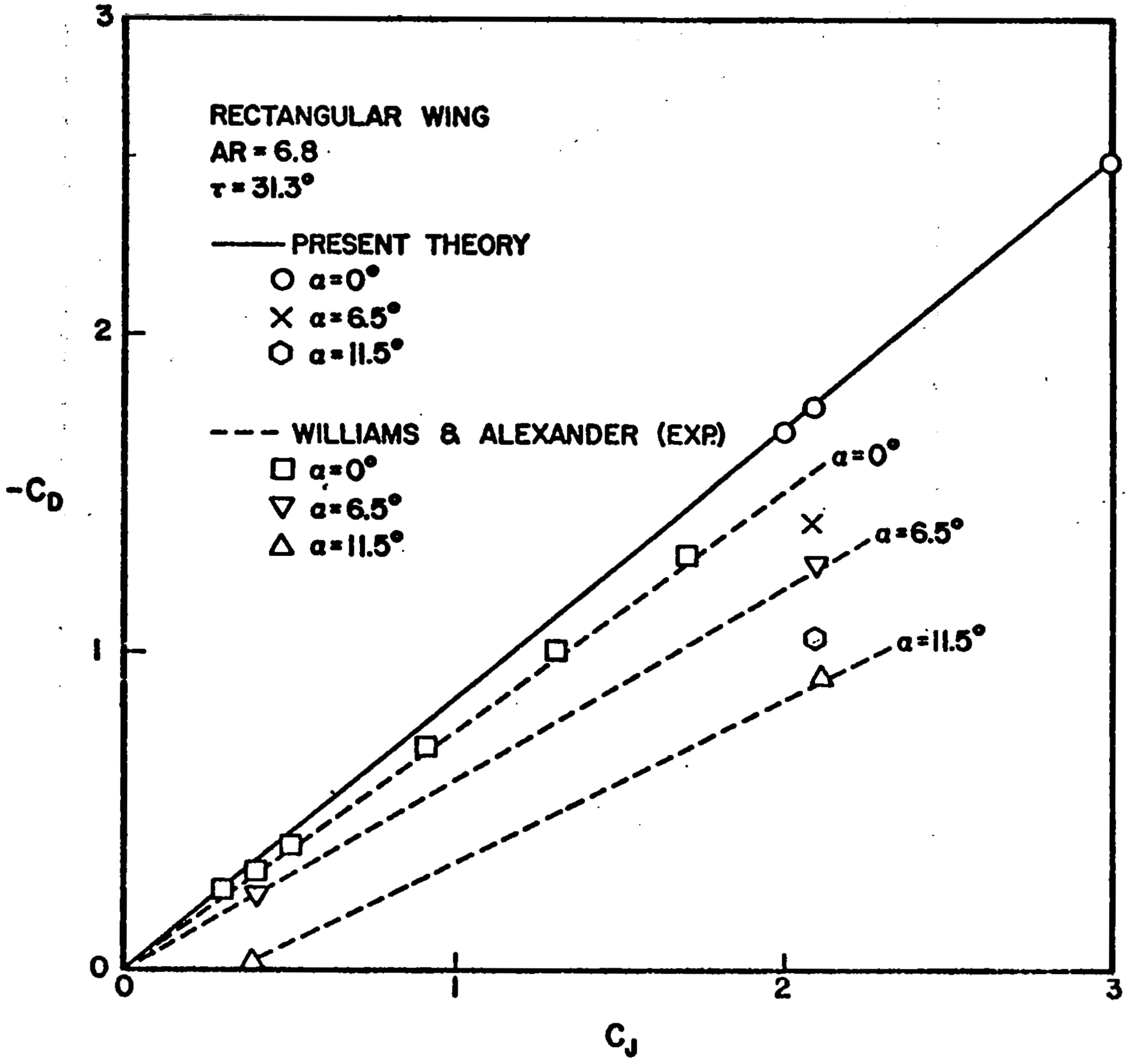

Figure 13. Variation of the Drag Coefficient with Jet Momentum Flux.

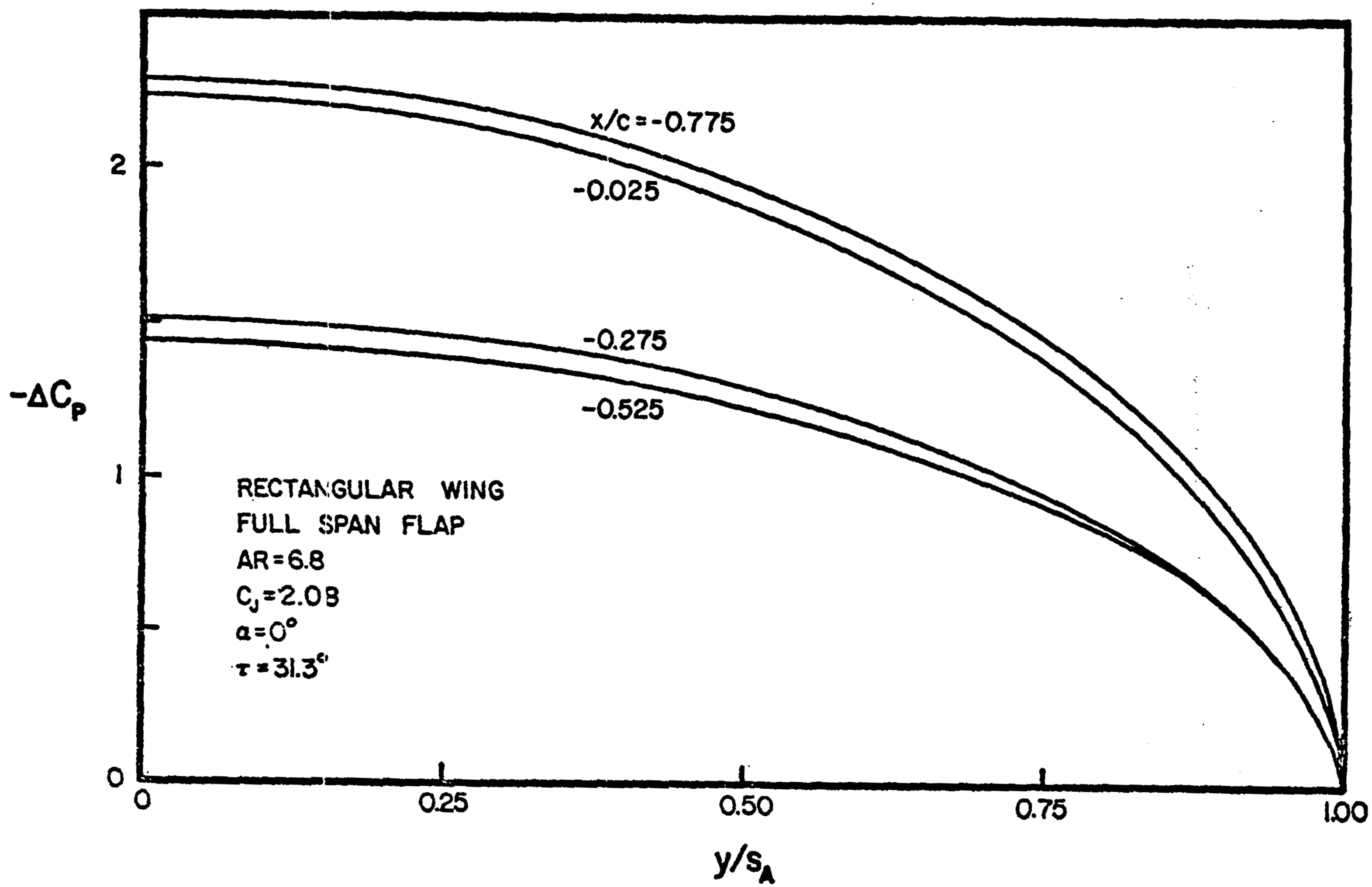

Figure 14. Spanwise Distribution of the Pressure Difference Across the Airfoil for $C_J = 2.08$ and $\alpha = 0°$.

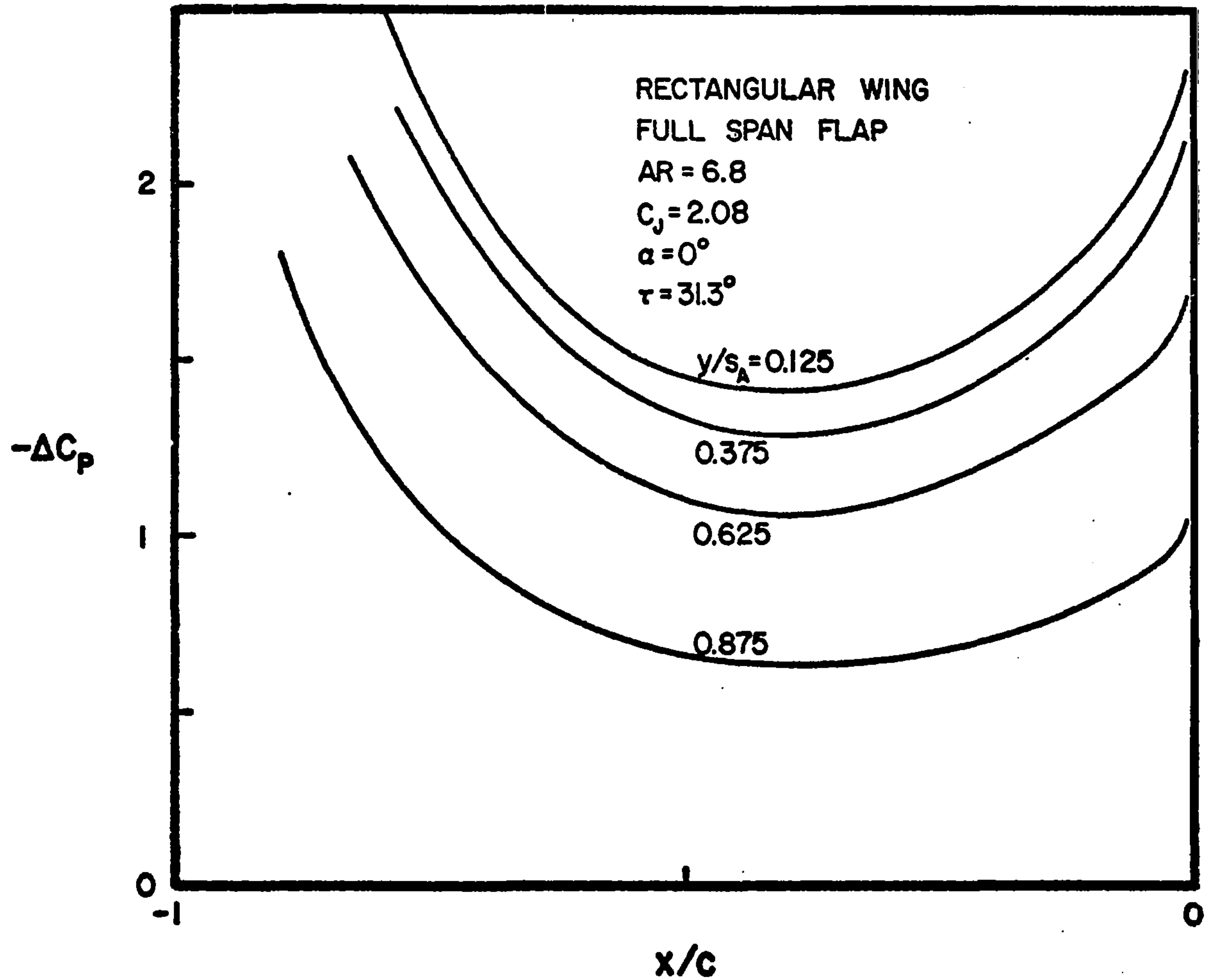

Figure 15. Streamwise Distribution of the Pressure Difference Across the Airfoil for C_J = 2.08 and α = 0°.

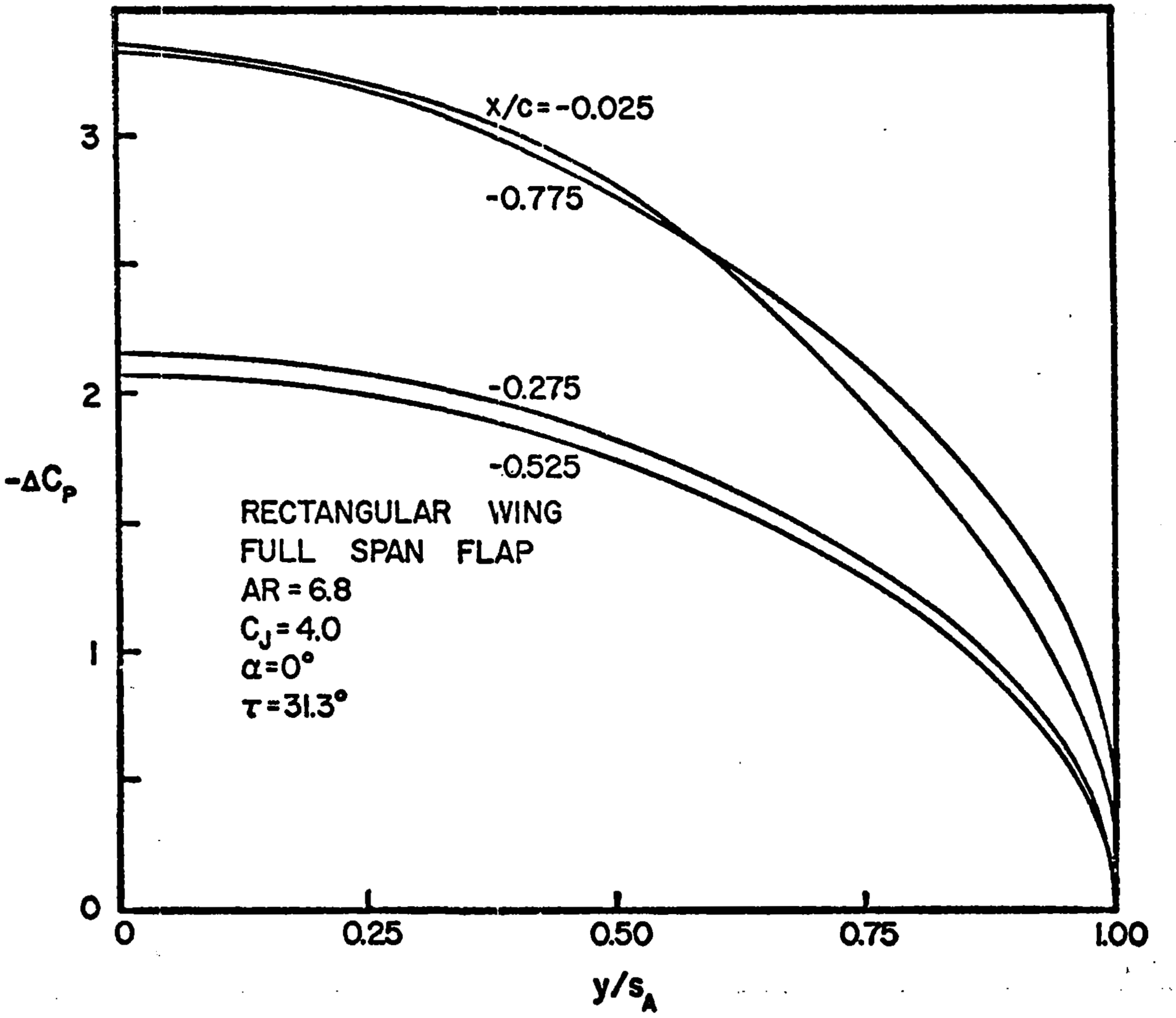

Figure 16. Spanwise Distribution of the Pressure Difference Across the Airfoil for $C_J = 4.0$ and $\alpha = 0°$.

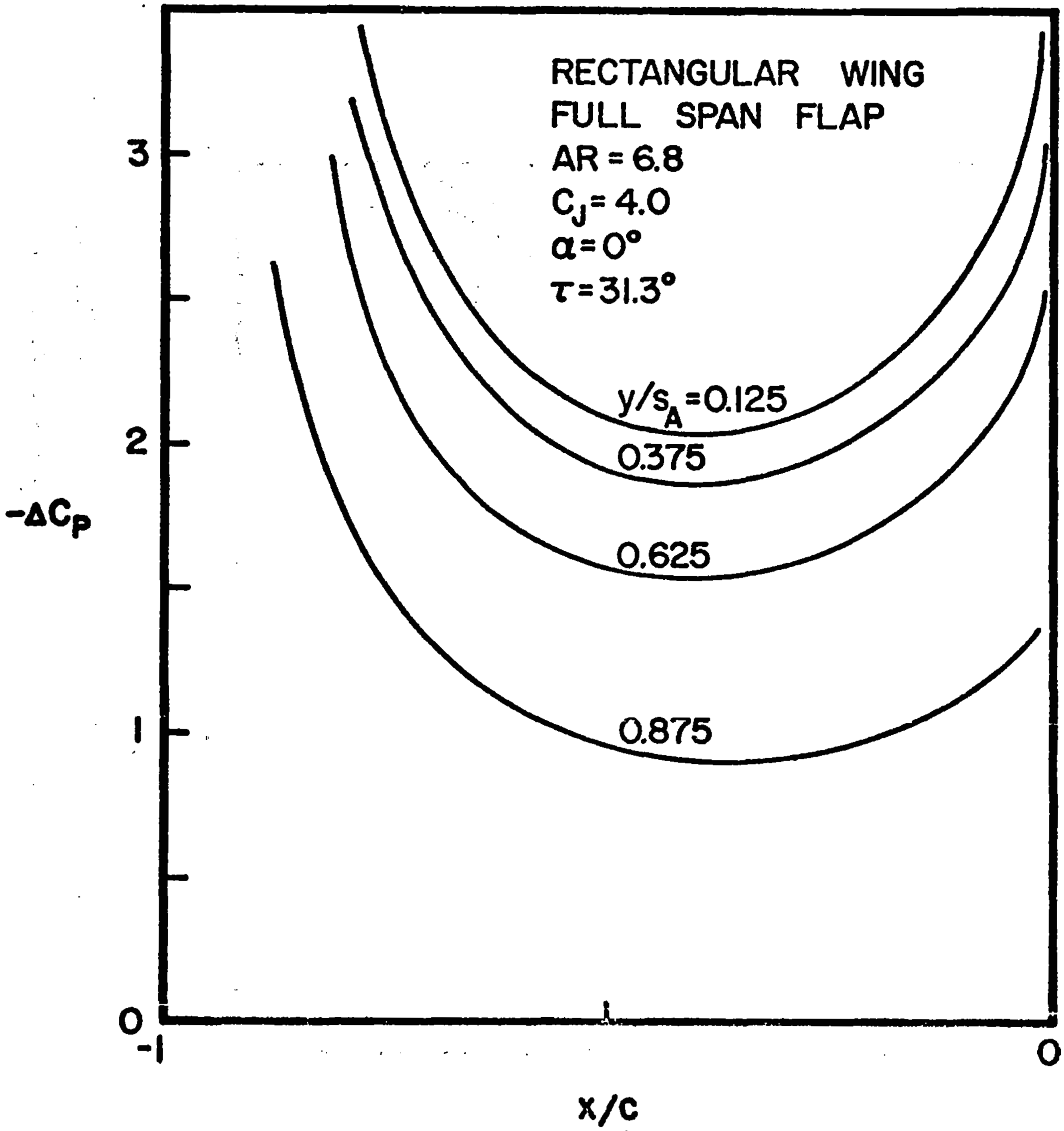

Figure 17. Streamwise Distribution of the Pressure Difference Across the Airfoil for $C_J = 4.0$ and $\alpha = 0°$.

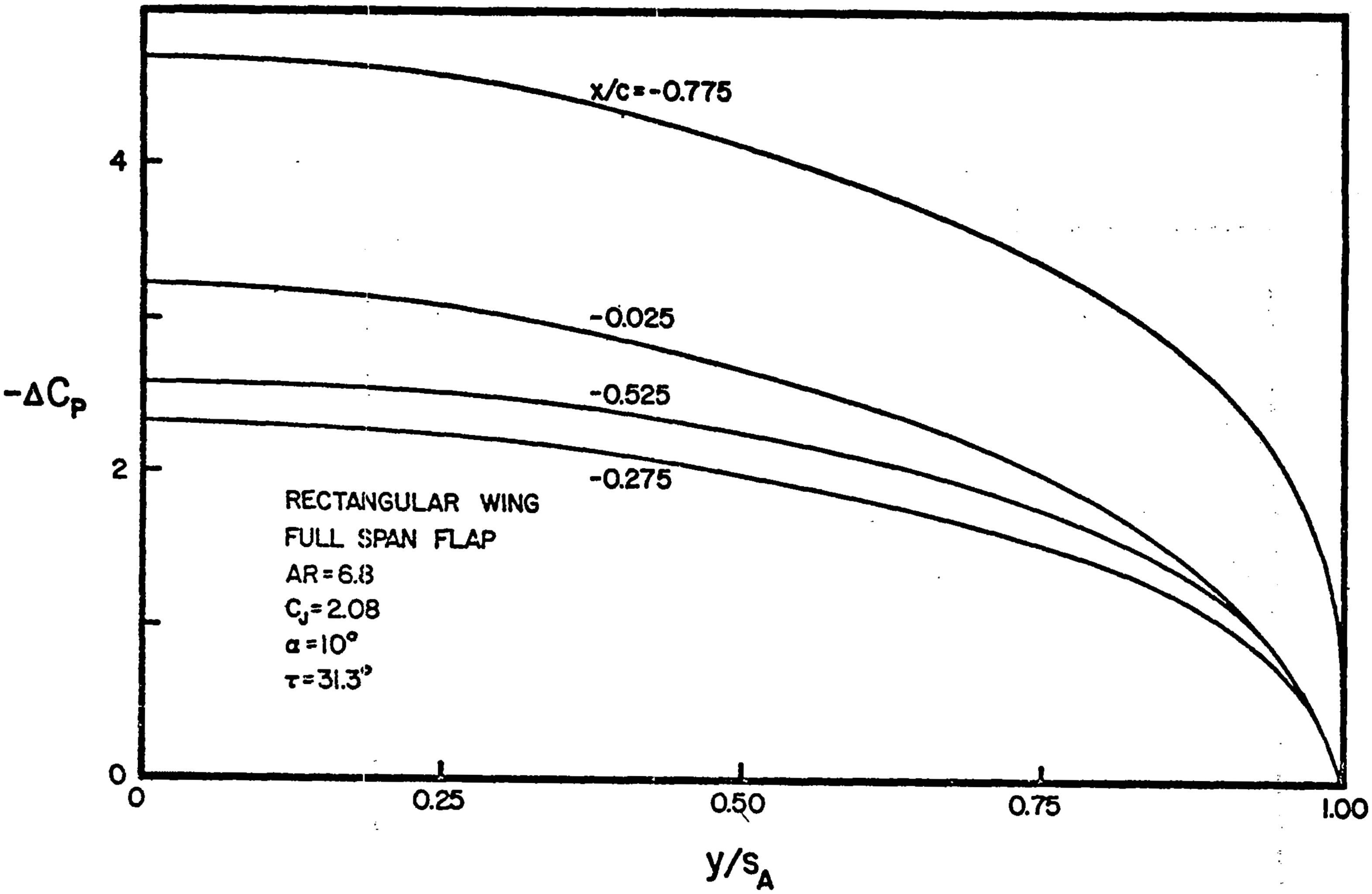

Figure 18. Spanwise Distribution of the Pressure Difference Across the Airfoil for C_J = 2.08 and α = 10°.

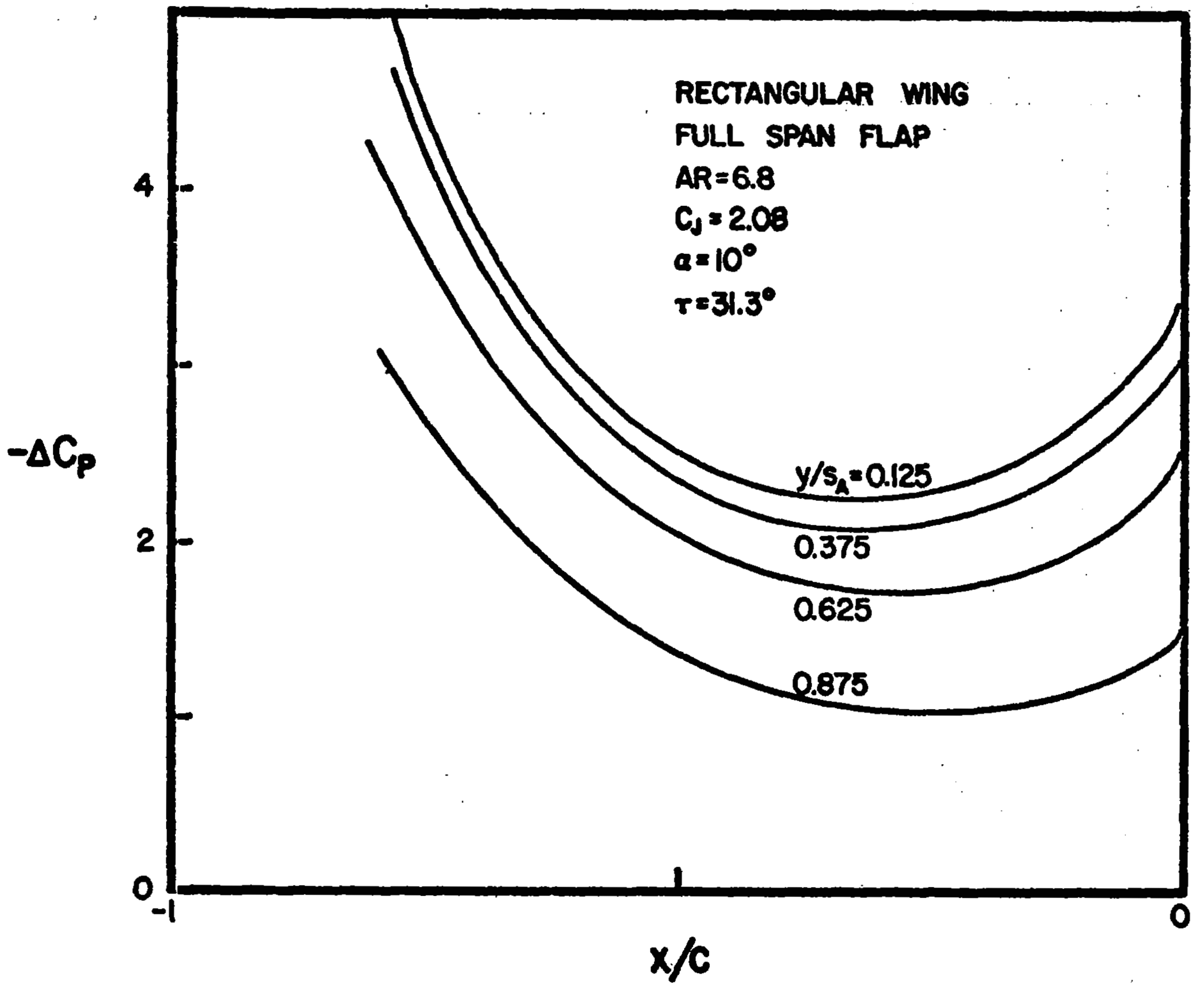

Figure 19. Streamwise Distribution of the Pressure Difference Across the Airfoil for C_J = 2.08 and α = 10°.

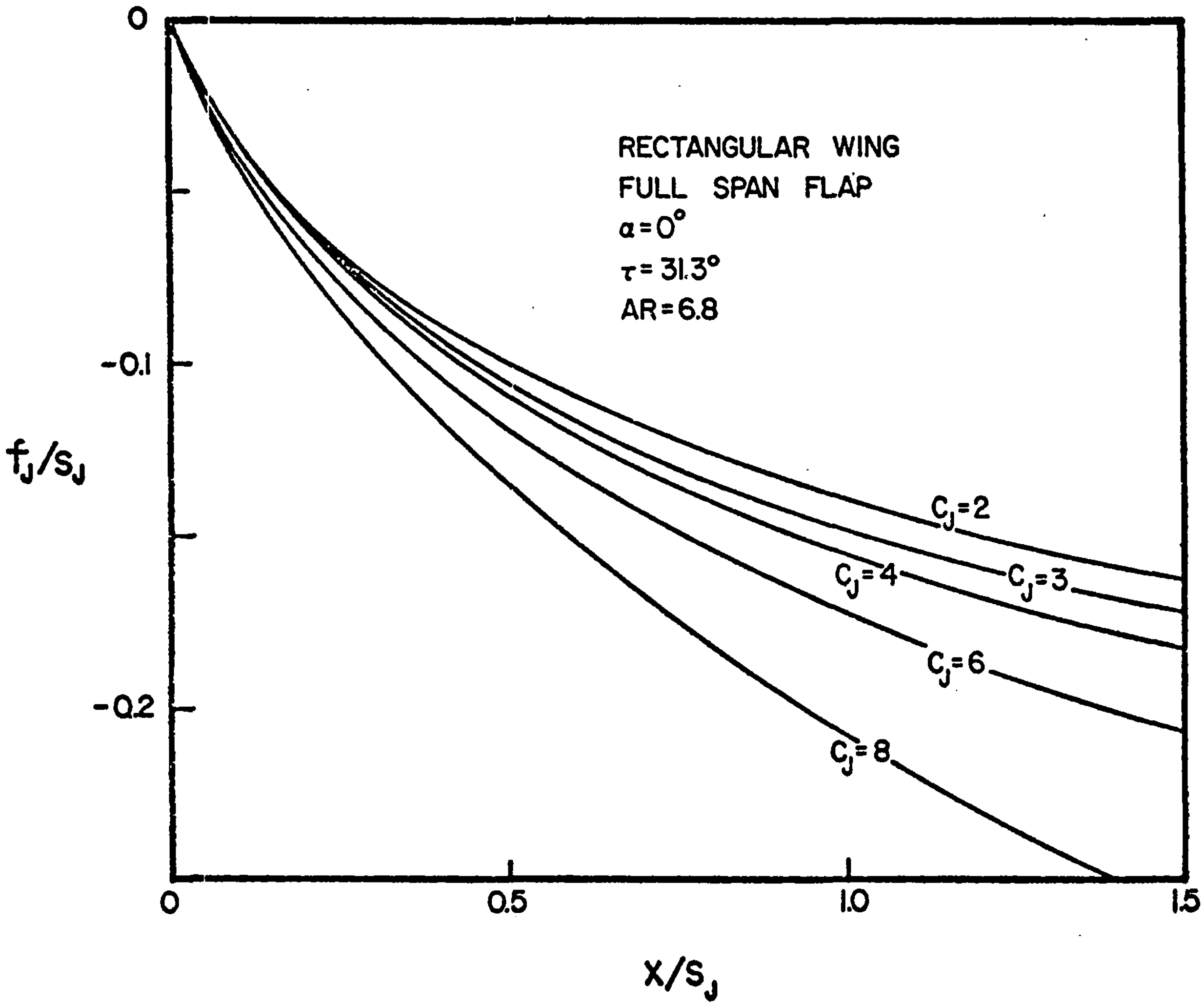

Figure 20. Locations of Jet Sheet in the Plane of Symmetry for Variations in the Jet Momentum Coefficient.

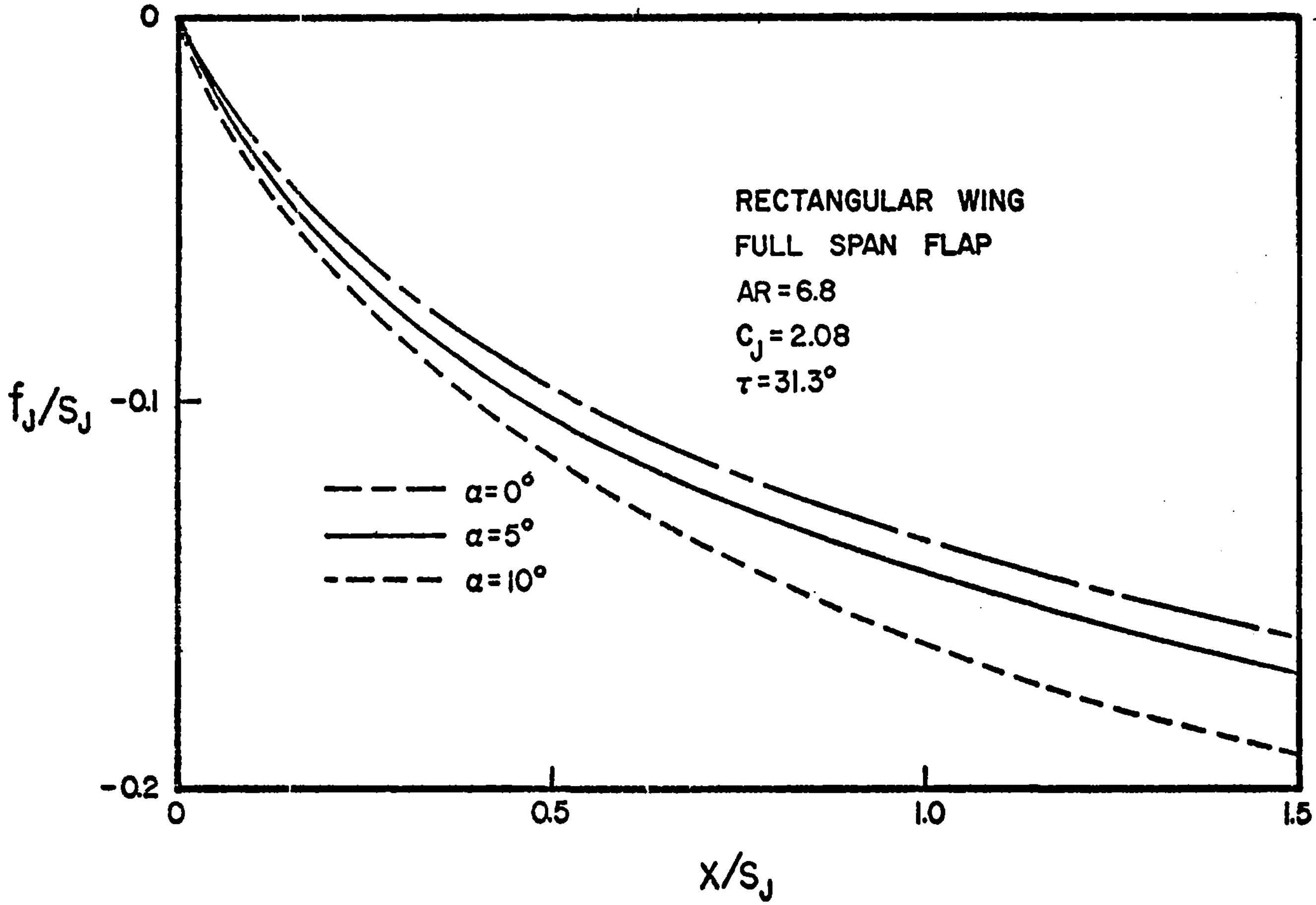

Figure 21. Locations of the Jet Sheet in the Plane of Symmetry for Variations in the Angle of Attack.

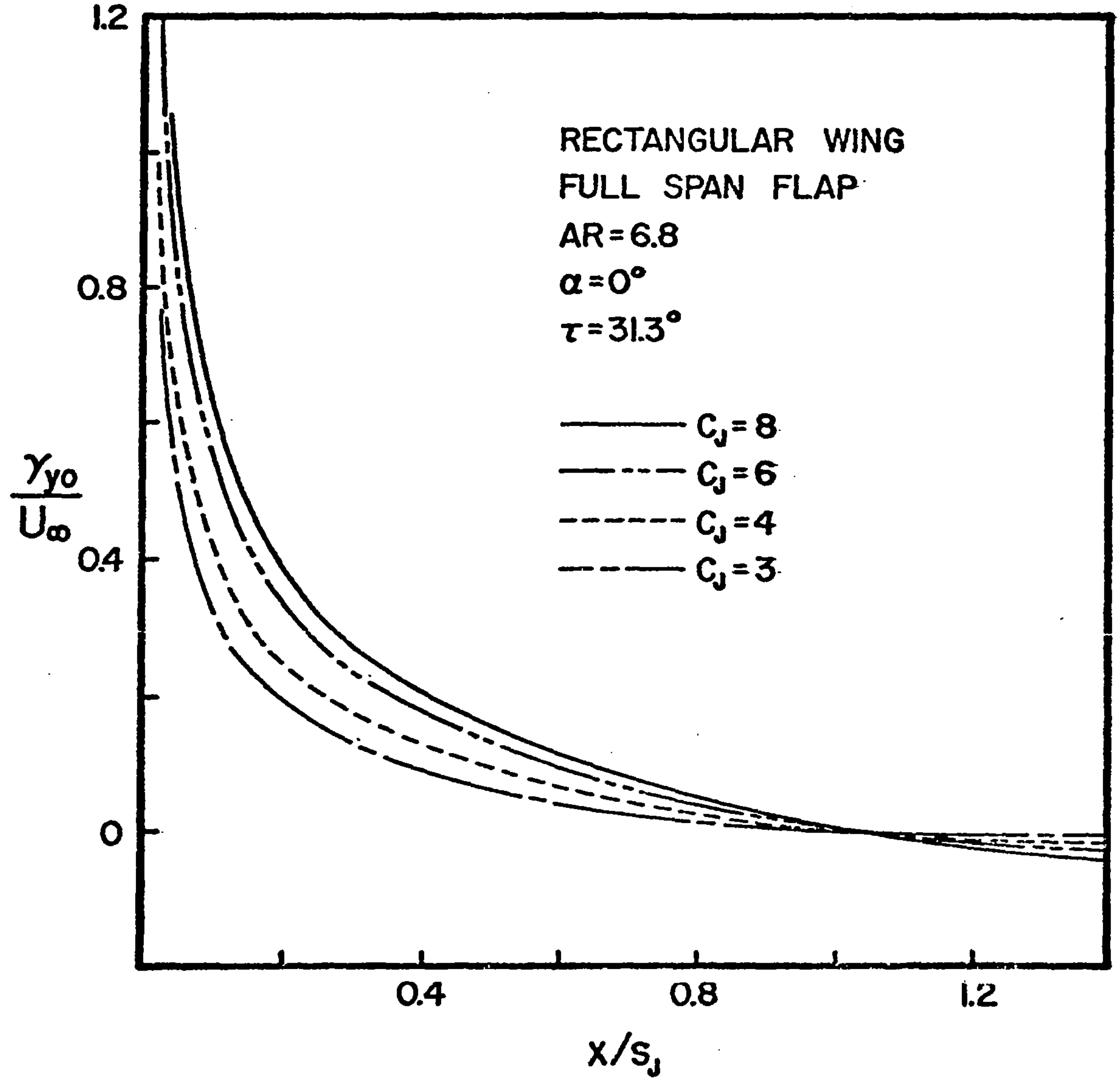

Figure 22. Variation of the Jet Vortex Strength in the Plane of Symmetry with Changes in the Jet Momentum Coefficient.

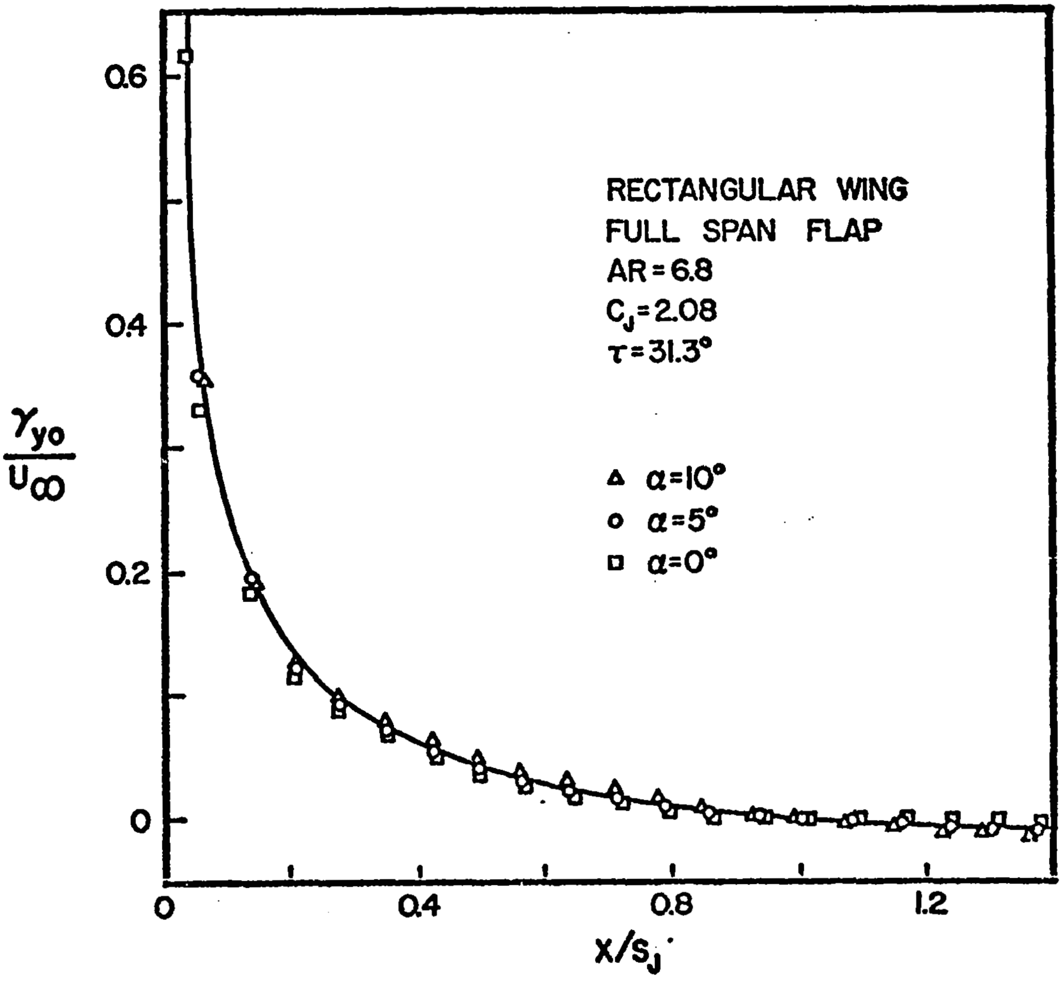

Figure 23. Variation of the Jet Vortex Strength in the Plane of Symmetry with Changes in the Angle of Attack.

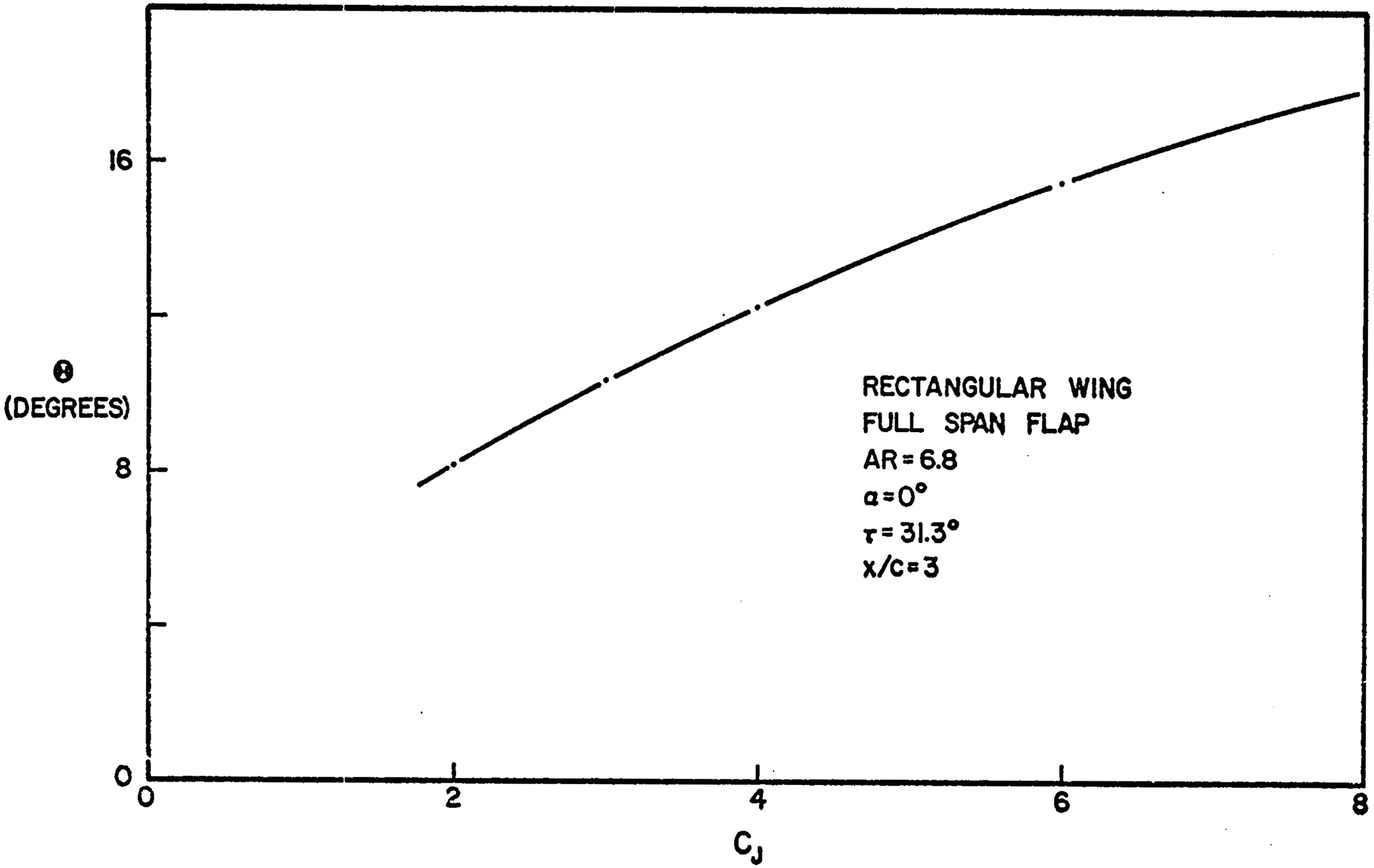

Figure 24. Variation of the Downwash Angle with Jet Momentum Coefficient for $\alpha = 0°$.

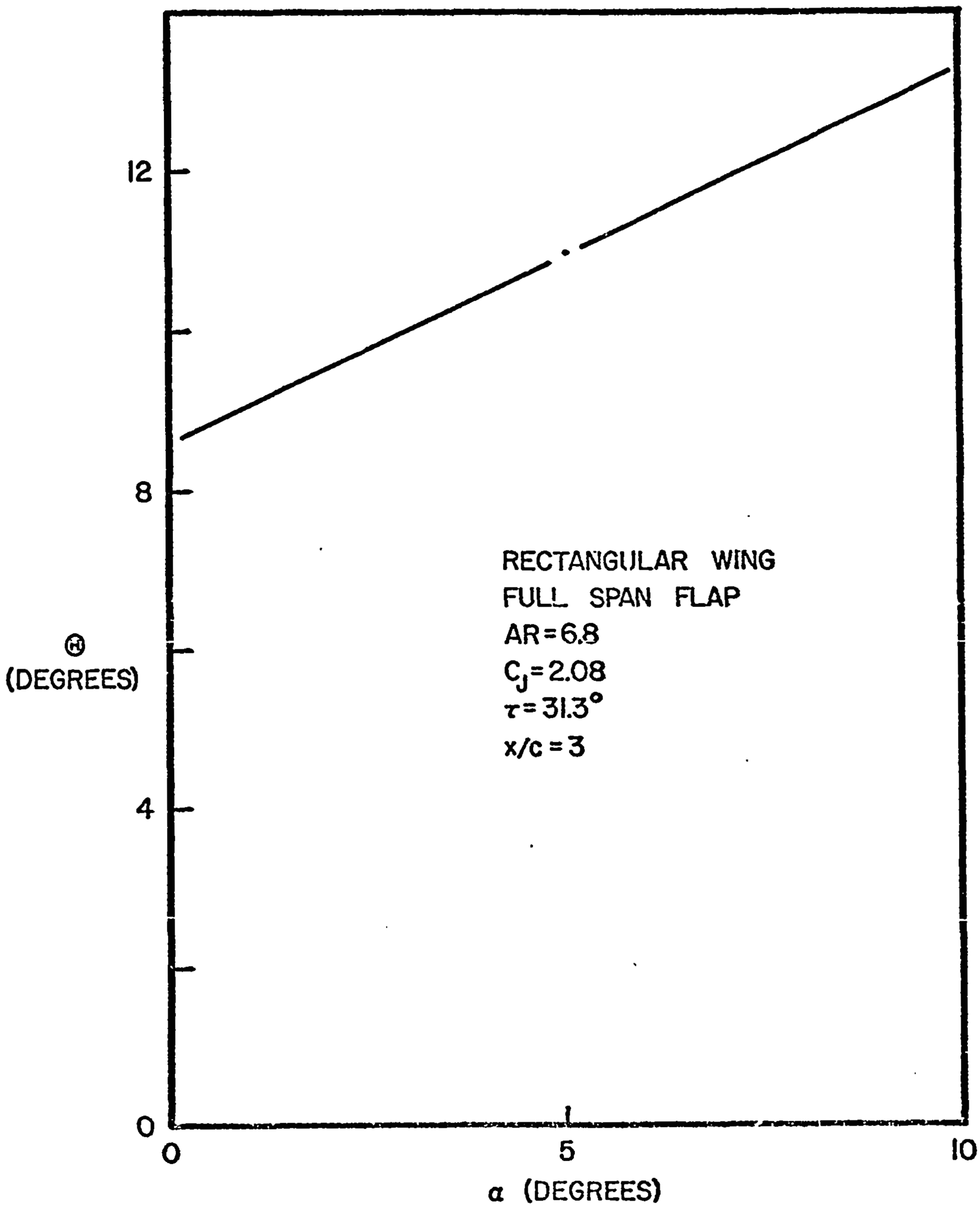

Figure 25. Variation of the Downwash Angle with Angle of Attack for C_J = 2.08.

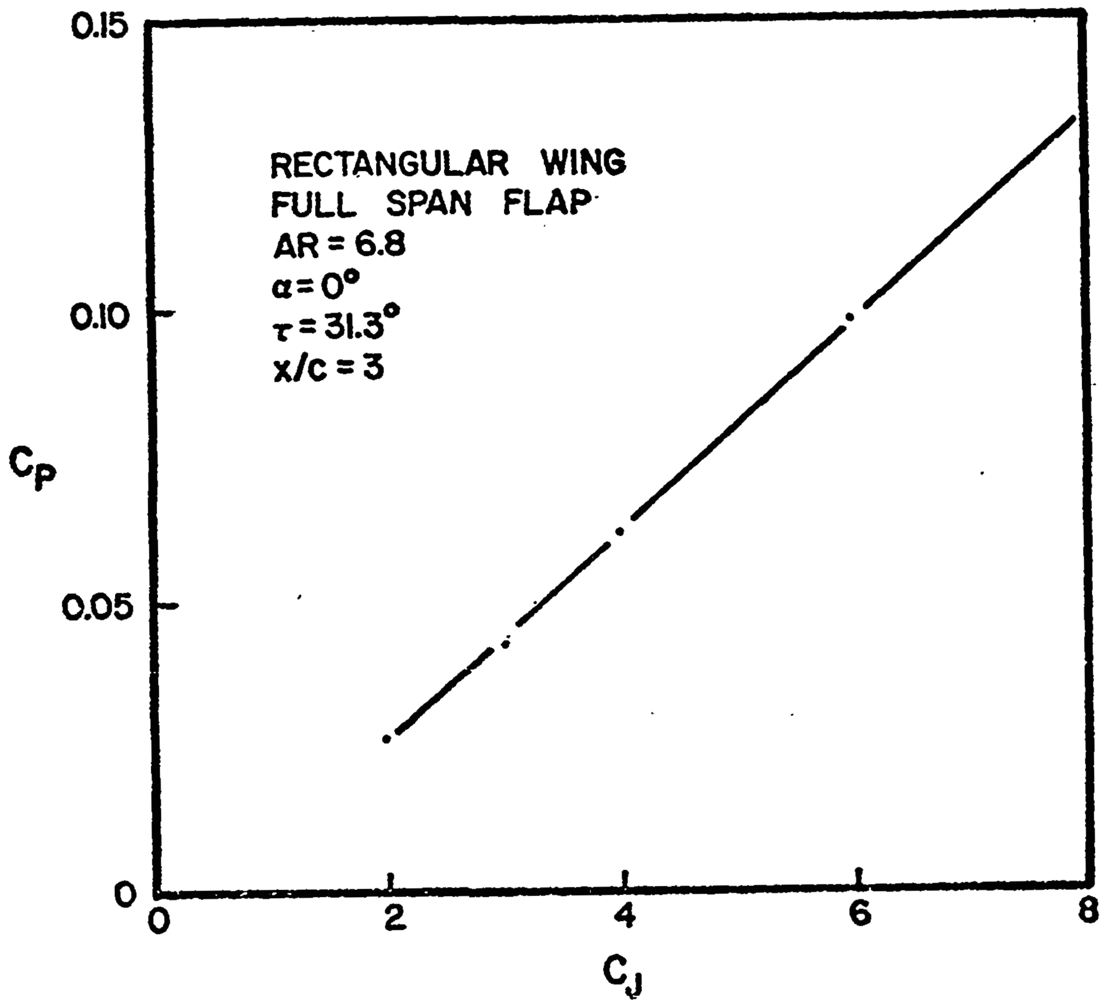

Figure 26. Variation of the Pressure Coefficient with Jet Momentum Coefficient for $\alpha = 0°$.

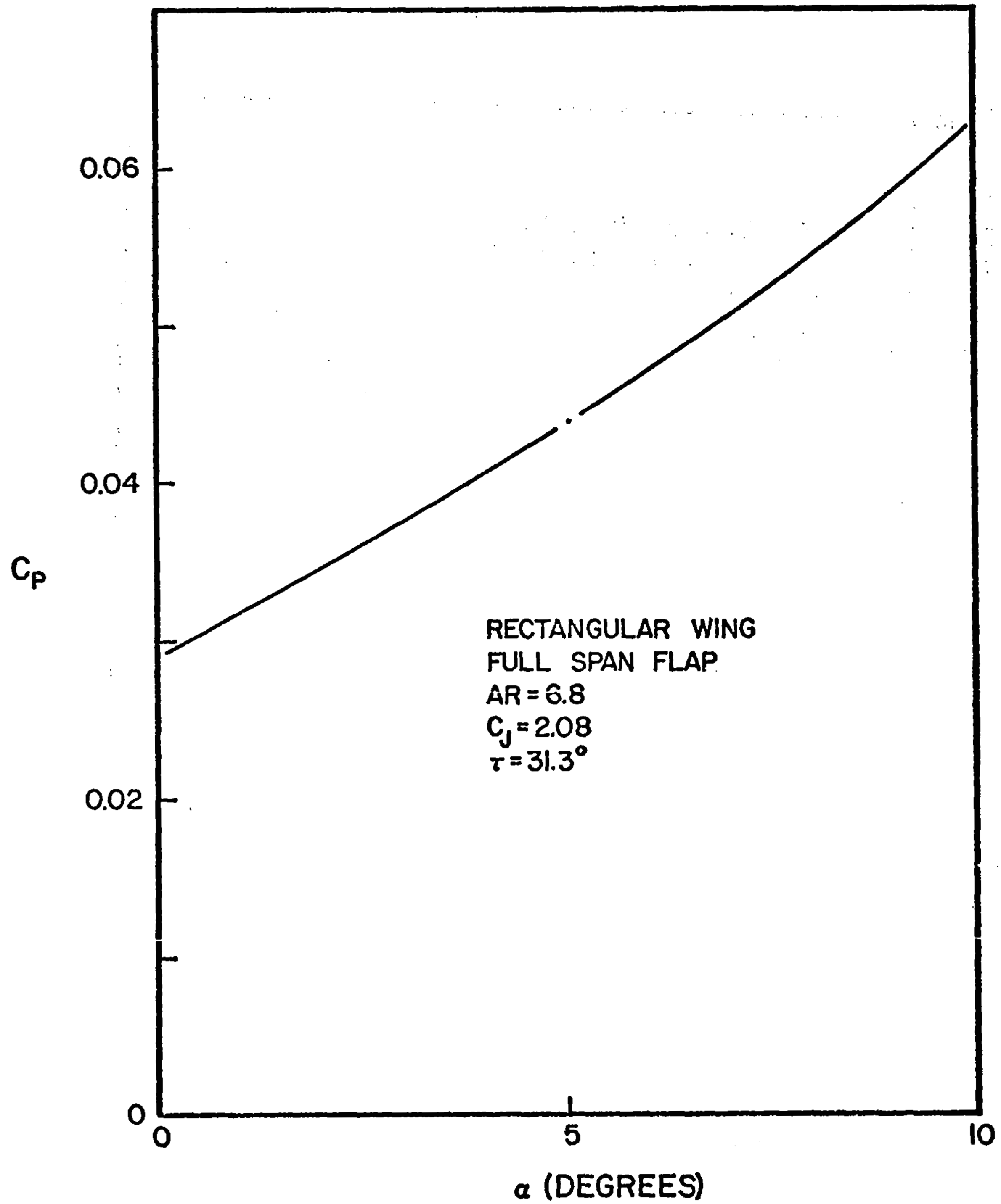

Figure 27. Variation of the Pressure Coefficient with Angle of Attack for $C_J = 2.08$.

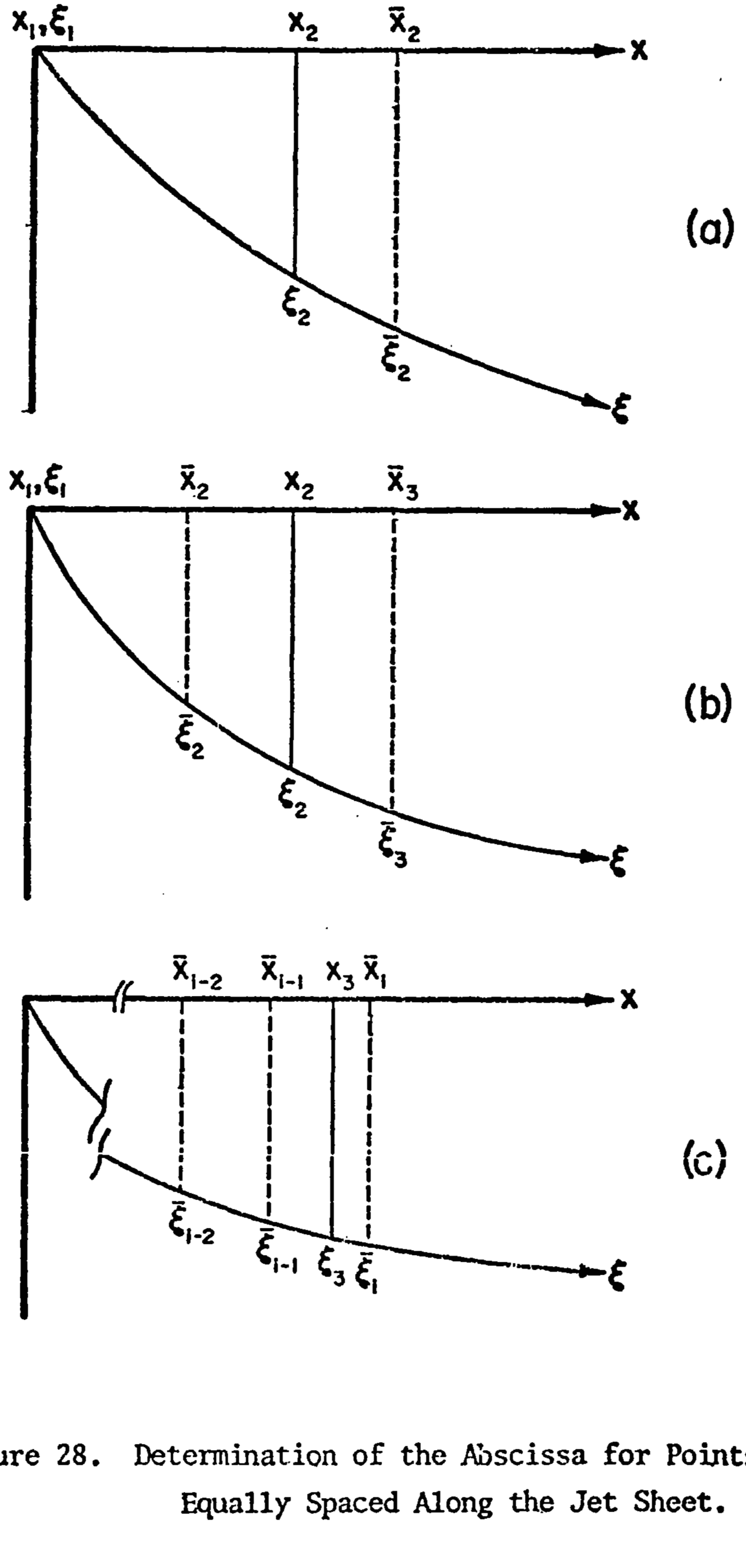

Figure 28. Determination of the Abscissa for Points Equally Spaced Along the Jet Sheet.

*U.S. GOVERNMENT PRINTING OFFICE: 1975 - 635-275/5